# Enhanced Engine Mechanical Efficiency through Tailoring of Lubricant Formulations to Localized Power Cylinder Wall Conditions

by

Ian P. Tracy

S.B, Mechanical Engineering
S.B., Aerospace Engineering
Massachusetts Institute of Technology, 2011

Submitted to the Engineering Systems Division
in Partial Fulfillment of the Requirements for Degrees

of

Master of Science in Technology and Policy and
Master of Science in Mechanical Engineering

at the

Massachusetts Institute of Technology

June 2015



Signature of Author……
Engineering Systems Division
Department of Mechanical Engineering
May 14, 2015

Certified by……
Dr. Victor Wong
Principal Research Scientist, Thesis Supervisor

Accepted by……...
Dava J. Newman
Professor of Aeronautics and Astronautics and Engineering Systems
Director, Technology and Policy Program

**Enhanced Engine Mechanical Efficiency through Tailoring of Lubricant Formulations to Localized Power Cylinder Wall Conditions**

by

Ian P. Tracy

Submitted to the Engineering Systems Division
on May 14, 2015, in Partial Fulfillment of the
Requirements for the Degrees of
Master of Science in Technology and Policy and
Master of Science in Mechanical Engineering

## Abstract

Numerical and experimental studies were performed on an internal combustion engine power cylinder wall's lubricating oil film in order to assess the possibility of tailoring engine lubricants to specific engine configurations and operating conditions for significantly enhanced fuel economy without an accompanying increase in engine wear. An array of different base oil-viscosity modifier type combinations were developed, tested, and analyzed in order to seek trends that link lubricant mixtures to certain rheological behaviors along the cylinder wall of a fired internal combustion engine. Viscosity modifiers were applied in an unconventional manner so as to increase viscosity at high operating temperatures rather than decreasing viscosity at low temperatures for promoting reliable cold-cranking. Consequently, a novel form of multi-grade lubricant was developed and simulated for determining potential fuel economy gains through its use. Both numerical simulation and a physical, laser-induced fluorescence diagnostic apparatus for an Isuzu 4JJ1 light-duty diesel engine were implemented in parallel to aid the development and validation of a reliable engine friction and wear model. Preliminary results have been insightful and coincident with classical continuum mechanics theory. Internal consistency across the developed model and physical diagnostics was considerable.

It is concluded that the tailoring of lubricant formulations can realize substantial fuel economy gains, and that oil & gas companies may realize significant competitive advantage and profit should they successfully inspire customers to consider purchasing lubricants that have been designed specifically for their automobile and driving habits. It is further proposed that the standards associated with lubricant classification be improved so as to consider the use of viscosity modifiers as mitigators of engine power cylinder wear at high cylinder temperatures near top dead center (TDC).

Thesis Supervisor: Dr. Victor W. Wong
Title: Principal Research Scientist

# Acknowledgements

I have had a fantastic experience over the past three years as a Master's degree student in both MIT's Engineering Systems Division and its Department of Mechanical Engineering. I have significantly extended both my fundamental technical knowledge, and perhaps more so achieved grand insight into systems level approaches and thinking. From a technical standpoint, I have relished the opportunity to first step into the world of systems safety under MIT's Dr. Nancy Leveson, and then delve deeply into the theory of tribology and engine lubrication under Dr. Victor Wong at MIT's Sloan Automotive Lab. I have been fascinated with continuum mechanics theory since it was first introduced to me during my undergraduate studies here at MIT, where I've been able to apply my intrinsic curiosity to problems that affect a great number of people. From a policy perspective, I feel that I have been enlightened as to the reasons for the existence of organizational protocols and policies that play dominant roles in determining what is created (be it products, ideas, or values) and how it is implemented in society. I have found these topics to be genuinely fascinating and directly applicable to my ambitions involving driving large-scale change in society through technological innovation and effective policymaking.

None of my studies or research would have been possible were it not for the gracious support of a number of individuals. I would foremost like to thank Dr. Victor Wong, my research advisor, for always being available for me when I needed assistance or advice on virtually all facets of my MIT experience. He has maintained great confidence in my abilities and provided me with more than amble opportunity to develop myself and guide my work streams as I deem fit. This level of trust and respect demonstrated by Dr. Wong is something of which I am truly appreciative. I would also like to acknowledge Dr. Nancy Leveson of MIT's Aeronautics and Astronautics for taking me under her wing during my first year as a graduate student and teaching me an entirely new way to think about systems safety and complex systems in general. Her work and research opportunities have radically redefined way that I view and approach the world around me. It was because of Dr. Leveson that I first felt the magnificent value of an MIT graduate education. I was no longer solving canned (albeit very challenging) technical problems; instead I was considering the very nature and origins of those problems, as well as whether the questions I am posed are the right ones to ask in the first place.

I further want to extend my thanks to Dr. Frank Field of MIT's Technology and Policy Program for teaching me to question my assumptions and seek to truly understand the fundamental drivers of decisions and policies. Barbara DeLaBarre has been of so much help in ensuring that I am aware of deadlines, opportunities, and university policies that may be of interest to me. Her generous support clearly extends to all of her TPP students.

Of particular significance to me is the assistance I've received and friendships I've developed with my Thai colleagues at PTT: thank you Komkrit Sivara, Somnuek Jaroonjitsathian, Chutinan Promdej, and Sunthorn Predapitakkun.

Finally, and as in every phase of my life, my greatest thanks is extended to my family for supporting me through thick and thin, whatever the situation—thanks Mom, Dad, Tommy, Ben, Mike, Dave, and of course Phil. Without them all, I would not be here today.

# Table of Contents

# List of Figures

# List of Tables

# Chapter 1. Introduction and Project Background

This Master's thesis summarizes the key accomplishments of work done in a collaboration between PTT Public Company Limited and the MIT Sloan Automotive Laboratory on lubricants optimization between August of 2013 and May 2015. It is in effect a detailed progress report on the developments over the first two years of a five-year project whose focus is to investigate the possibility of tailoring engine lubricant formulations to specific engines and operating conditions for enhancing automobile fuel economy by several percentage points. The benefits of reduced fuel consumption are clear—fewer emissions, decreased demand for global nonrenewable energy resources, and an accompanying reduction in dependence on foreign goods. From an individual's perspective, improved fuel economy results in transportation cost savings through reductions of both fuel consumption and engine contamination, time savings in the form of increased driving range, and improved air quality, among a host of other benefits. It is estimated that strategic lubricant tailoring has the potential to enhance overall automotive fuel economy by upwards of 5%. A single percent fuel economy boost is considered greatly significant in the automotive industry at present.

One of the primary focuses of my research over the past twenty or so months has been analyzing rheological data for several lubricants while modeling both boundary and hydrodynamic friction components along the wall of an internal combustion engine's power cylinder. This was done in order to enable the tailoring of lubricants to a given engine for minimal friction losses while maintaining adequate cylinder wear. Both numerical models and physical measurement apparatuses were developed for the purpose of understanding the rheological and tribological phenomena that occur along the cylinder wall during fired engine operation. A well-understood tradeoff exists between overall frictional power losses and cylinder wall wear rate, which will be explained shortly. For a given wear rate, however, it is shown herein that lubricants even within the same SAE oil grade classification can yield significant differences in frictional power losses. It is therefore possible—and important—to tailor lubricant formulations to specific engine geometries, or classes of geometries, and operating conditions. The significant impact of tailored lubricants on engine efficiency and—consequently—reduced emissions should inform the development of policies that govern intelligent lubricant development for internal combustion engines. A key recommendation for updating the classifications of modern multi-grade lubricants is included near the conclusion of this thesis.

## 1.1 Fuel Economy Enhancement through Lubricant Optimization

The objective of the present research effort is to gain an understanding of lubricant behavior in internal combustion engines to a sufficient extent such that base oil-additive blends can be successfully tailored to a light-duty diesel Isuzu 4JJ1 engine undergoing a characteristic drive cycle with a resulting efficiency improvement of at least 3%. The degrees of freedom of the prescribed approach include selection of lubricant base stock and additives that desirably impact the rheological properties of the resulting blend. Fruitful selection of a base oil and additives is accomplished in a manner that promotes reduced wear and overall energy consumption reduction through careful consideration of both boundary and hydrodynamic power loss contributions from the ring-pack and skirt reciprocating in the fired engine. The Isuzu 4JJ1 engine selected for optimization has basic specifications: four cylinders, displacement of 3.0 liters, and rated power of approximately 115 kilowatts.

This research has been conducted in close collaboration with PTT Public Company, an oil and gas company headquartered in Bangkok, Thailand. A key focus of this work specifically entails the tailoring of lubricants in regions with warm climates that do not experience temperatures well below freezing. Such areas do not require lubricants to possess cold-cranking capabilities, since lubricants in warm climates do not thicken to an extent beyond that which is deemed unacceptably resistant to pumping oil through to components that require lubrication. The current research shifts from a traditional focus on mitigating cold temperature effects on behavior of lubricant blends to addressing the impact of higher temperatures on engine oil control volumes within a fired power cylinder. Such high temperatures are known to reside near the source of fuel combustion at the top of the cylinder. At high temperatures near top dead center (TDC), fuel economy reduction due to mechanical friction-induced power losses is mild compared to the lower temperature regions further down along the cylinder. However, engine scuffing and wear, which can ultimately lead to combustion gas leakage and engine failure well within its design lifetime, occur most significantly in the high temperature region. Since engines are not to fail for hundreds of thousands of miles, wear near top-dead center (TDC) is a substantial limiter for the behavior of a lubricant in the power cylinder. If wear can be reduced, greater flexibility will be embedded in lubricant development, ultimately leading to a drop in power loss (and thus fuel consumption) over a given drive cycle. Figure 1-1 provides a schematic

of the current project's overall goal of 3% engine efficiency improvement through lubricant base stock and additive tailoring.

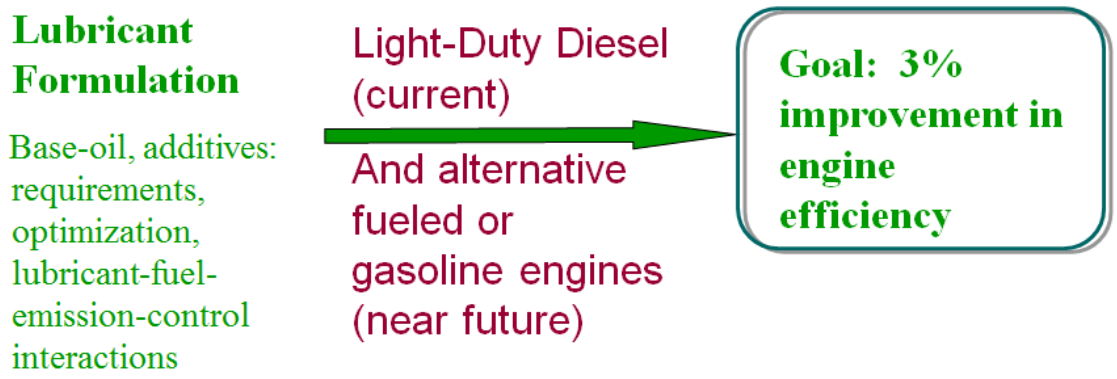


**Figure 1-1.** Project Overall Objective Map

The research project is partitioned into four major tasks, each contributing to enhancing a numerical model for engine friction and wear that can be applied in order to predict the impact of a given lubricant formulation on performance with regard to those two primary parameter metrics. The approach is given by:

**Program Tailored to Light-Duty Diesel Study**

**Approach:**

1. **Base oil and VI optimization for prevalent duty-cycles in Thailand – methodology and analyses in leveraged program**
2. **Light-Duty Diesel Engine and Oil Film Thickness Measurement System Installation based on Laser-Induced Fluorescence Diagnostics**
3. **Minimum oil film thickness (top ring) – determine practical limit of viscosity reduction (consider combination with 1. above)**
4. **Relative mix of boundary friction modifiers/anti-wear additives that optimize given light-duty diesel for piston-assembly friction versus valve-train and bearing friction**
5. **If acceptable, consider "in-situ" lubricant composition/property controls that supplement additive package. Engine technology to supplement lubricant technology – e.g. reduced oil control ring tension**

Items 1 and 2 have been accomplished thus far, and have paved the way for considerable progress on items 3-5, which will all be addressed herein. 1 and 2 will be discussed in greater

depth, with the 3-5 making appearances throughout this text, effectively foreshadowing the work that is upcoming.

### 1.1.1 Base Oil and VM Optimization via Numerical Simulation

Item 1 describes the practice of designing, testing, and analyzing several lubricant formulations in numerical simulation so as to determine that or those which are most desirable with regard to the fuel economy-engine wear tradeoff that is central to this project. After all, as we seek to develop a lubricant that substantially reduces fuel consumption without increased wear, a means of comparing the effectiveness of one lubricant over another is thus of core importance to the project. Lubricants are segmented based on (1) the class of base oil, and (2) type of viscosity modifier mixed to generate a resulting final lubricant solution. Purposeful partitioning enables the correlation of friction-wear results to groups of base oil-viscosity modifier pairs.

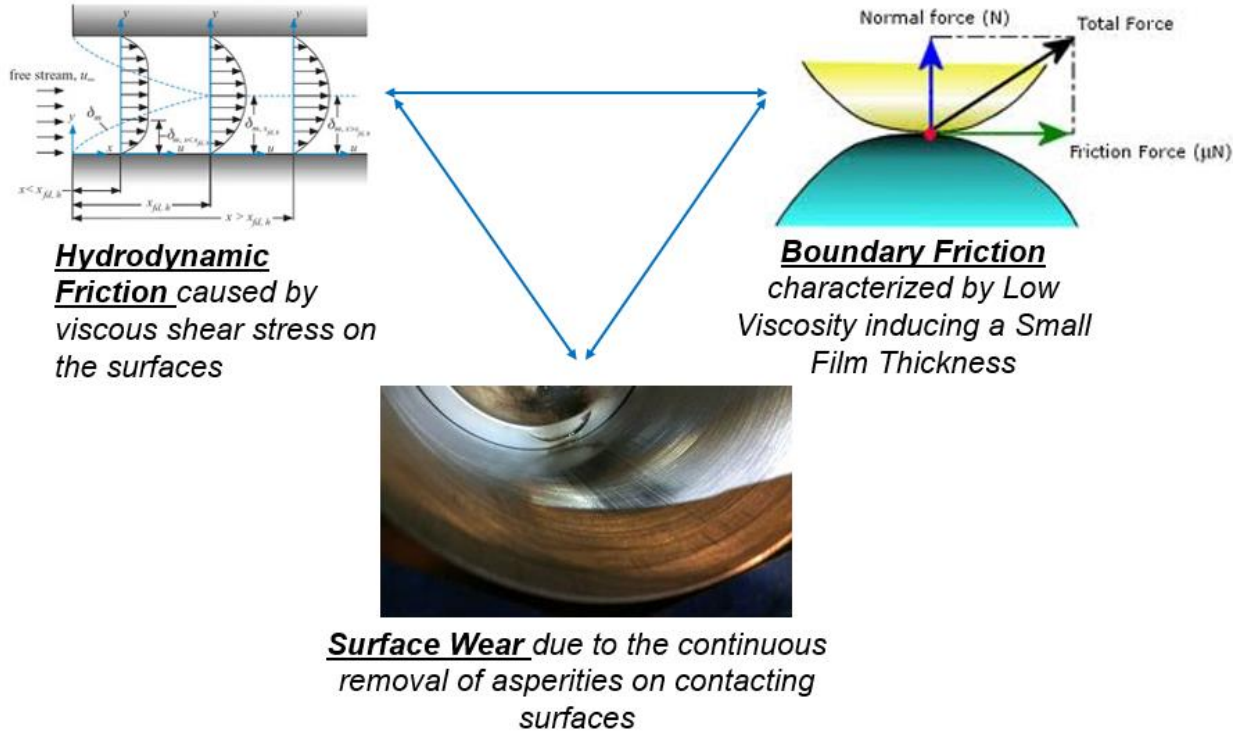


**Figure 1-2.** Depiction of the three output parameters of primary interest

The outputs of the simulation developed are simplified to an overall frictional power loss value (further decomposed into boundary and hydrodynamic components) and a quantitative result for

a wear parameter that is to reflect the effective engine cylinder wear rate. A grid of power loss and wear values are generated in order to enable the selection of the single "best" lubricant for an engine at a particular operating condition. "Best" refers to the lubricant that optimizes one's utility function, balancing incremental improvements in fuel economy with the accompanying increase in wear. In other words, it is important to determine the relative value of an incremental improvement of both metrics relative to one another in order to select one lubricant's performance as superior to the others'. Sensitivity analysis and multi-dimensional regressions (fitting) may likely play roles in converging upon an optimal lubricant formulation. An engine can be simulated at several operating points, and the results of those simulations may be subsequently combined via appropriate weighting to reflect the simulation of an entire engine

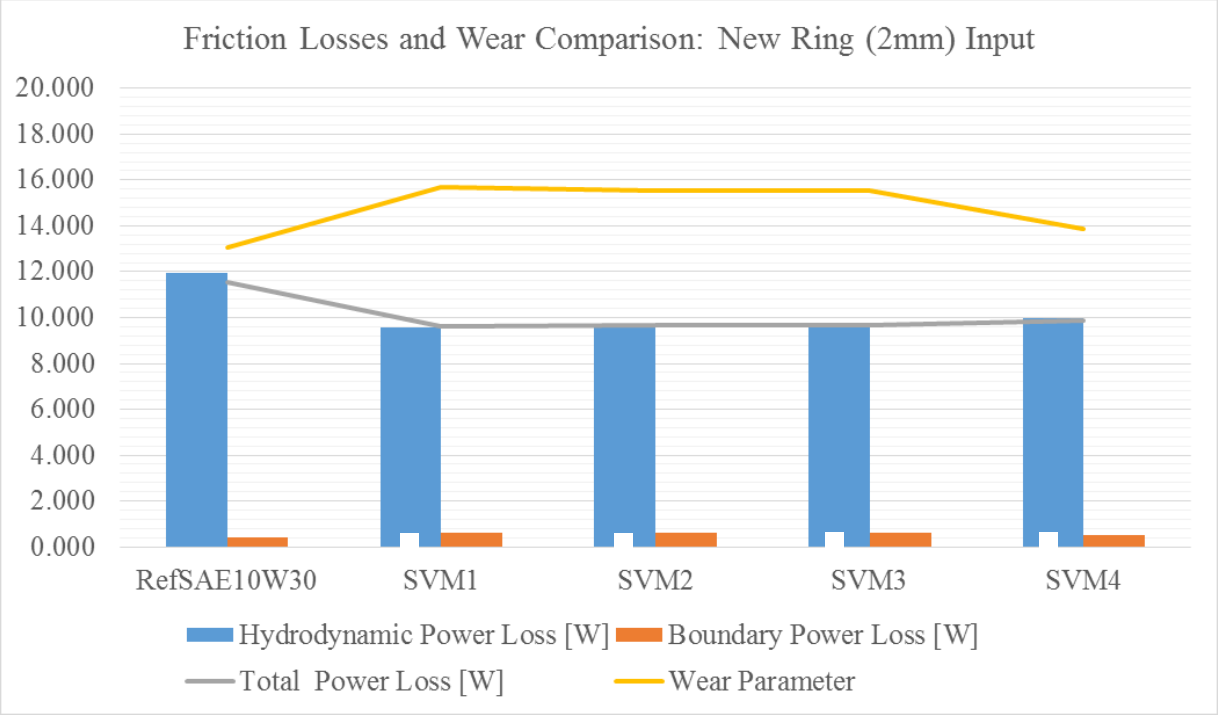


**Figure 1-3.** Sample numerical results from the friction-wear model central to this project.

test cycle, such as the New European Drive Cycle applied herein. For example, if a drive cycle consists of idle for 100 seconds, a mid-range load value for 200 seconds, and peak-torque for 100 seconds, then it may well be reasonable to assign respective weightings of 0.25, 0.50, and 0.25 to idle, mid-range, and-peak torque operating condition simulation results in order to yield an effective full-cycle simulation.

**Table 1-1.** Sample output data organized by power loss component and wear parameter

| | Hydrodynamic Power Loss [W] | Boundary Power Loss [W] | Total Power Loss [W] | Wear Parameter |
|---|---|---|---|---|
| RefSAE10W30 | 11.120 | 0.424 | 11.540 | 13.070 |
| SVM1 | 9.039 | 0.605 | 9.644 | 15.677 |
| SVM2 | 9.061 | 0.599 | 9.660 | 15.556 |
| SVM3 | 9.063 | 0.596 | 9.658 | 15.518 |
| SVM4 | 9.389 | 0.494 | 9.883 | 13.886 |

A full graphical representation of four-stroke cycle film thickness, friction components, and temperature is given in Figure 1-4, where orange curves represent the base oil + VM blend. Film thickness is shown to scale with the square root of viscosity.

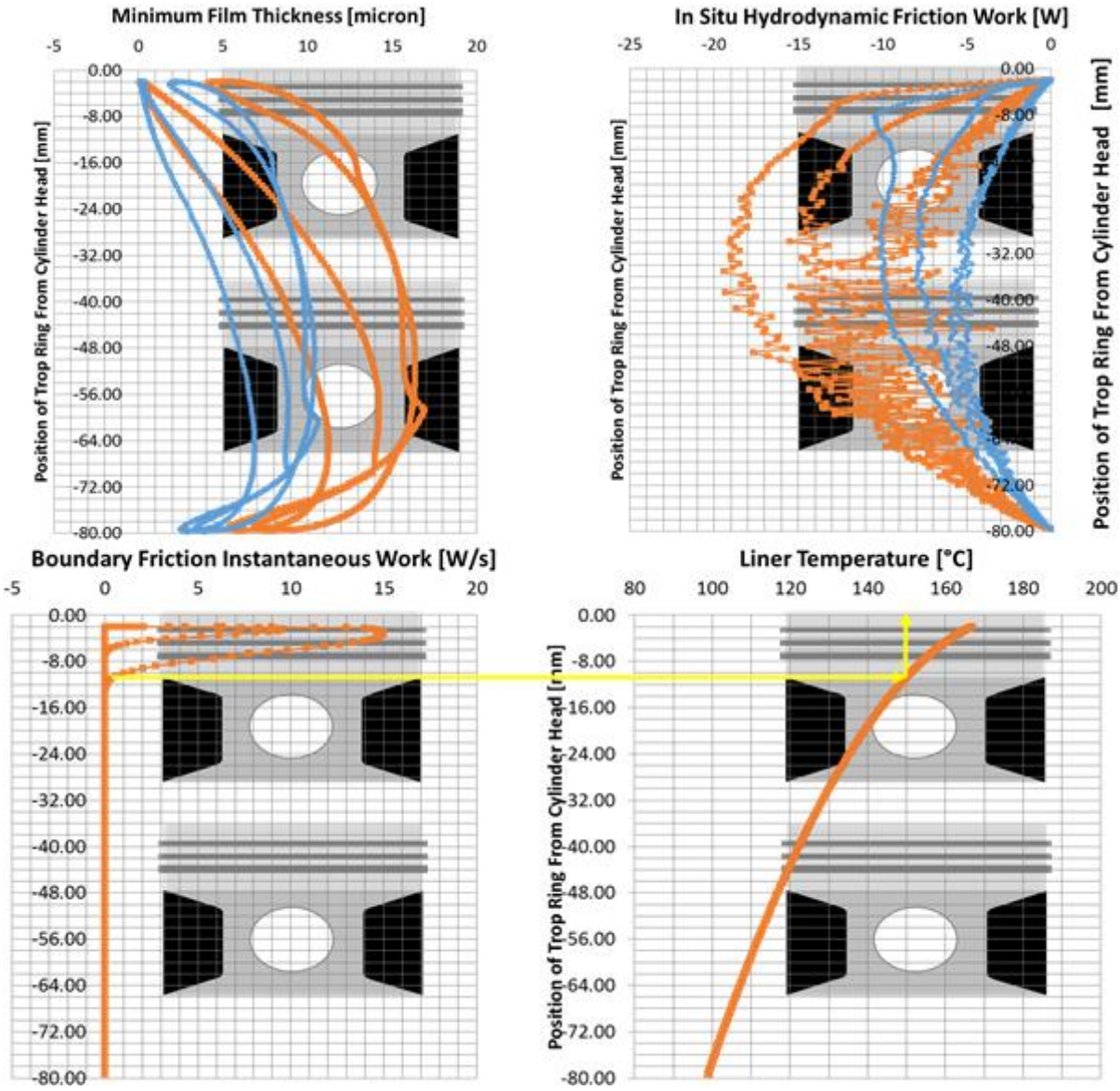

| Specimen | Total Power Loss | Total Boundary Power Loss | Total Hydro Power Loss | Wear Parameter |
|---|---|---|---|---|
| Base oil | 4.75 | 0.83 | 3.92 | 18.4 |
| Base oil + VM | 7.42 | 0.265 | 7.15 | 9.4 |

**Figure 1-4.** Graphical representation of key friction-wear model output values

### 1.1.2 Oil Film Thickness Verification through Laser-Induced Fluorescence

Item 2 of the project tasks references the laser-induced fluorescence (LIF) apparatus designed, manufactured, installed, and maintained by the author and his colleagues at PTT. Its purpose is to physically measure lubricant film thickness at point locations along engine cylinder walls—in large part to help validate outputs from numerical simulation. It further serves to provide greater insight into the rheological behavior of lubricants along the cylinder, while varying temperatures, engine geometries, and operating conditions. The LIF device is able to probe at discreet locations along the power cylinder wall, and was thus positioned to provide data representative of cylinder wall regions of interest. The two regions selected for the purposes of this project are: (a) the mid-stroke area where the piston travel at high velocity and oil films

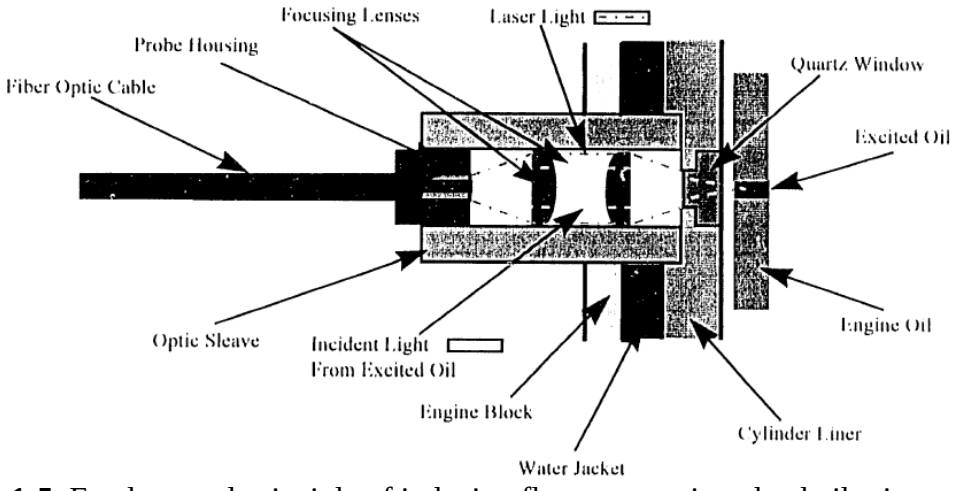


**Figure 1-5.** Fundamental principle of inducing fluorescence in a dyed oil mixture via laser light

are thickest, yielding heavy viscous losses; and (b) a point near TDC where lubricant temperatures are highest, and high cylinder pressures cause significant wear along the wall (or liner if one is present) due to the predominance of solid-to-solid contact in that particular region.

### 1.1.3 Minimum Oil Film Thickness: the Practical Limit of Viscosity Reduction

Item 3 seeks to determine the reduction of lubricant viscosity adjacent to the top ring that is permissible given the requirement to maintain a wear rate at or less than that generated by a reference multi-grade engine oil. That is, to what extent was the optimal lubricant solution selected in Item 2 thinned relative to the reference oil solution to which it was compared and whose wear rate it was required to match or best? Figure 1-6 displays the range of oil temperatures adjacent to the piston rings and skirt during a sample engine operating cycle.

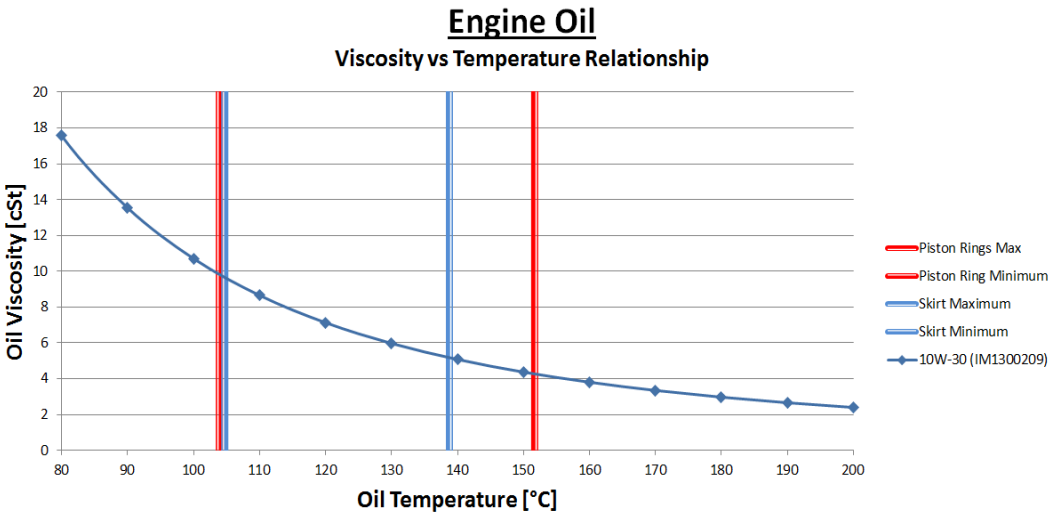


**Figure 1-6.** Oil temperature ranges experiences by both the piston and the skirt

Figure 1-7 shows that in situ piston speed is approximately parabolic, terminating with zero speed at both TDC and BDC where the piston stops and begins moving in the opposite direction. A further visual representation Figure 1-8 illustrates the regions of peak wear due to boundary friction and maximum power loss resulting from high piston speeds and heavy viscous dissipation.

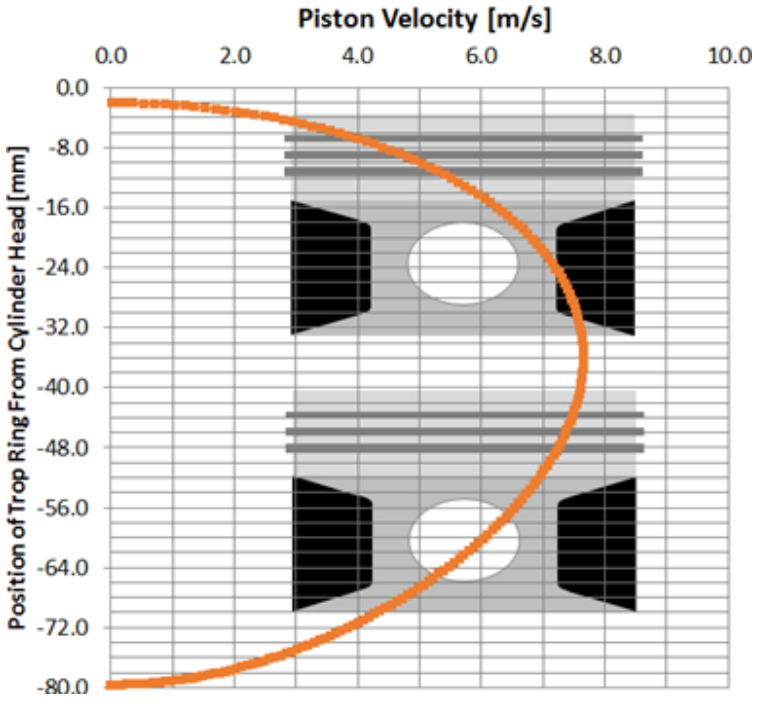


**Figure 1-7.** Sample engine piston speed profile

The high speed of the piston approximately half-way between its peak and trough points generates significant pressure that helps separate the piston from the wall via hydrodynamic lubrication. At high speed, the viscous stress is great due to a strong gradient in fluid velocity as a function of distance normal to the cylinder wall (recall the classical solution for fluid shear stress $\tau = \mu \frac{\partial u_x}{\partial r}$). Viscous dissipation thereby generates substantial frictional losses, and is in fact responsible for the majority of them over most conditions tested thus far by the author. Sensitivity analysis conducted on approximately twenty base oil-viscosity modifier blend combinations indicated a range of boundary power loss contributions between 5% and 25% of the total power cylinder power loss, with idle generating the greatest boundary losses. As load decreases, the potential for friction reduction increases to a maximum at idle, where all power is being converted to wasted thermal energy. Since the cycles of predominant concern to the author and many key players in the industry operate primarily at idle, significantly reducing overall cycle friction at idle is of primary concern. As many modern engines operate at up to 90%+ mechanical efficiency at rated power conditions, considering cycles with part- and low-load operating conditions will yield a greater overall mechanical friction percentage decrease.

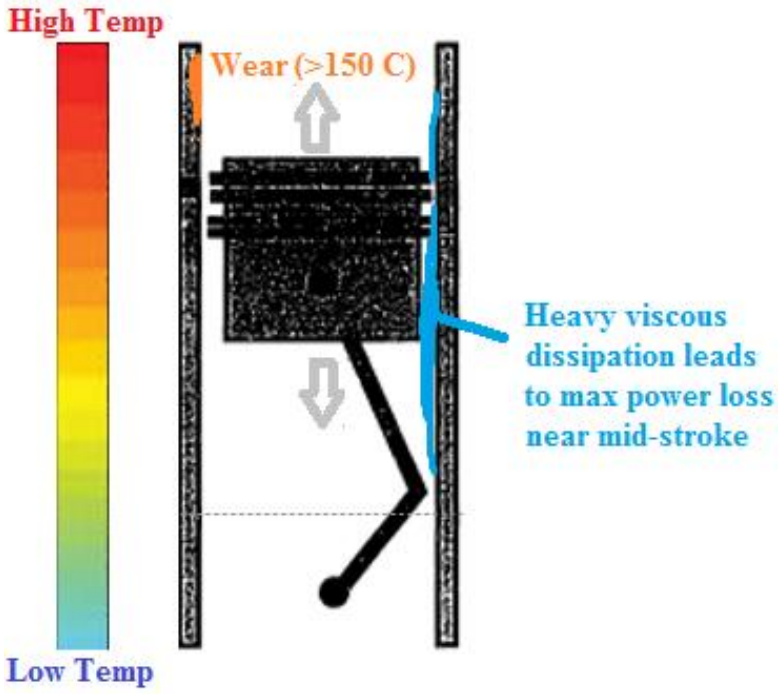


**Figure 1-8:** Regions of peak wear (thin oil film) and high power losses (via viscous losses) [1]

Absolute temperature value bounds can vary substantially across different engine sizes (or displacements), for example. We notice that the ring-pack experiences higher temperatures than the piston and determines the minimum tolerable film thickness that can be present near TDC while maintaining adequate levels of cylinder wall wear. The author would like to note that recent studies by Mark Molewyk indicate the possible presence of significant cylinder wall wear near mid-stroke due to skirt oscillatory motion and consequent scuffing during the exhaust stroke. [1]

### 1.1.4 Friction Modifiers and Anti-Wear Additives in the Piston-Assembly

Item 4 brings to light the fact that other lubricant additives exist for the express purposes of both reducing boundary friction via friction modifiers and decreasing material removal from the engine cylinder wall by way of including anti-wear agents such as ZDDP (referenced later as well). For the purposes of this project, combined analyses of lubrication regimes for specific engines and their corresponding prevalent duty cycles are conducted to determine the statistical distributions of hydrodynamic, mixed, and boundary lubrication at each of the relevant piston-assembly, bearing, and valve train components. Based on these statistical results and the empirical relationships (both synergistic and antagonistic effects) among the additives, e.g.

competitive actions of ZDDP and friction modifiers, and their effects on friction, optimum formulations will be developed for specific engine and duty cycles applications. A simple model for friction modifiers has been developed and included for the sake of demonstration. It varies friction coefficient based on friction modifier concentration, and its boundary work loss output for a reference lubricant with and without friction modifiers that result in a 15% drop in cylinder wall friction coefficient is given in Figure 1-9.

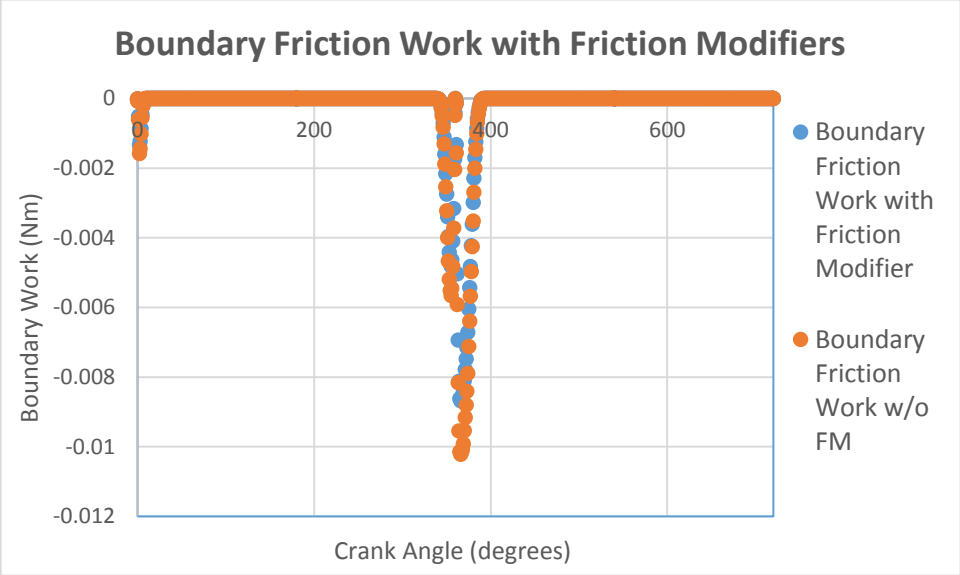


**Figure 1-9.** A decrease in boundary power loss results from the addition of friction modifiers.

The importance of both friction modifiers and anti-wear agents in enabling significant improvements in engine efficiency should not be discounted. Their mutual interactions are known to affect one another and their abilities to effectively complement the work of lubricants are dramatic. Anti-wear agents are known in some cases to introduce tribofilms between two rubbing surfaces, which in turn increases friction coefficient while providing a form of solid lubricant that promotes power machinery component longevity. Friction modifiers often consist of surface agents like oxide layers that, when interacting, yield a low friction coefficient. Investigating the optimal use of combined friction modifier and anti-wear agents within lubricant formulations is of great significance and represents the next step in the author's research.

# Chapter 2. Introduction to Lubrication Theory

## 2.1 Power Loss Contributions in Internal Combustion Engines

The primary objective of this research is improving internal combustion engine efficiency through understanding variations in frictional power losses and wear rate that result from the use of different formulations of lubricants in the power cylinder. Doing so will furthermore enable the selection of a most desirable available lubricant for a given engine such that mechanical efficiency is optimized and adequate wear mitigation is achieved. A quantitative appreciation for the fuel economy benefit inherent in this technique can be attained through understanding the relative power loss contributions of an internal combustion engine to the automobile that it propels. According to Richardson (2000), Figure 2-1 reasonably accurately categorizes the contributions of power loss in a diesel engine [2].

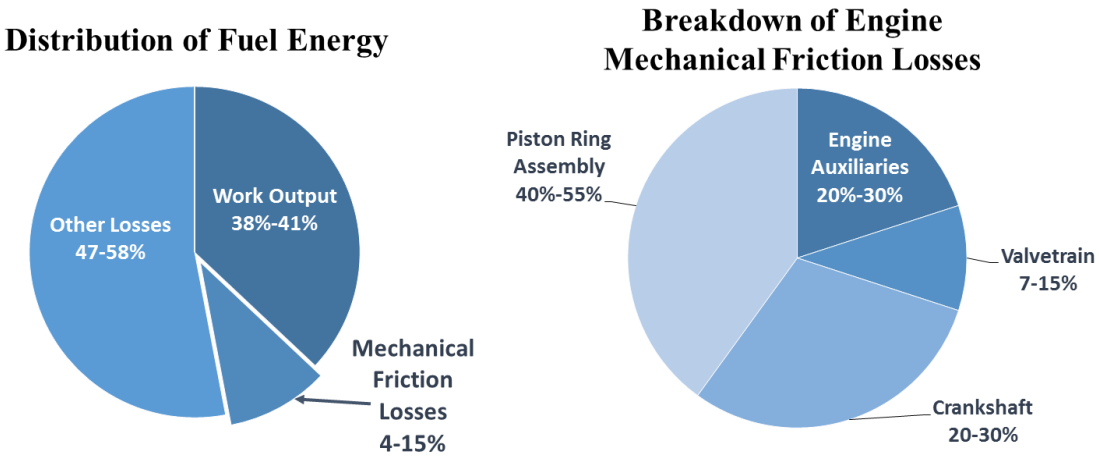


**Figure 2-1.** Distribution of diesel engine power loss by source

Allegedly, anywhere between 1.6% and 8.3% of total engine losses are attributable to power cylinder friction. Richardson further segments the piston ring assembly (power cylinder) power loss contributions as 18-33% for the rods, 28-45% for the rings, and 25-47% for the piston. Recall, however, that mechanical friction's contribution depends on engine load. These values can therefore be taken as representative of popular engine operating cycles. A single percent improvement in fuel economy is considered very significant in automotive circles, and achieving three times this fuel economy gain is the goal of the research endeavors described in this thesis.

## 2.2 Viscosity-Temperature Relationship

There exists a strong sensitivity of viscosity to temperature. In fact, along the power cylinder of a typical engine, the viscosity of the lubricating oil varies on the order of five-fold!

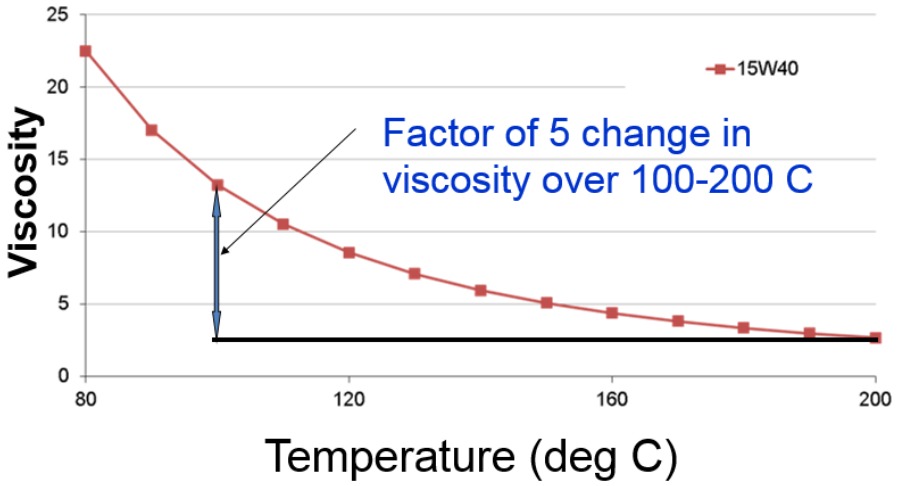


**Figure 2-2.** Viscosity of engine oil is very sensitive to temperature change

The temperature of the cylinder peaks near top-dead-center (TDC) where combustion is initiated, and is minimal near bottom-dead-center (BDC). Typical oil film temperatures near TDC are around 180 Celsius, whereas those at BDC hover around 90 Celsius, depending of course on the size, load, and speed of a particular engine. Figure 2-3 illustrates the temperature profile of the oil film along the cylinder liner of a single-cylinder, one-liter engine operating at relatively light

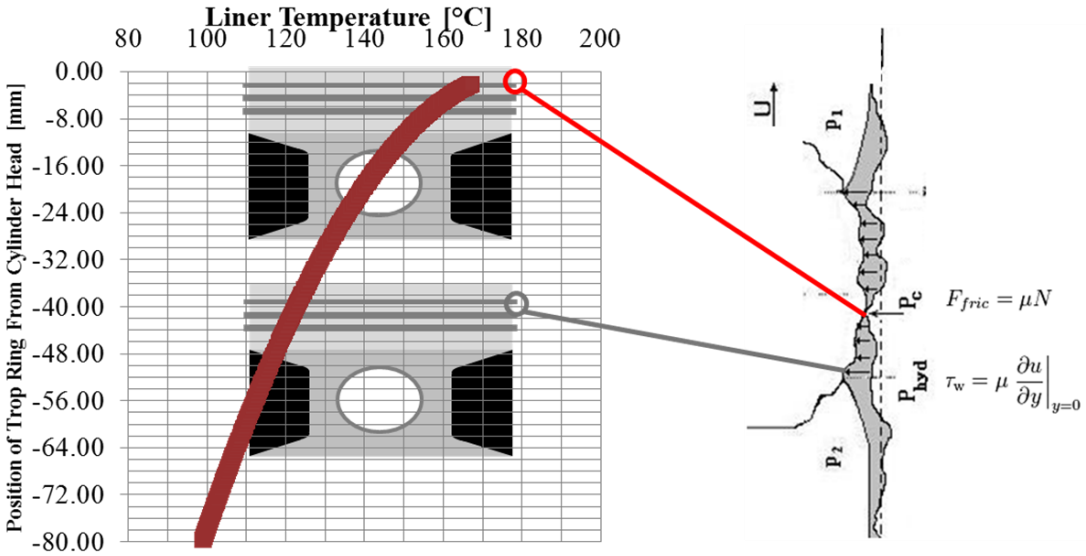


**Figure 2-3.** Engine power cylinder wall oil temperature profile

load and a steady-state speed of 2000 RPM. The lines correlating engine temperature to friction behavior will be explained shortly in a section on friction and lubrication fundamentals. Figure 2-4 demonstrates the sensitivity of viscosity to temperature for several lubricants. Each curve represents a different engine oil, so there is a wide array of SAE classifications represented. Note that at lower temperatures viscosity is higher and friction through viscous dissipation dominations. Near a transition temperature of around 150 Celsius, the mode of lubrication changes from fluid separation to solid-to-solid contact because of the thinning of the lubricant and consequent inability of that lubricant to support full separation between two mutually reciprocating solid surfaces. In the coming discussion, a reference to the Stribeck curve will elucidate the relationship between viscosity, lubricant fluid film thickness, and subsequent frictional power losses.

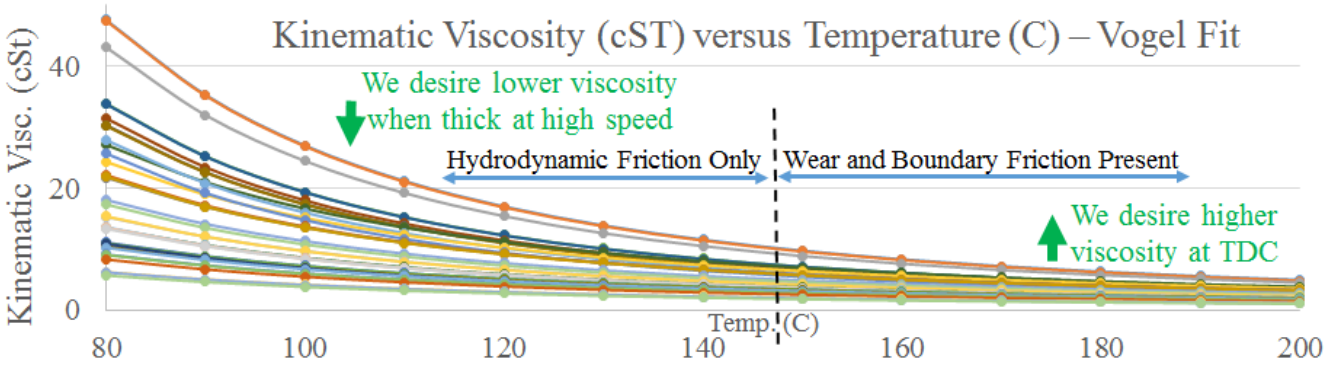


**Figure 2-4.** Viscosity-temperature curves for several candidate lubricants

Having seen the temperature distribution versus location along the power cylinder wall, we can map viscosity to those locations knowing the viscosity-temperature relationship for a given lubricant. At nether locations along the cylinder wall, temperatures are lowest and viscosity is greatest, which promotes separation of adjacent solid surfaces sliding relative to one another. As we move toward TDC, we notice a thinning of the oil and eventual transition from complete separation of the piston and wall (hydrodynamic lubrication) to mixed and contact (boundary) lubrication when film are thinnest at the region surrounding TDC.

Considering the thickest oil (arbitrarily), we notice that it has kinematic viscosity of around 45 centistokes at 80 C, and around 6 centistokes at 200 C. This drop in viscosity over what is a possible engine operating temperature range is therefore quite dramatic, and shows that at a given point in time, the lubricant near TDC and that closer to BDC have wildly different

kinematic viscosities. This is important because the viscosity of an oil directly impacts the type of friction that two sliding surfaces lubricated by that oil experience. At low temperatures when the piston moves rapidly and induces a relatively high shear rate in the oil film, high viscosity leads to great viscous power losses. At higher temperatures near the site of combustion, the protecting oil film thins and asperity contact coupled with high pressures on the piston crown yields significant boundary friction and engine wear. One can intuit that a thicker oil will provide greater protection from both solid-to-solid friction and wear. The next section discusses the basic principle of friction, and highlights the concept that friction coefficient is minimized for a given oil viscosity (and film thickness) with engine operating conditions held constant.

## 2.3 Overview of Lubricants and their Constituents

In general, a lubricant is simply any substance introduced between two surfaces in motion relative to one another that reduces the friction generated between those surfaces. Its basic function is two-fold: reduce friction and prevent wear. Additional functions include: cooling, corrosion prevention, capturing of contaminants such as harmful combustion products and solid deposits, and sealing of fluids. Lubricants can take the form of a gas, liquid, or solid, and have been used intentionally by humans for thousands of years. For example, Egyptian murals dating to around 2000 B.C. show liquids being poured in front of large statues that are dragged along the ground, presumably in order to reduce the work required by people to accomplish the dragging [3].

Lubricants in engines must possess some key operating characteristics so that they operate as specified and do not degrade too rapidly over time. A reader of this thesis who has switched from organic to synthetic oil and experienced a significant reduction in required annual oil changes is likely appreciative of that aspect of their transition. Commonly cited characteristics of engine lubricants include: low volatility, sufficient absence of foam during engine operation, stability to oxidation and degrading chemicals, absence of deleterious impact on other engine components like seals and surface coatings, low toxicity and acceptable odor, and reasonable cost to manufacturers and consumers. In order to achieve the functions required of it during its given operating cycles, an engine lubricant consists of both a base stock (base oil)

and several additives that are blended into that base stock in order to yield a final lubricant solution. Lubricants are therefore very complex substances from a rheological perspective. Accurately modeling each of their characteristics across the range of operating conditions they may experience is extraordinarily challenging. Heuristics and best practices consequently abound in the lubricants industry.

For example, oil temperature is often characterized not by that found in the power cylinder, but instead by the oil that resides in the oil sump and pumping area beneath regions of higher temperatures in which the lubricant actually acts. This is the result of an industry that seeks to mitigate the risk associated with not adequately understand the properties of fluids and lubricants as they lubricate power machinery across a variety of operating conditions.

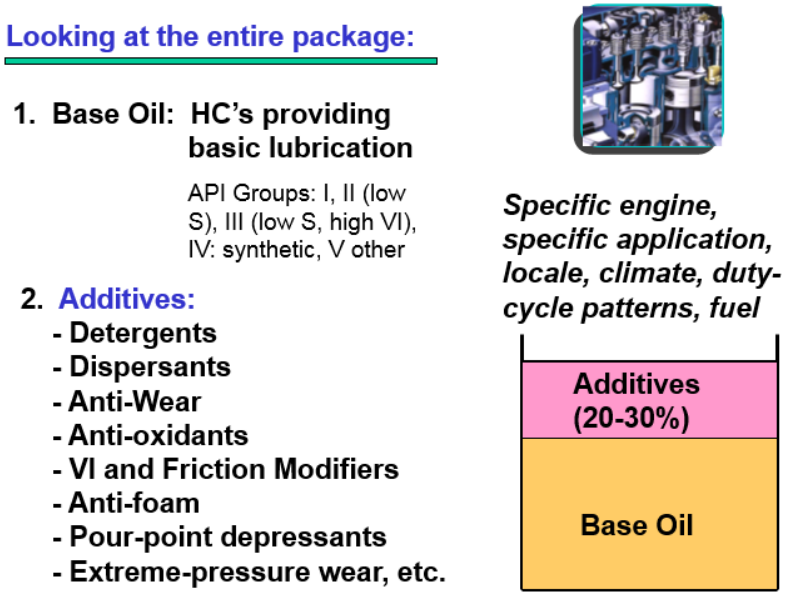


**Figure 2-5.** Lubricant solutions consist of base stocks mixed with several additives

Engine oil is far more than a simple, arbitrary hydrocarbon used in a primitive manner to somehow promote the separation of solid surfaces from one another. Detergents, typically composed of metal salts and organic acids, are used to control engine deposits and neutralize acidic products of engine combustion that have diffused into the oil film along the cylinder wall. Dispersants are designed to separate particles that may form sludge and deposits that can interfere with lubricant passageways. Such particles may include combustion products like soot from diesel engines, wear debris, water condensate, intake air, or other particulate matter. Anti-wear additives, as the name implies, protect solid layers during the wear process by decomposing

thermally into reactive byproducts that generate tribofilms or other protective layers on the surface. Such layers are continuously created through the tribochemical interactions between the additives and metal surfaces. The most common anti-wear additive is zinc dithiophosphate (ZDDP). Anti-oxidants serve to retard the process of oil oxidation and subsequent transition to sludge given the high temperatures present in the engine. Viscosity modifiers, central to this thesis, are typically high molecular-weight polymers added to an existing lubricant blend in order to reduce the sensitivity of the oil to temperature variation. Viscosity index, a measure of viscosity robustness to temperature fluctuation at low temperatures (40 to 100 Celsius), must be sufficiently high so that engines are able to start in cold weather and resist wear that comes about through undesirable thinning of a lubricant between two adjacent, sliding solid components.

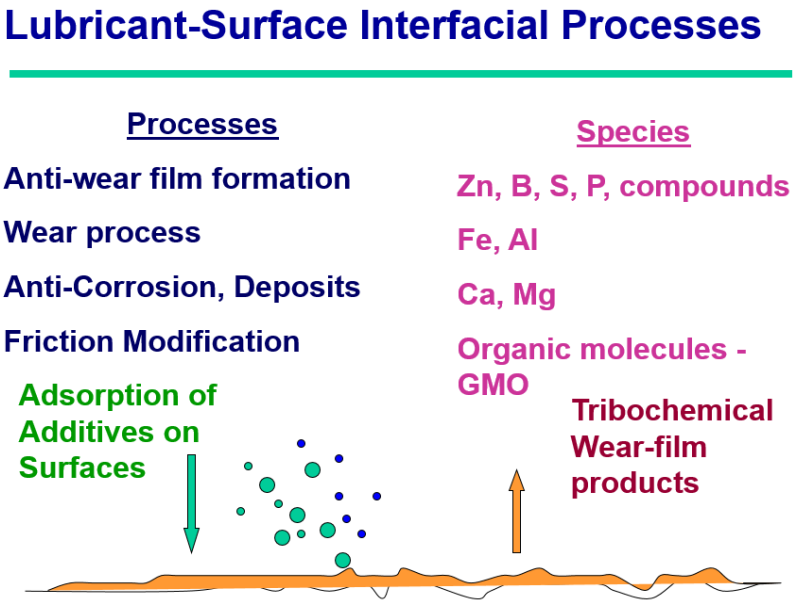


**Figure 2-6.** A depiction of additive-induced surface phenomena affecting engine wear

## 2.4 Friction: General and Along the Power Cylinder Wall

A reasonable means of explaining the components of boundary and hydrodynamic friction as they pertain to a fired internal combustion engine is via the Stribeck Curve. For a given velocity and engine load, decreasing a thick oil's viscosity reduces engine friction power losses up to a point. A thick oil film is produced by elevated piston speeds and provides complete separation between two solid surfaces. The fast rate of motion, however, results in substantial viscous shear stresses and thus hydrodynamic power losses. These are dominant along the piston

skirt and present between the piston rings and cylinder wall. Decreasing the viscosity in the hydrodynamic lubrication regime reduces the shear stress associated with surfaces sliding relative to one another, which results in reduced power losses for most operating conditions. The

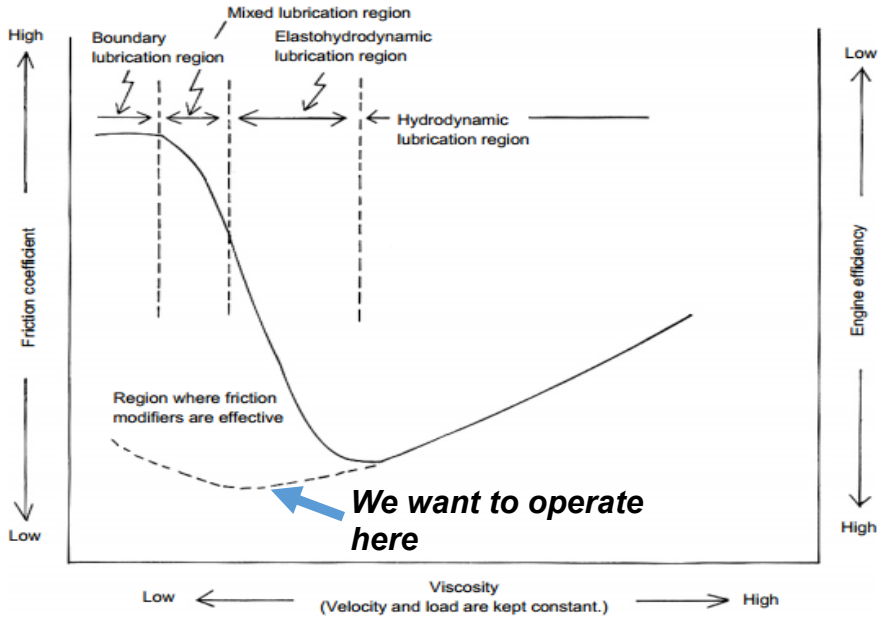


**Figure 2-7:** Stribeck curve relating friction coefficient to viscosity, load, and relative speed [4]

latter qualifier was included because at low loads and speeds, it is possible that boundary friction becomes a dominant source of frictional power loss. As the oil viscosity is decreased, the lubricating film between the sliding surfaces thins until solid-to-solid asperity contact is initiated.

The minimum friction coefficient is achieved in a mixed lubrication regime in which there is partial asperity contact and some support from a fluid hydrodynamic film. Thus, the optimal lubricant viscosity at a given location along the liner promotes a combination of boundary and hydrodynamic friction so that overall frictional power losses are minimized at the trough of the particular representative Stribeck curve. As viscosity is further decreased, solid contact grows until the boundary lubrication regime is entered.

In pure boundary lubrication, the friction coefficient is generally very high, and virtually no change in friction coefficient is obtained through viscosity variation. This is because there is no hydrodynamic pressure support provided by the fluid film to separate the two sliding surfaces, and all lubrication is done through metal-to-metal contact in which the metal surfaces rub against one another. The fundamental nature of frictional power loss in the boundary friction regime is relatively unaffected by the application of variable pressure—that is, the friction coefficient

serves as an approximately unchanging proportionality constant for determining friction force. This reflects the case in which the classic formula for solid friction is applied: $F = \mu N$, where μ here is of course not viscosity but friction coefficient, and N is the normal load applied orthogonal to the surfaces between which boundary friction transpires.

The boundary lubrication regime is also costly in terms of wear, since the Archard's model used in this research for predicting engine wear implies a linear correlation between wear rate and boundary friction. Thus, operating in the boundary lubrication regime is deleterious because of both the substantial power losses and engine wear that transpire. Engine manufacturers therefore recommend that users operate slightly to the right of the minimum point on the Stribeck curve, so that variations in velocity and load err on the side of greater hydrodynamic lubrication, where wear is reduced and increase in friction coefficient is more gradual for a given variation in the load parameter $\frac{\mu P}{u}$ , where $\mu$ is viscosity, P is pressure or load forcing the sliding surfaces together, and u is the relative velocity of the surfaces along their directions of motion—the speed of the piston the case of an engine. Note that the abscissa of the Stribeck Curve is more commonly given by the aforementioned load parameter rather than viscosity with the other elements of the parameter—load and velocity—held constant. It is interesting to note that the minimum friction coefficient can be lowered further through the introduction of polar friction modifiers, which independently reduce the friction generated between two sliding surfaces. Anti-wear agents also exist, and round out the common boundary lubricant additives, though they tend to increase the friction coefficient between solid bodies by introducing a rather rough tribofilm.

## 2.5 Developing a Cylinder Wall Oil Film Friction Model

Understanding basic tribology as per the Stribeck Curve explained above motivates the need to understand how a minimum friction coefficient value can be achieved during engine operation through appropriate lubricant selection. That is, it would be helpful to develop a numerical model that takes defining characteristics of lubricants as inputs, and generates engine power losses and wear rate as outputs such that proper tailoring of lubricants to particular engines can be reliably accomplished. This section describes the development of such a model,

which was subsequently complemented with a physical fluid film thickness measurement apparatus that relies on the principle of laser-induced fluorescence (LIF).

Intuitively, a numerical model of this type must predict the rheological and tribological behavior governing the lubricant situated along an engine cylinder wall. In the present case, the wall can be modeled as stationary with respect to a reciprocating piston that is partitioned into ring-pack and skirt regions. The piston then slides with variable velocity—zero at TDC and BDC, and peak near mid-stroke. As the piston moves, both viscous (Couette) and pressure-driven (Poiseuille) flow are present. A shearing boundary layer forms due to the lubricant viscosity resisting fluid motion over other layers of fluid. Combustion gases contribute to elevated pressure above the piston crown. High-pressure combustion gases extend along the cylinder walls and down to the ring-lubricant interface. The rings, after all, are designed in large part to seal combustion gases above the piston so that adequate pressure is retained for power delivery to the drivetrain, thereby ideally minimizing wasteful blow-by.

A version of the Reynold's equation in one dimension formed the basis of the numerical fluid model applied in this research effort to understand the behavior of lubricants situated on the cylinder wall of a fired internal combustion engine. Analysis of the equation was performed on a model of a curved ring (slider) reciprocating relative to a flat, stationary surface representing the cylinder wall. Figure 2-8 illustrates this principle.

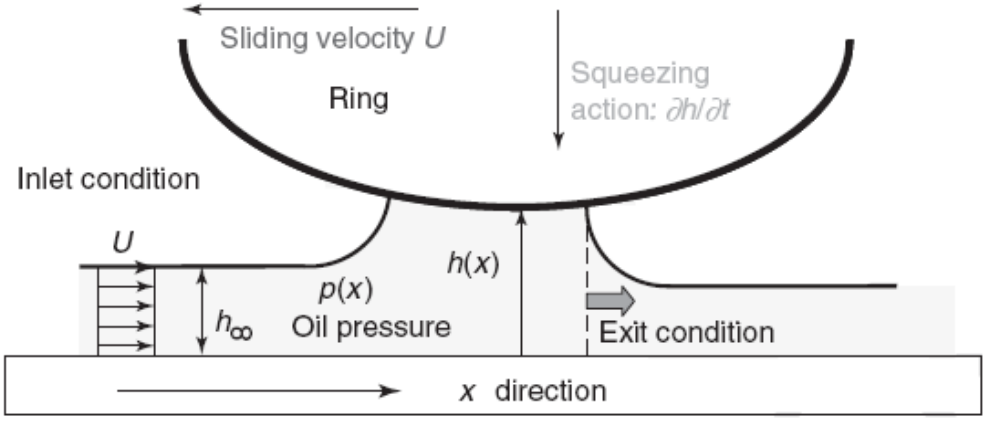


**Figure 2-8.** Ring-Liner Friction and Lubrication Model [5]

Considering a balances of forces on the roughly barrel-shaped ring: radially outward forces include pressurized combustion gases trapped within the ring groove behind the ring and the ring

tension with which the ring was manufactured. The forces on the ring outward toward the liner are then balanced by inward pressure of the lubricating oil film in the case of hydrodynamic friction, and support from solid asperities along the cylinder wall when boundary friction is present. Both forms of inward radial support (fluid pressure and asperity contact) are of course present in the mixed lubrication regime. As displayed previously in the Stribeck curve, for such a reciprocating system, the supportive pressure generated in the oil film depends strongly upon the velocity of the piston and viscosity of the oil. A simplified version of the Reynolds Equation in one dimension that omits properties such as surface roughness is given by Figure 2-9, where x is the distance from some reference location in the direction of piston motion, h(x,t) is the space- and time-depend film thickness at the trough of the ring profile (theoretical minimum oil film thickness), U is the speed of the sliding fluid, μ is the oil viscosity, and P is the hydrodynamic pressure in a cross-section of the oil film [5]. A time-independent version (with the last term removed) is known as the Sommerfeld solution, not shown here.

$$\frac{\partial}{\partial x}\left(\frac{h^3}{\mu}\frac{\partial P}{\partial x}\right) = 6U\frac{\partial h}{\partial x} + 12\frac{\partial h}{\partial t}$$

**Figure 2-9.** One-Dimensional Reynolds Equation for Thin Fluid Films

Surface characteristics such as roughness, waviness, and other texturing are included as flow factors that modify the time-independent terms of Figure 2-9 above. The four equations of Figure 2-10 represent flow factors that Dr. Tian Tian of MIT included in his development of such a

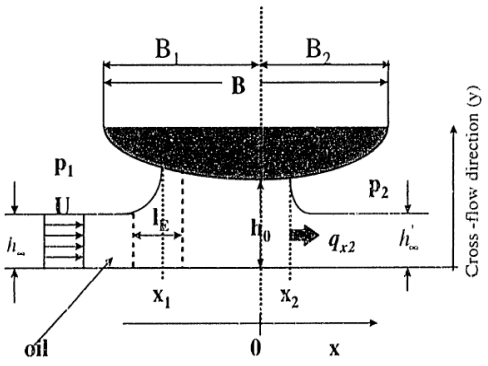


$$\bar{q}_x = -\phi_x \frac{h^3}{12\mu}\frac{dp}{dx} + \frac{U}{2}(\bar{h}_T + \sigma\phi_s)$$

$$\bar{\tau} = \frac{\mu U}{h}(\phi_f + \phi_{fs}) - \phi_{fp}\frac{h}{2}\frac{\partial p}{\partial x}$$

$$\bar{q}_x = \bar{q}_{x2} + \frac{dh_0}{dt}\int_x^{x_2}\phi_c\,dx$$

$$h'_\infty = \frac{\bar{q}_{x2} - \bar{h}_T(x_2)\frac{dx_2}{dt}}{U - \frac{dx_2}{dt}}$$

**Figure 2-10.** One-Dimensional Reynolds Equation including Surface Flow Factors

ring-pack lubrication model. The top-left equation gives the oil flow rate for rough surfaces [6]. The top-right provides an expression for shear stress (causing hydrodynamic friction) on a given

ring [6]. On the bottom-left is a form of mass conservation in the control volume bound by x and $x_2$ on the left and right, respectively. Finally, the bottom-right equation gives the oil film thickness on the liner after a ring has passed, given that the Reynolds outlet condition $\frac{dP}{dx}(x_2) = 0$ is applicable [7]. The Reynolds outlet condition is an empirical result considered accurate for steady-state lubrication at loads above 2 bars.

The minimum oil film thickness under the ring h is determined via a force balance of the outward radial load against the lubricating oil pressure, along with pressure and mass continuity boundary conditions along the wetted edges of the ring [5]. An asperity contact model that calculates boundary pressure is applied when mixed or boundary lubrication is present and is included in the radial force balance [8]. The film thickness that remains following the passage of one ring serves as the inlet thickness condition for the following ring. Piston tilt and ring angular changes through tilting in its groove effectively modify the angular orientation of the curved ring relative to a flat, stationary cylinder wall surface.

### 2.5.1 Wear Parameter Calculation

Wear refers to the progressive degradation and removal of particles from the surfaces of solid components leading to permanent loss of material from those components. In the context of the current systems, such components primarily wear from the physical contact they make as they slide with nonzero speeds relative to one another. Another form of wear results from contact with intake or combustion contaminants and solid particles that are absorbed by the oil film. There are multiple fundamental mechanisms responsible for wear—its existence can be attributed to combined or individual effects of corrosion, adhesion, and abrasion. As the piston-cylinder wall interface can effectively be modeled as a surface of contacting asperity peaks, the pressure at such small localities is enormous during periods of heavy boundary friction, and often causes asperities to weld themselves together and deform plastically above a critical shear strength. Such a strong bonding effect explains the term adhesive wear. Significant work is required to break these temporary bonds as the surfaces continue to slide past one another, and much of the energy released is effectively dissipated as a form of frictional power loss [9]. Abrasive wear occurs due to the presence of impurities in the lubricating substance. Such impurities may originate from the ambient air, metallic debris from corrosive and adhesive wear,

and combustion products. Lastly, corrosive wear results from acidic products of combustion at low temperature.

Wear is the parameter with which power loss is compared and compromises are made. In general, fuel economy is enhanced through the selection of a relatively thin (low-viscosity) lubricant that substantially reduces hydrodynamic power losses realized by the piston at high speeds near mid-stroke. The drawback of thinning the oil near mid-stroke where the lubricating film is thick due to a high load parameter per the Stribeck Curve is that the lubricant's viscosity is reduced all along the cylinder wall. Consequently, near TDC where boundary friction and wear peak, their values will be increased with a selection of a thinner lubricant. Consequently, as viscosity is reduced and enhanced fuel economy is achieved, contact friction and cylinder wear are increased accordingly. This results in the primary tradeoff faced by lubricant designers: that of fuel economy versus engine wear. Mitigating factors for wear do exist in numerous forms: friction modifiers, anti-wear surface agents, and solid lubricants in the form of tribofilms. The latter are solid lubricants between two sliding surfaces that wear in the place of the two surfaces themselves, thus leaving the actual cylinder wall relatively shielded from boundary contact and the resulting wear, but at the cost of a typically higher friction coefficient.

The wear model implemented in the concerned numerical application was premised on the notions that boundary friction drives wear, and that wear is a local phenomenon dominated by the location of greatest wear rate. It is based on the asperity contact theory of friction, in which adhesive wear dominates and fully plastic flow occurs across all contacting asperities. With these assumptions in place, friction is shown to vary linearly with respect to the applied load between the two surfaces, as required by Amontons' First Law. Adhesive wear is illustrated in Figure 2-11 in which localized adhesion is initialized on a surface and material is repeatedly transferred onto that accumulation of asperities. Asperities eventually detach and act as loose wear debris in the engine, potentially serving an anti-wear function by contributing to the development of a tribofilm

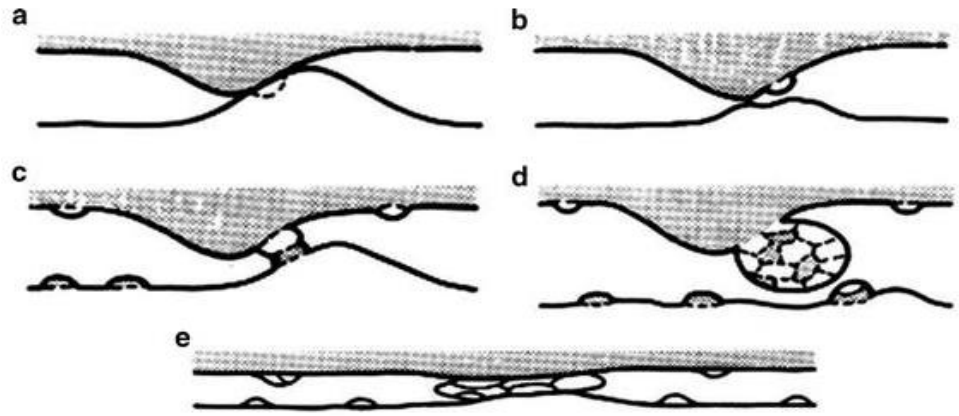


**Figure 2-11.** Illustration of adhesive wear [10]

The figure below illustrates the nature of the boundary (contact) model applied in the numerical model of the present research. As per Greenwood-Tripp, contact pressure can be approximated as zero if the lubricant film thickness value exceeds four times the effective roughness at the piston-wall interfaces. Contact films thinner than four times the characteristic roughness, which is taken as the Euclidiean norm of ring and liner roughness, are assumed to increase contact pressure exponentially. A force balance equates the ring groove pressure force and the ring tension to the forces provided by the lubricating oil and supporting asperity contact.

$$p_c = \begin{cases} 0 & h/\sigma > 4 \\ K_c(4 - \frac{h}{\sigma})^z & h/\sigma < 4 \end{cases} \qquad \sigma = \sqrt{R_{a,liner}^2 + R_{a,ring}^2} \qquad \dot{Q}_{wear} = U \int_A P_{contact}$$

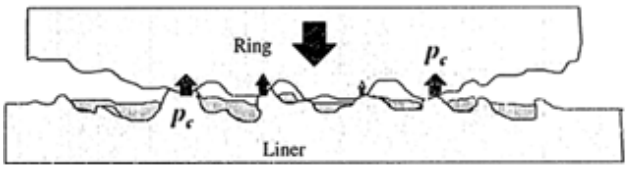


$$\int_A P_{ring} + T_{ring} = \int_A P_{hydro} + \int_A P_{contact}$$

**Figure 2-12.** Greenwood-Tripp Wear Model Fundamentals [6]

Given the distribution of contact pressure and velocity between the two surfaces, effective wear can be modeled as the greatest local wear rate. The location of max wear rate depends on the engine operating conditions, but it generally appears near TDC due to high pressure and ring-reversal. The wear rate written above in Figure 2-12 illustrates that wear at any local region can be modeled as the product of piston velocity and area integral of the contact pressure within that region—effectively representing boundary power loss. Further inspection yields the Reye's/Homes'/Archard's equation, which is a simple model for sliding wear based on asperity contact theory.

To derive the applied wear model, one may begin with an expression for the volume of wear debris:

$$V_D = K_{const} \frac{F_{load} L_{sliding}}{H_{softest}},$$

where wear volume is directly proportional to both the applied load and sliding distance, and inversely proportional to the hardness of the softest material used in sliding. Assuming plastically-deforming asperities of radius a, a wear particle may result.

$$dF = \pi a^2 H,$$

Where H is mean contact pressure during full plasticity. A worn particle can be modeled as having volume

$$dv = \frac{2}{3}\pi a^3,$$

With sliding happening over a distance x = 2a, after which asperity contacts break and take on a new load. Then:

$$\frac{dv}{dx} \propto \frac{dF}{H}$$

Taking a fraction k of all encounters that produce wear, and differentiating to yield an instantaneous rate of wear, we find that

$$v \propto \frac{kFL}{H} \Rightarrow v \propto \frac{kFL}{H} \Rightarrow \frac{dv}{dt} \propto \frac{kF\frac{dL}{dt}}{H} + \frac{k\frac{dF}{dt}L}{H} \approx \frac{kF_{Boundary}V_{piston}}{H} \qquad (1)$$

In the limit as time steps are very small, the second term vanishes, and we are left with an expression for wear rate that is directly proportional to both boundary contact force and piston velocity. This of course assumes that material hardness is unchanged throughout the testing cycle. Hence, the wear rate calculated in the present power cylinder friction-wear model was taken as the maximum of the product of boundary contact force and piston speed at every modeled point along the cylinder wall. While k and H values can be included with relative confidence, the purpose of the wear parameter is to compare the proportion of wear rates across

testing cycles for the purpose of trading off fuel economy gains with increases in wear. Thus, an absolute representation for the wear rate at the piston-cylinder wall interface was neither sought nor calculated. Unsurprisingly given the high combustion pressures and transient behavior of the piston near TDC, wear was considered greatest near TDC, where boundary friction dominates.

### 2.5.2 The Vogel Equation and Lubricant Rheological Behavior

The property of an engine lubricant that plays the most dominant role in affecting both hydrodynamic and boundary friction components along the cylinder wall is viscosity. As expressed in the Stribeck Curve above, with a given engine load and piston velocity, the viscosity determines the lubrication regimes in which several key engine components will operate. The author applied the Vogel equation as a means to interpolate and then extrapolate fluid viscosity across a temperature range typical of light-duty diesel vehicles. The research team eventually decided upon three temperatures that were considered appropriate for solving the Vogel equation, where $k, \theta_1, and\ \theta_2$ are model constants determinable by three independent data points.

$$\boldsymbol{v = k \times e^{\frac{\theta_1}{\theta_2 + T}}}$$

A script was written in MATLAB in order to solve for the three Vogel parameters, given here:

```
clc
clear

syms k theta1 theta2

nu40=6.911;
T40=100;

nu80=3.331;
T80=150;

nu100=2.117;
T100=200;

S = solve(nu40 == k*exp(theta1/(theta2+T40)), nu80 ==
k*exp(theta1/(theta2+T80)), nu100 ==
k*exp(theta1/(theta2+T100)));

S.k
S.theta1
S.theta2
```

The temperatures corresponded to low temperature (at 80 Celsius), fuel economy (at 100 Celsius), and wear reduction (150 Celsius) "zones," where a transition temperature has been included to mark the temperature at which boundary power loss begins to exceed losses due to viscous dissipation.

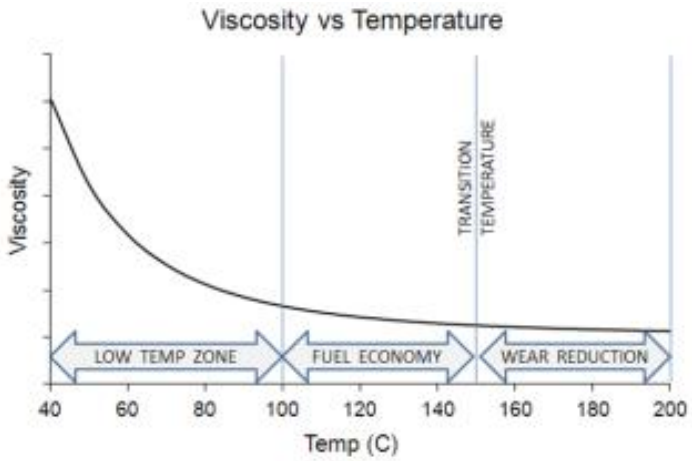


**Figure 2-13.** Cylinder wall zones defined by lubricant temperature

Another input parameter of interests—albeit little interest—to the numerical simulation suit is density of the lubricant at a given operating condition (or versus temperature). A density solver was generated in MATLAB that extrapolates 150 Celsius density from those at lower temperature.

```
clc
syms beta1 beta2

T0=20;
rho0=1000*[0.8379 0.8383 0.8381 0.8380 0.8692];

T1=50;
rho1=1000*[0.8196 0.8201 0.8198 0.8197 0.851];

T2=80;
rho2=1000*[0.8016 0.8012 0.8011 0.8012 0.8322];

for i=1:length(rho0)
S = solve(rho1(i) == rho0(i)*(1-beta1*(T1-T0)), rho2(i) ==
rho0(i)*(1- beta2*(T2-T0)));
beta_avg = ((double(S.beta1)+double(S.beta2))/2);
rho150=rho0(i)*(1-beta_avg*(150-T0));
[vpa(rho0(i)) sprintf('%0.3d', beta_avg)  sprintf('%0.3d',
rho150)] %print rho0 value to identify lubricant
End
```

### 2.5.3 Shear Thinning

The shearing properties of a given lubricant and engine geometry/operating conditions were also considered during simulation, and where incorporated via single function often referred to as the Cross equation. Shear in multi-grade oils significantly affects their viscosities when the shear rate is great enough. As polymers coil and uncoil, their strands eventually lose stiffness and/or shear off, reducing their ability to thicken as fresh viscosity index improvers would. Not considering long-term effects, high shear rates promote the uncoiling of VMs, which reduces their abilities to impede fluid flow. In the case of a reciprocating piston in the power cylinder, at high enough speeds, the shear applied to the wall oil film causes polymers in the lubricant to "stretch" and align with the flow such that viscosity boosting additives have diminished effect on thickening the oil near mid-stroke. Consequently, high shear rates cause thinning of the oil. This is desirable because power losses at high speeds are the result of viscous dissipation, and a decrease in lubricant viscosity (and thus Stribeck load parameter) results in a depressed friction coefficient, especially around mid-stroke. The equation, which served as the basis of shear thinning behavior in the present model and characterizes the viscosity of a Cross fluid, calculates instantaneous viscosity as a function of zero- and infinite-shear viscosities in addition to shear rate and two model constants.

$$\eta = \eta_{\infty} + \frac{(\eta_0 - \eta_{\infty})}{1 + C\dot{\gamma}^m}$$

**Figure 2-14.** Cross Model for Shear Thinning (the constant C is the Cross Time Constant)

Figure 2-15 represents the effect of shear rate on a sample multi-grade oil. Note the dramatic drop in viscosity with respect to shear rate. While this result is an exaggeration of the consequences of shear thinning in an internal combustion engine's power cylinder, it nevertheless highlights the sometimes dramatic thinning effect caused by shearing.

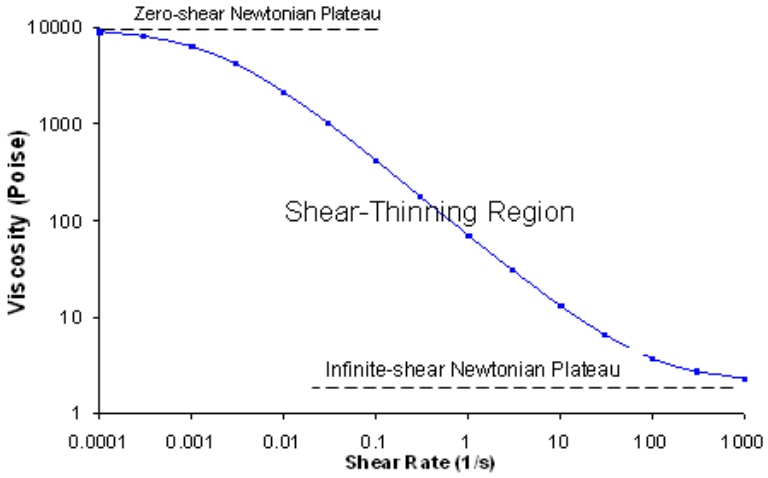


**Figure 2-15.** The dramatic effect of shear thinning on oil viscosity (theoretical)

## 2.6 Blending Equations and Relations

Of particular interest to the author was determining a reliable means of modeling the rheological properties of virtually all blend combinations of base stocks with viscosity modifiers. Significant attempts were made to develop blending equations from the considerable volume of data provided to the author by PTT. Specifically, a predictive model that takes the base stock viscosity-temperature profile, viscosity modifier solution concentration of actual solid polymer, viscosity modifier viscosity-temperature data, and the concentration of viscosity modifier solution in the base stock as input parameters, and outputs the resulting blend's viscosity-temperature data was sought. Graphically, that gives the following array of nested boxes, where the overall lubricant contains much base stock in addition to a viscosity modifier solution, which itself contains the VM solid polymer suspended in another base oil.

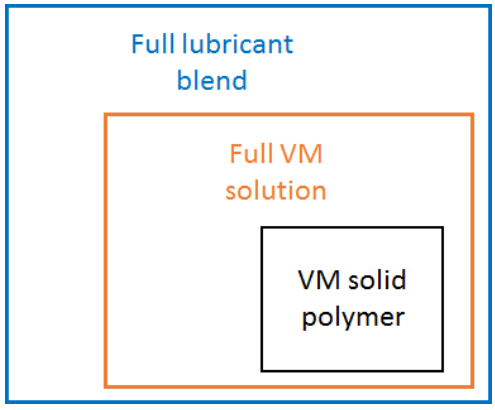


**Figure 2-16.** Viscosity Modifier in its Lubricant Hierarchy

Developing a model from correlating the provided oil data alone would ultimate prove fruitless, and the best the author could ask for is the acquisition of a "thickening efficiency." This value is the percentage increase in viscosity that a given concentration of a given VM would induce in a given base stock. The thickening efficiency was found to be relatively linear with respect to temperature given known base stock and VM data. Consequently, the only prediction that could reasonably be achieved is for oils and additives with known rheological properties over some temperature range. The concept of thickening efficiency is highlighted in Figure 2-17. Notice the consistent linearity in thickening percentage the 20 to 100 degree temperature range. This behavior was shown to extend into engine operating temperatures as well. Such behavior was assumed to hold even if not explicitly demonstrated for all base oil and VM combinations.

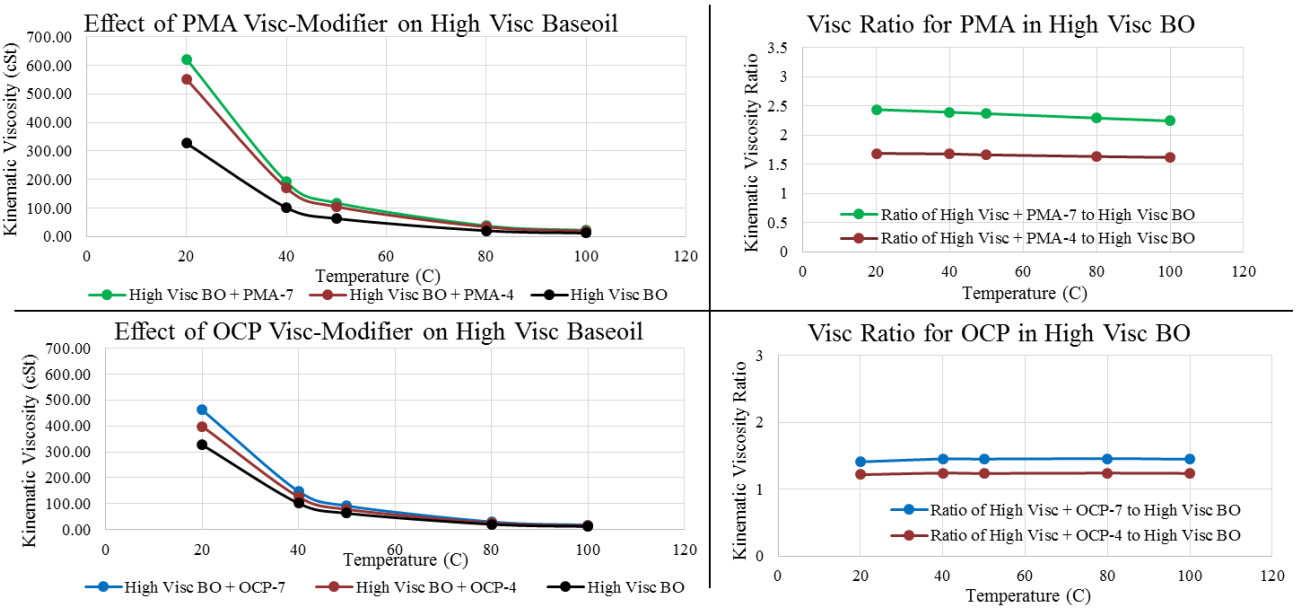


**Figure 2-17.** Thickening efficiency is relative linear with respect to temperature for a given oil

# Chapter 3. Base Oil-Viscosity Modifier Numerical Optimization

## 3.1 Input Parameters

In order to successfully simulate engine lubrication behavior, especially friction between reciprocating surfaces and wear developed due to asperity contact between solids, the relevant engine specifications and operating conditions must be appropriately included in the model. In the present case, both engine and lubricant parameters are required to yield an accurate depiction of rheological behavior at the piston-cylinder wall interface. These two sets of parameters were included separately and considered independent so that iteration across one set could be easily accomplished with the other unaffected. The set of input parameters for the engine was organized in a text file organized by engine and condition specification type (e.g. load and RPM) versus engine component geometries. This implementation was not particularly conducive to rapid iteration across operating conditions, which leaves room for improvement in the future should comparisons across many different RPM and load conditions be deemed important.

The input text file including the relevant lubricant properties conveniently amounted to just five parameters as described in the previous section on the Vogel equation. They included lubricant solution name, density, and $\theta_1, \theta_2, and\ k$ Vogel model constants. It was quite conducive to automated iteration of several lubricants, which enabled rapid simulation and testing of several candidate lubricants. A sample file containing lubricant input parameters is given in Appendix A, and input parameters for multiple lubricants to be simulated in an automated, continuous manner is given in Appendix A.

## 3.2 Output Data

The data output from the power cylinder friction-wear model consisted of key rheological parameters and results calculated every crank angle degree or fraction thereof—tenths and halves for regions near the end of the power cylinder (TDC and BDC) where strongly transient engine and lubricant behavior transpires. Higher resolution was desired near the cylinder ends more specifically because of the quickly varying piston behavior and presence of boundary friction peaks. Ring-reversal and high pressures near TDC made the friction profiles of the ring-liner interaction particularly prone to shifting and fluctuation. Data represents a full engine cycle at a fixed operating condition (load and RPM), and thus ranges in crank angle from 0 to 720 degrees,

where 0 represents TDC at the beginning of the intake stroke. Furthermore, a section of the output is summarized results data, the most important of which are arguably the power losses due to both hydrodynamic and boundary lubrication, and the overall "wear factor," which represents peak local wear rate at a point along the cylinder liner for that particular engine cycle. As expressed in the above (1), wear rate was modeled as an effective material removal rate to due adhesive wear, or the contact of asperities that deform plastically and break away from their respective surfaces. Such a rate was calculated at each time step in the simulation by taking the product of the instantaneous boundary contact (solid-to-solid) force and instantaneous piston velocity. F in (1) represents the boundary force, and the time-derivative with respect to distance along the cylinder wall is given by piston velocity, with the assumption of a stationary cylinder wall. The instantaneous wear rate was tabulated for all time steps and the maximum absolute value was taken as the representative wear rate for the engine at the operating conditions specified in the input parameters.

## 3.3 Friction-Wear Simulation Results

The result of simulation was an output of instantaneous and overall power loss from both boundary and hydrodynamic friction, in addition to a wear parameter that reflected effective wear rate by finding the maximum such value along the cylinder liner.

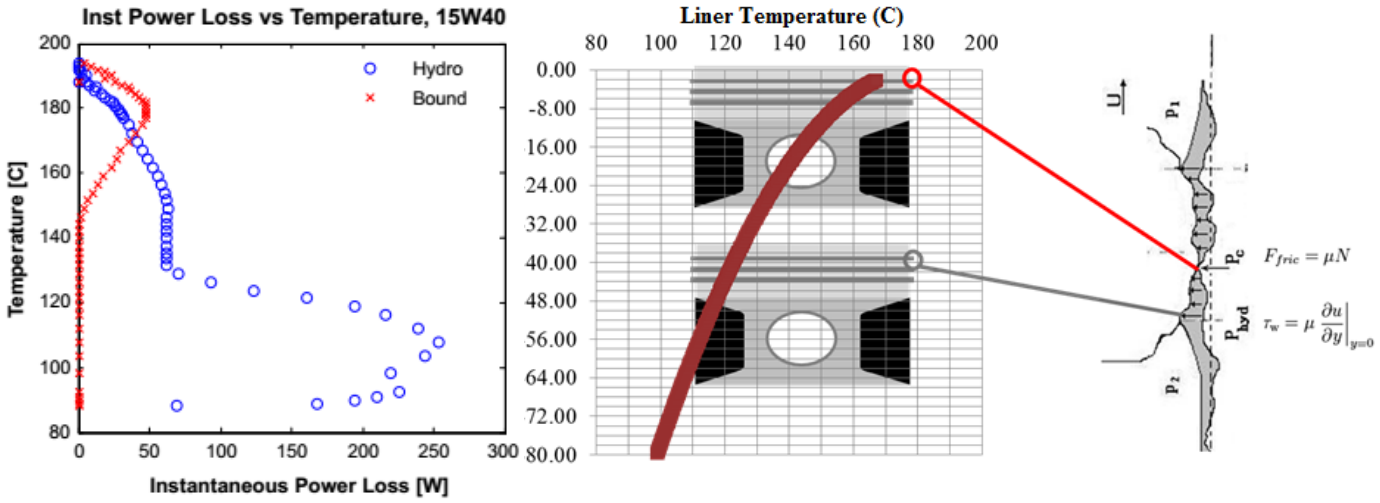


**Figure 3-1.** Independent Modeling of Hydrodynamic and Boundary Friction

The model enabled the team to select a most favorite lubricant among several options. It was shown that, neglecting secondary effects, lower viscosity lubricants provided the greatest

fuel economy, albeit at a correspondingly greater wear rate. The following table illustrates a theoretical attempt to generate an optimal lubricant with both minimal power loss and adequate wear. The viscosity-temperature profile of the optimized oil would be relatively parabolic in nature, which has not been realized in testing thus far. The finding, however, is instructive in that it provides both an idea as to potential improvements in efficiency and a guide for means to improving existing lubricants through relatively minor alterations in rheology. Note that this first-pass attempt at deriving an optimal viscosity-temperature profile returned a power loss value less than half of the original with a 40% or so increase in wear rate.

**Table 3-1.** Comparison of Theoretically Optimized Lubricants to Existing Samples

| $V_{100}$ [cSt] | $V_{140}$ [cSt] | $V_{170}$ [cSt] | Boundary Power Loss [W] | Hydro Power [W] | Total Power Loss [W] | Wear Parameter |
|---|---|---|---|---|---|---|
| Reference Baseoil + Visc. Modifier | | | 0.5 | 9.4 | 9.9 | 13.9 |
| 2.0 | 0.8 | 3.0 | 1.1 | 3.5 | 4.6 | 19.6 |
| 2.0 | 1.0 | 4.0 | 0.7 | 3.8 | 4.4 | 13.5 |

A tradeoff matrix was consequently developed, illustrating the relative sensitivities between fuel economy and wear across different lubricants.

**Table 3-2.** A demonstration of the tradeoff between wear and fuel economy

| Lubricant Species | Total Hydro. Power Loss [W] | Total Boundary Power Loss [W] | Total Power Loss [W] | Wear Parameter |
|---|---|---|---|---|
| | | | 11.14 | 13.19 |
| | | | 11.14 | 13.31 |
| | | | 11.13 | 13.25 |
| | | | 11.37 | 12.60 |
| | | | 11.13 | 13.346 |
| | | | 11.8 | 10.750 |
| S | | | 11.33 | 11.31 |
| | | | 11.42 | 12.144 |
| | | | 11.69 | 12.82 |
| Ref.SAE_5W-30 | 11.85 | 0.34 | 12.19 | 11.56 |

We notice a 7% improvement in fuel economy over the reference 5W-30 engine oil, which **corresponds to greater than 3% improvement in engine mechanical efficiency, which is our objective**!

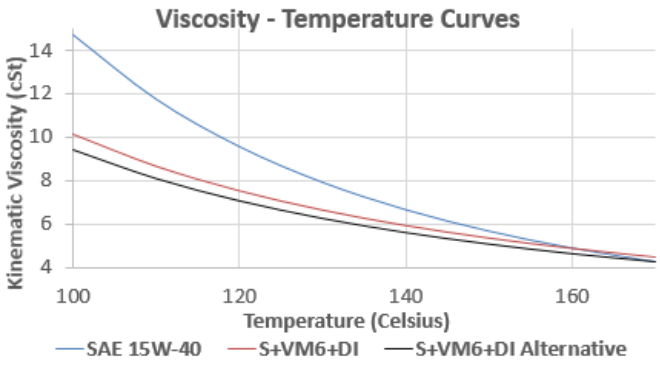


A shift from the 15W-40 reference oil to the S + VM6 + DI generated a 3.3% fuel economy gain as per NECD test cycle analysis.

| Name of Specimen | Hydro Power Loss [W] | Boundary Power Loss [W] | Total Power Loss [W] | Effective Wear Rate |
|---|---|---|---|---|
| **15W-40** | 8.72 | 0.31 | **9.03** | **8.98** |
| | | | **7.92** | **8.62** |

**Figure 3-2.** Simulation results demonstrating fuel economy improvement over the reference oil

Plotting, for example, a profile of film thickness for two different lubricants in simulation yields the expected result. The reference lubricant plus viscosity modifier mixture generates truncated film thicknesses near mid-stroke where the piston velocity is at a maximum. Further, observe that the (minimum) thicknesses at high temperatures near TDC are rather similar, generating equal wear rates for both lubricant species. Consequently, the modified lubricant is the clear preference when considering the fuel economy and wear tradeoff. The results from the skirt model—modeled using the same Reynolds Equation-based hydrodynamic and Greenwood-Tripp boundary friction algorithms—are also included. They indicate substantially less variation between the two simulations, which his expected given our focus on increasing lubricant viscosity only in the high temperature regime. Recall that the piston skirt is not exposed to high temperatures given its location several crank angle degrees below the ring-pack, and therefore is not thought to experience boundary friction near TDC. It does, however, undergo considerable boundary friction near mid-stroke given piston oscillations within the cylinder [11]. Consequently, as evinced in 3-2, skirt film thickness is relatively unaffected by a viscosity modifier designed to thicken lubricants at higher temperatures.

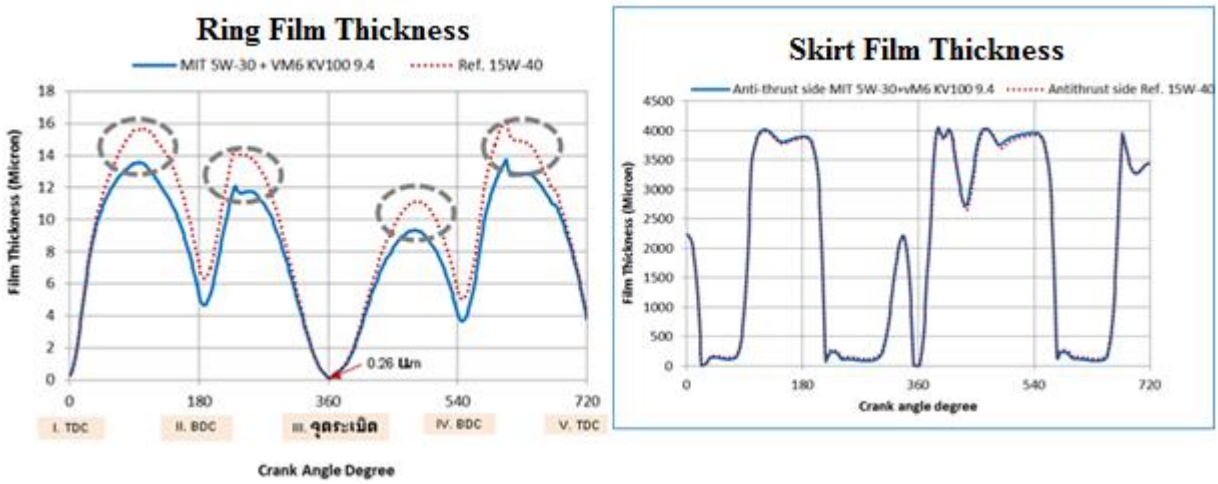


**Figure 3-3.** Numerical simulation thickness profiles for both the ring and skirt

### 3.3.1 Follow-up Work

These studies have inspired our follow-on work that includes investigating friction modifier and anti-wear additives, in hopes that fuel economy can be further enhanced with acceptable wear to the cylinder wall in a fixed-liner configuration. Vaporization and oil transport models will also be included. Such studies have already been carried out to some extent in the past in our Sloan Lab, and have been extended by a few of my lab mates, including Ms. Grace

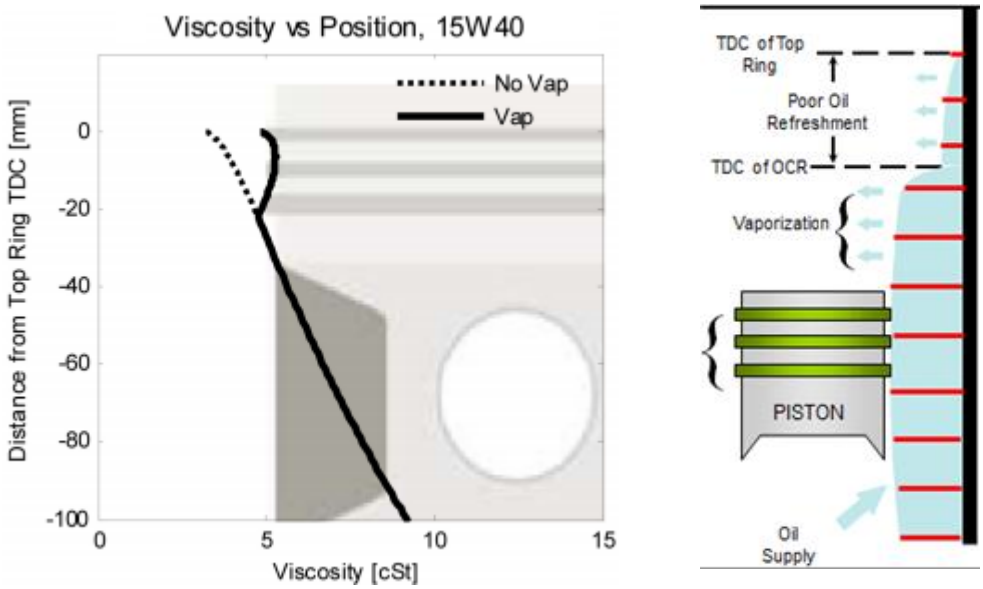


**Figure 3-4.** The lubricant film near TDC is thickened as light HCs evaporate off [12]

Gu and Dr. Michael Plumley. The (validated) qualitative intuition that underlies cylinder oil vaporization in the power cylinder indicates that the lighter hydrocarbons of a lubricant

formulation are the first to evaporate, ultimately yielding a heavier (more viscous) lubricant as time progresses. Since the conditions promoting vaporization transpire primarily in the combustion region of the cylinder near TDC, vaporization tends to thicken the portion of the oil film situated nearest the top of the engine cylinder. This is, according to our previous discussion describing the nature of the tradeoff between fuel economy and wear inherent in an optimal balance between boundary and hydrodynamic friction contributions on an engine cylinder, wear is effectively defined by the boundary friction occurring near TDC due to a combination of high pressures pressing the piston along the wall and high temperatures reducing the viscosity (and film thickness) of the lubricating film to a minimum. Thus, a thicker lubricant is desired and natural vaporization of the lighter hydrocarbons embedded in the oil film near TDC yields a higher viscosity in that region, promoting a reduction in engine wear. Since the piston velocity is low near TDC, hydrodynamic friction is relatively insignificant compared to boundary friction, especially near the location of peak wear rate. Consequently, a fuel economy improvement is also realized through reduced boundary and only marginally increased hydrodynamic friction components. Ongoing efforts exist in order to enhance the fidelity of vaporization models prior to their implementation into the friction and wear models presently discussed. The phenomenon of poor oil refreshment near TDC may contribute to a thinning of the lubricant in that region, countering the beneficial effects associated with increased viscosity of that lubricant volume.

### 3.3.2 Observed Patterns

An initial observation among the data returned by the Reynolds-based friction solver is the presence of substantially more viscous friction than boundary friction. Figure 1-4 illustrates that boundary friction is only noticeably present near TDC, and that it spikes at the point of maximum wear rate. Thickening the oil via inclusion of viscosity modifiers for a depressed sensitivity of viscosity on temperature further decreases the fraction of friction that stems from asperity contact. Furthermore, the overall power loss decreased for all oil sample input data applied to the model, implying that the thinnest commercial lubricants provide the greatest fuel economy. A key reason for their absence in most engines is the tradeoff between engine efficiency and wear. Consequently, it seems that if boundary contact in the region of peak wear illustrated in Figure 1-4 be reduced through strategic manipulation of lubrication rheological properties and/or modification of the surface properties (chemical or mechanical) of the cylinder

wall, then wear can be greatly mitigated. The first step in such an investigation is isolating precisely the location of wear for a given engine and specific operating conditions, and determining variation in both the location of peak wear rate and the distribution of wear (effectively boundary friction) in the region surrounding that peak wear point.

Of particular importance for a given engine was the temperature at which peak wear occurs. This is the case because in order to reduce wear at a given location strictly through lubricant design, the viscosity of the lubricant at that location is to increase. The viscosity can be increased locally if the temperature corresponding to a particular location is well understood so that the viscosity-temperature curve can be appropriately tweaked outside of the engine. Manual curve modification can be physically attained through the mixing of additives into a given lubricant blend. Specifically, viscosity modifiers are additives whose purpose is to reduce the sensitivity of lubricant viscosity on temperature. Their nature enables the selective thickening of a lubricant at a given viscosity modifier transition temperature. Before proceeding further along this line of reasoning, it may be instructive to briefly review the physical mechanisms underlying lubricant thickening via viscosity modifiers.

Viscosity modifiers (VMs), also referred to as viscosity index improvers, are polymer additives that can be modeled as solid coils that expand and shrink according their solubility in the surrounding lubricant, which varies significantly with temperature. As solubility increases with temperature, VMs uncoil as they are further attracted by the surrounding oil base stock. Their intrusive interactions with the lubricant molecules resists the resulting solution flow, effectively increasing viscosity.

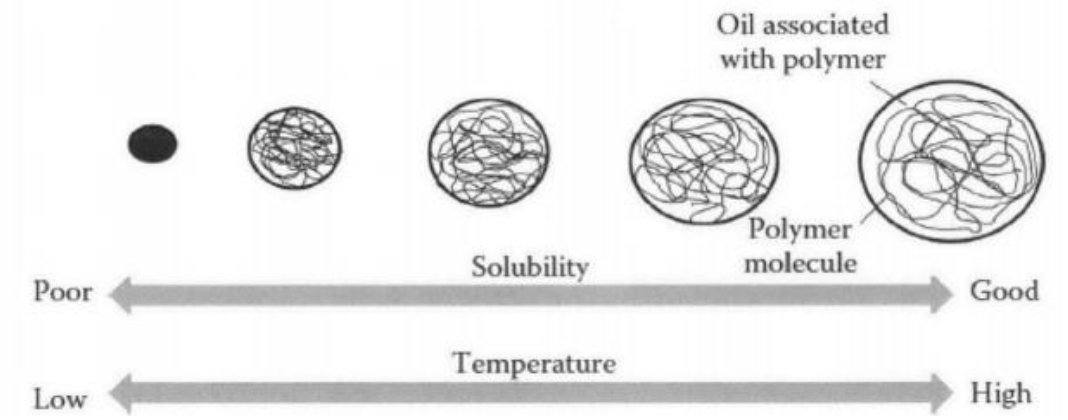


**Figure 3-5.** Viscosity modifiers uncoil as temperature increases, increasing fluid viscosity [13]

When temperature decreases, solubility decreases and the VM coils are more attracted to themselves, causing them to coil into smaller flow resistors for the surrounding baseoil. Consequently, viscosity the solution thins. VMs were originally developed in order to depress the viscosity of a lubricant at low temperatures such that cold cranking could be accomplished. Since a single oil blend is used throughout an engine—in both regions of boundary-dominated and hydrodynamic-dominated friction—it is important to both ensure reliable cold cranking and preventing excessive wear on any engine component. Successful cold cranking then necessitated a reduction of viscosity at low temperatures while sustaining sufficient viscosity at higher temperatures, especially for engine components that experience great asperity contact. VMs added to lubricants have thus historically been designed to activate, or become increasingly soluble in the surrounding lubricant, at temperatures above those typically experienced during cold cranking attempts. A thicker basestock can then be selected to mitigate pumping problems associated with high viscosity oil during low temperature cranking, and it will reliably thin to thicknesses below its nominal viscosity-temperature profile at steady-state operating conditions—typically between 100 and 200 degrees Celsius.

The approach proposed in this research, and the reason that it should be considered in implementing policy and regulatory changes related to lubricants, is that the VMs are applied on the opposite end of the relevant temperature spectrum, as they are no longer required to address low temperatures. In warm climates of Thailand and other tropical nations, cold-temperature cranking is not of real concern, since temperatures do not dip below freezing, and certainly do not reach -40 Celsius levels that are used to define the Society of Automotive Engineers specifications for multi-grade oil classifications [14]. In other words, the current research proposes and demonstrates various instances of lubricants being tailored to enhance the mechanical efficiency of internal combustion engines. This is done by addressing the thinning of the protective layer of the lubricant near TDC that induces wear and is responsible for the efficiency-wear compromise which impedes the implementation of lubricants that are optimized strictly for engine efficiency. Specifically the thermal activation of VM additives in the lubricant solution described above is set to occur at the onset of wear, such that significant incremental thickening occurs in the region of maximum wear. In other words, VMs are to remain relatively unaffected and insoluble in the oil solution until the ambient conditions reach a temperature just below that at which the onset of wear occurs near TDC. As temperature further increases into the

wear region, such tailored VMs would uncoil and cause maximum resistance to fluid shear (i.e. maximum viscosity) at the point of maximum wear rate. Since the VM was dormant at lower temperatures, the viscosity-temperature profile of the fluid would be virtually unaffected at cylinder wall locations below the boundary contact region near TDC. Thus, the thickening of the lubricant near TDC would not theoretically induce any additional hydrodynamic power losses near mid-stroke or other regions of significant viscous dissipation, resulting in both reduced enhanced efficiency and drastically reduced wear.

## 3.4 Theoretical Improvements through Viscosity Modifier Design

An initial strategy in seeking potential fuel economy gains from VM design and implementation into existing lubricants is to generate ideal cases for a lubricant's viscosity-temperature profile and assess fuel economy and wear reduction gains that have been realized and could further be generated through modifying the rheological behavior of the fluid at particular temperatures. Figure 3-5 illustrates the concept of modifying the viscosity of lubricants by reducing their viscosity's sensitivities to temperature to varying degrees at lower temperatures. Viscosity above the transition temperature (150 Celsius) is unaffected. Viscosity modifiers VM3 and VM4 are theoretical attempts to model lubricants with lower viscosity indices from a reference 15W-40 multi-grade oil such that the low temperature characteristics of the lubricant blends are amenable to high-speed mid-stroke piston behavior such that viscous losses are mitigated. That is, for a given quantity of boundary contact and wear near TDC, the hydrodynamic friction-dominated regions at lower temperatures along the cylinder liner experience less power loss through manual reduction of lubricant viscosity in those regions. While such a strategy does a considerable amount to reduce power losses in the lower temperature regions along the power cylinder, it does little to reduce effective power cylinder wear because of the phenomenon's relative isolation in the high-temperature regime near TDC.

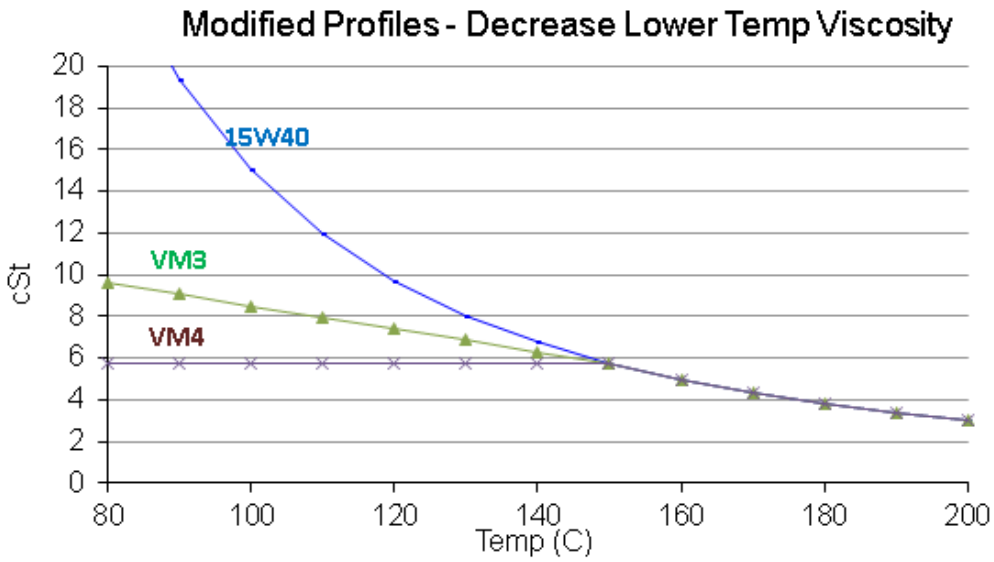


**Figure 3-6.** Decreasing viscosity at low temperatures improves fuel economy [12]

An alternative approach involves selectively modifying the rheology of a lubricant at high temperatures, as proposed throughout this thesis. Doing so affects primarily the wear characteristics of a lubricant due to increased film thickness supporting a separation between the solid power cylinder wall and piston exterior surface. Since the majority of power loss is attributable to viscous friction, the reduction of boundary friction near TDC with this method generates a mild to minor contribution to fuel economy enhancement. However, the practical impact of this latter approach has major implications on potential fuel economy gains. Since the lower bound of lubricant viscosity for a given engine is dictated by engine wear such that the power cylinder will not fail within a few hundred thousand miles of typical engine operation, increasing viscosity near TDC enables the use of generally much lower viscosity lubricant at low temperatures because the general requirement for maintaining adequate wear is only that viscosity at the region of peak wear is held relatively constant. Clearly, viscosity reduction lower along the cylinder wall, especially where piston speed is maximal, will decrease mechanical power losses, and perhaps radically so. Figure 3-6 presents the wear mitigation and friction reduction effects of VM1 through VM4 when each is independently blended with a reference 15W-40 lubricant.

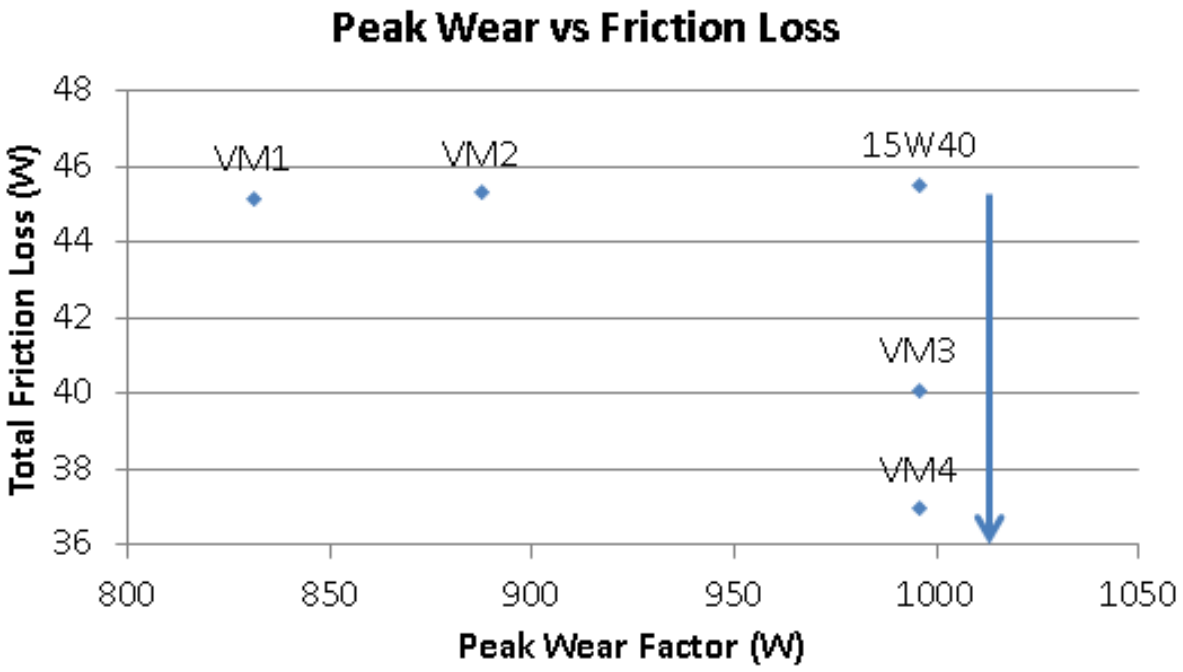


**Figure 3-7.** Fuel economy and wear mitigation comparison across VM 1-4 additives [12]

It was shown that fuel economy increased monotonically with reduced viscosity for all lubricants tested. It was therefore natural to inquire as to the film thickness at which power losses were minimized, while neglecting wear concerns. That is, what is the minimum film thickness attainable prior to fuel economy beginning to degrade with further lubricant thinning? Several "flat" lubricant viscosity-temperature curves in which viscosity was constant across temperature were then tested in the friction model, and the following data was generated. The data demonstrates that power loss did indeed reduce to minimum values between 1 and 1.5 microns. Wear varied substantially and with multiple local minima. Thus, according to the model, film thicknesses as low as a single micron are potentially optimal. This result of course begs the question: why does the industry not focus on friction modifier and more effective anti-wear agents so that the true optical fuel economy can be attained, especially with increasingly stringent government regulatory standards in the areas of fuel consumption and greenhouse gas emissions. Further, it is clear that significant formulation improvement can be made beyond an initial flat-line, constant viscosity theoretical formulation, since in the best case viscosity should be significant lower near mid-stroke than it is near TDC for the purposes of addressing the wear-fuel economy tradeoff mentioned several times in this thesis.

**Table 3-3.** Minimum power loss was observed with film thickness in the 1-1.5 micron range

| Density [kg/m$^3$] | Viscosity (cSt) | Boundary Power Loss [W] | Hydro Power [W] | Total Power Loss [W] | Wear Parameter | Max Wear Degrees ATDC |
|---|---|---|---|---|---|---|
| 600 | 1.5 | 1.97 | 3.60 | 5.57 | 34.5 | 18.2 |
| 700 | 1.3 | 1.95 | 3.63 | " | 34.2 | " |
| 800 | 1.1 | 2.02 | 3.56 | " | 35.1 | " |
| 850 | " | 1.89 | 3.69 | " | 33.5 | " |
| 900 | 1.0 | 1.97 | 3.60 | " | 34.5 | " |
| 1000 | 0.9 | " | " | " | 34.5 | " |
| 2000 | 0.5 | 1.77 | 3.84 | 5.60 | 31.8 | " |

Upon determining an optimal constant-viscosity value for purely reducing overall frictional power loss, a more realistic multi-grade oil whose grades reflect characteristic rheological behaviors at mid-stroke and near TDC was sought. This was accomplished by fitting a curve adhering to the Vogel equation and holding a constant kinematic viscosity of 42.04 cSt at 40 degrees Centigrade and about 3.5 cSt at 167 Celsius. The latter viscosity was set at the point of consistent maximum wear rate so that a greater thickness could be ensured near TDC, as the location of max wear rate on the test engine was simulated as possessing a temperature of around 167 Celsius. The 80-degree Centigrade viscosity was then adjusted until a minimum power loss viscosity was found. This maximum efficiency value for viscosity at 80 Celsius was approximately 1 cSt. Interestingly and surprisingly, the wear parameter was also at a minimum! In such a case, the best lubricant is that which simultaneously presents the least power loss and lowest wear rate. Note that yielding such obviously optimal formulations are generally the exception, not the rule. However, with concise lubricant design, power losses can be significantly reduced with an accompanying decrease in wear parameter.

Constant-viscosity and constant-wear lubricants have now been tested, and it would therefore be interesting to optimize Vogel parameters until a truly optimal results is returned. The resulting viscosity-temperature curve would be parabolic in nature, with peak values at TDC and BDC to mitigate boundary frictional power losses in those regions, and a trough in the area of highest piston speed where mixed lubrication is strongly desirable.

**Table 3-4.** Holding viscosity at 40 and 167 Celsius constant while $V_{80}$ is adjusted

| $V_{40}$ [cSt] | $V_{80}$ [cSt] | Boundary Power Loss [W] | Hydro Power [W] | Total Power Loss [W] | Wear Parameter | Max Wear Degrees ATDC | Max Wear Temperature [C] |
|---|---|---|---|---|---|---|---|
| 42.04 | 11.98 | 0.494 | 9.39 | 9.88 | 13.886 | 8.2 | 167.06 |
| " | 1 | 0.499 | 6.41 | 6.91 | 13.302 | 9.1 | 166.69 |
| " | 2 | 0.492 | 6.82 | 7.31 | " | " | " |
| " | 3 | 0.489 | 7.16 | 7.65 | " | " | " |
| " | 4 | 0.486 | 7.47 | 7.95 | " | " | " |
| " | 5 | 0.483 | 7.75 | 8.24 | 13.304 | 6.1 | 167.8 |
| " | 6 | 0.481 | 8.02 | 8.50 | 13.315 | " | " |
| " | 8 | 0.476 | 8.59 | 9.06 | 13.355 | " | " |
| " | 10 | 0.472 | 9.16 | 9.63 | 13.357 | " | " |

Similarly, holding $V_{80}$ and $V_{167}$ constant while varying viscosity at 40 Celsius resulted in the following table. Note that, again, the optimal lubricant is that which also minimizes wear, neglecting the first line of incomparable data. This is attributable to the fact that the fixed viscosity value serves as a hinge about which the others vary. In this case one would question why a rise in $V_{40}$ would result in decreased power loss. The reason is the nature of the Vogel Equation, which generates a lower mid-stroke viscosity for higher low-temperature viscosity given its need to compensate and reach those hinge viscosity-temperature values.

**Table 3-5.** Holding viscosity at 80 and 167 Celsius constant while $V_{40}$ is adjusted

| $V_{40}$ [cSt] | $V_{80}$ [cSt] | Boundary Power Loss [W] | Hydro Power [W] | Total Power Loss [W] | Wear Parameter | Max Wear Degrees ATDC | Max Wear Temperature [C] |
|---|---|---|---|---|---|---|---|
| 42.04 | 11.98 | 0.494 | 9.389 | 9.883 | 13.886 | 8.2 | 167.06 |
| 20 | 10 | 0.465 | 9.629 | 10.09 | 34.2 | 6.1 | 167.8 |
| 30 | " | 0.470 | 9.30 | 9.77 | 35.1 | " | " |
| 40 | " | 0.471 | 9.166 | 9.637 | 33.5 | " | " |
| 50 | " | 0.472 | 9.105 | 9.577 | 34.5 | " | " |
| 60 | " | 0.473 | 9.044 | 9.517 | 34.5 | " | " |
| 70 | " | 0.473 | 9.019 | 9.493 | 31.8 | " | " |

It is important to note that in each of these viscosity modifier-tailoring exercises, the viscosity at the location (via temperature correlation) of peak wear rate was held approximately constant. It was assumed though viscosities for temperatures around peak wear were fully customizable. Consequently, the author proposes that fundamental lubrication research focus in part on determining the mechanisms by which different classes of viscosity modifiers activate

(uncoil), and more importantly determine a reliable set of protocols for tailoring the temperature and rate at which that activation occurs. Doing so would enable the development of warm weather multi-grade lubricants that remain thin through the mid-stroke and only begin to uncoil and thicken near TDC where thickening is desired.

## 3.5 Simulating Engine Cycles

Of particular interest was the simulation of the engine of interest operating over the New European Drive Cycle (NEDC) cycle, which includes several operating points consisting of torque-speed pairs. This was accomplished by generating such pairs via an engines software suite ADVISOR that takes several automobile and engine specifications and operating conditions as inputs—including engine size, car weight and type, cycle speed versus time, ambient conditions, and more—and returns the torque-speed pairs that the engine generates over time in order to satisfy the drive cycle requirements input by the user. The model returns data well beyond the torque-speed points desired for friction and wear simulation via the Reynolds-based solver developed for this research. Figure 3-5 illustrates the drive cycle requirements of the NEDC. Note that there are four repeated urban cycles followed by a lengthier extra-urban component.

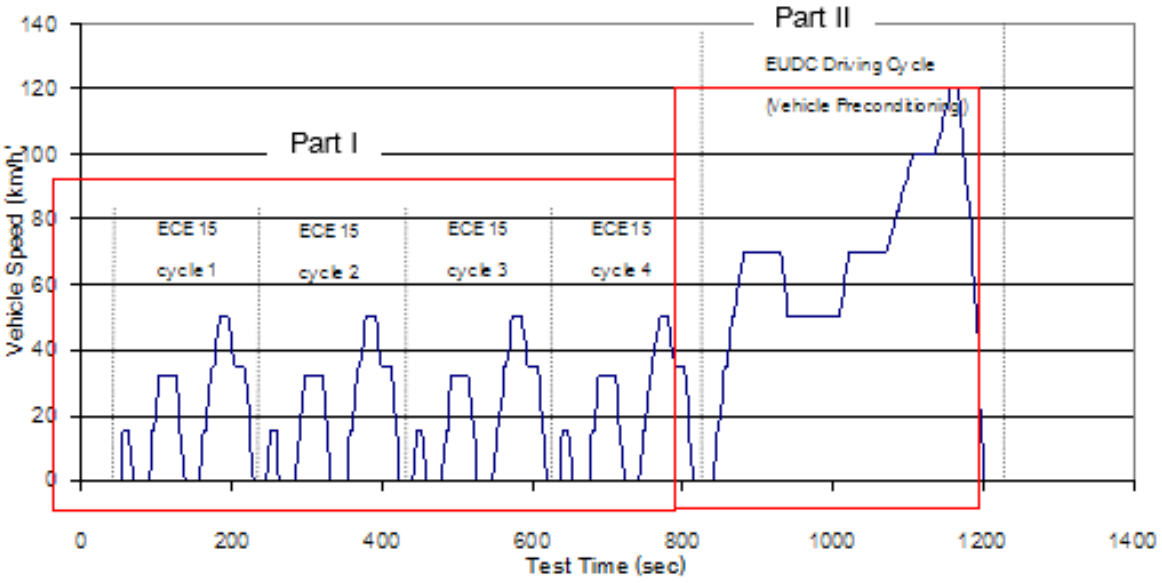


**Figure 3-8.** The NEDC Cycle is defined by vehicle speed over time

The ADVISOR program has user interface given by Figure 3-8. There is clearly quite a bit of customizability and flexibility imbedded into the program so that operating conditions can

be extracted for virtually any engine type and prescribed drive cycle. Several default and alternative values for engine type, vehicle size, and vehicle components types exist in the input pages, and representative values for a given engine of interest may serve as sufficient first-pass indicators of engine performance. Given the complexity of the input files read into ADVISOR, such an approach may be prudent for acquiring initial data over overriding all given sample files and engine data prior to running any numerical tests.

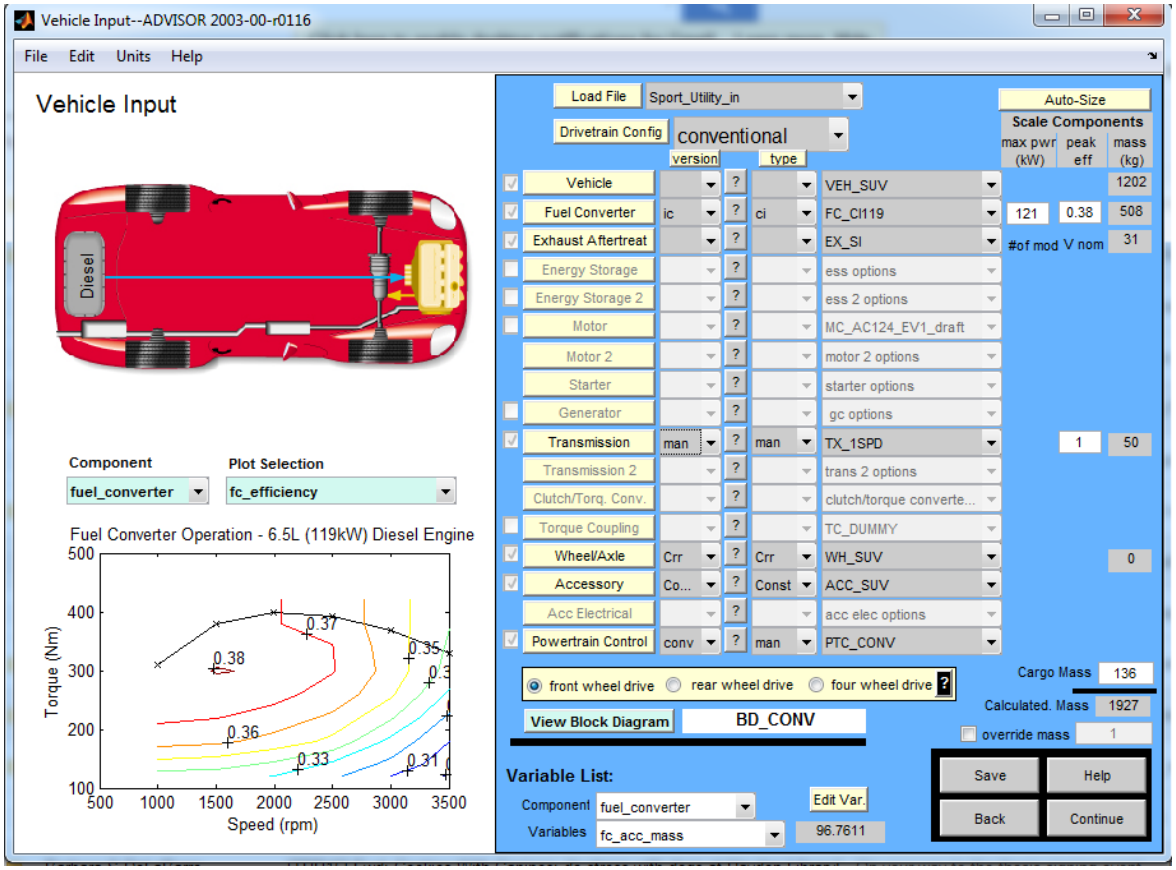


**Figure 3-9.** The ADVISOR user interface enabling the selection of several engine parameters

The speed and torque outputs by the engine as per ADVISOR's results are given in Figures 3-9 and 3-10, respectively. Note that there is a significant amount of repetition in the data, and that the transient regions cannot be ignored due to the significant torque, engine speed, and fuel consumption required during those ramp-up periods. Consideration of all operating points must thus be made when determining which are most relevant for the purposes of power loss simulation. A resolution of around one or one-half crank angle for data sampling may be acceptable in comparing torque-speed operating points.

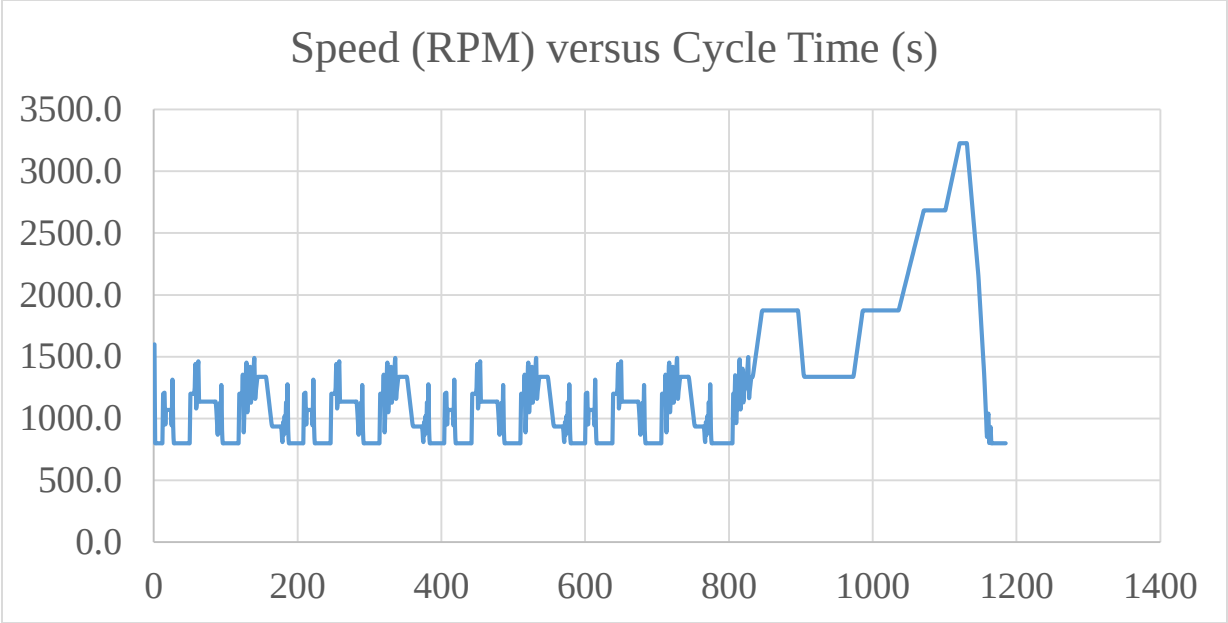


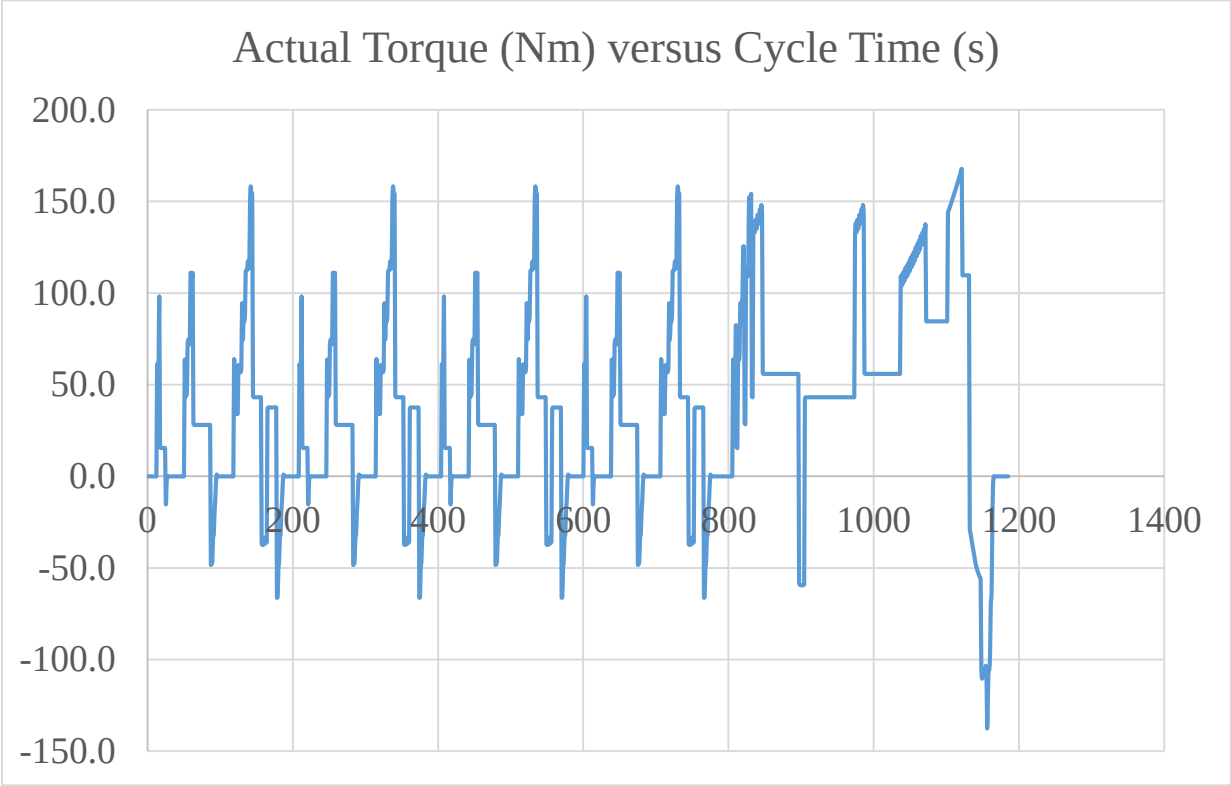


**Figure 3-10.** ADVISOR output: speed/torque required by the test engine during the NEDC cycle

Torque and speed output data were sampled at every crank angle and organized according to frequency of torque-speed pairings. It was noted that the top twenty pairs of operating points accounted for nearly 70% of those experienced by the engine over the entire operating range, and were considered an adequate representation of cycle engine behavior for initial data analysis. Given on the order of 1400 operating points, it was clear that the NEDC cycle is repetitive in nature and focuses an engine's torque and speed to a relatively narrow band of values. Note that in Figure 3-11, negative torque values correspond to downhill driving in which work is being done *to* the engine rather than by it.

| | A | B | C | D | E | F |
|---|---|---|---|---|---|---|
| 1 | Speed (RPM | Torque(Nm | | Frequency | | |
| 2 | | | | | | |
| 3 | 800.0 | 0.0 | | 309 | | |
| 4 | 1337.4 | 43.2 | | 119 | | |
| 5 | 1874.3 | 55.9 | | 100 | | |
| 6 | 1136.7 | 28.1 | | 96 | | |
| 7 | 935.7 | 37.6 | | 52 | | |
| 8 | 1069.6 | 15.5 | | 31 | | |
| 9 | 2683.5 | 84.6 | | 30 | | |
| 10 | 3226.3 | 109.7 | | 10 | | |
| 11 | 868.8 | -46.5 | | 8 | | |
| 12 | 883.9 | -31.9 | | 8 | | |
| 13 | 908.3 | 0.9 | | 8 | | |
| 14 | 1019.2 | -33.4 | | 8 | | |
| 15 | 1200.0 | 34.6 | | 8 | | |
| 16 | 1171.2 | 151.8 | | 5 | | |
| 17 | 1322.4 | 154.2 | | 5 | | |
| 18 | 809.7 | -65.9 | | 4 | | |
| 19 | 886.4 | -66.3 | | 4 | | |
| 20 | 898.8 | 60.8 | | 4 | | |
| 21 | 919.8 | -13.5 | | 4 | | |
| 22 | 926.9 | -13.7 | | 4 | | |
| 23 | 939.2 | 0.2 | | 4 | | |
| 24 | 951.2 | -14.8 | | 4 | | |
| 25 | 952.0 | 98.2 | | 4 | | |
| 26 | | | | | | |
| 27 | | | | | Sum | 829 |
| 28 | | | | | Fraction | 0.69958 |
| 29 | | | | | Nonempty Cells | 23 |

**Figure 3-11**. The ~20 operating points most frequently experienced during the NEDC cycle

Each of the 20 major operating points found in the previous sorting step was then input as a test in the main friction-wear modeled developed previously in this text. Unsurprisingly, it was found that full cycle analysis yielded an optimal lubricant that is different from that yielded through simulating a single, representative operating condition for a particular cycle. This result

can be explained largely because of the nature of the most frequent operating conditions, especially idle in this particular case, which is the condition reflecting over 20% of the cycle in terms of duration. At idle, low loads and engine speeds reduce hydrodynamic friction, and boundary lubrication thus plays a more dominant role. A lubricant that is thus more conducive to mitigating boundary friction and wear is more desirable at idle than one which is focused on depressing viscous dissipation near mid-stroke. Recalling Figure X from before, and comparing to the full-cycle results given in Figure X, we see considerable changes in ordering of VM that generates minimum power loss. For example, considering only our two primary metrics, SV3 and SV2 are now both potential candidates since one no longer has more desirable (lower) values in both categories. Thus, full-cycle testing is imperative if an optimal lubricant is to be selected from a batch of candidates.

**Table 3-6.** Single operating point friction-wear results

| | Hydrodynamic Power Loss [W] | Boundary Power Loss [W] | Total Power Loss [W] | Wear Parameter |
|---|---|---|---|---|
| RefSAE10W30 | 11.120 | 0.424 | 11.540 | 13.070 |
| SVM1 | | | 9.644 | 15.677 |
| SVM2 | | | 9.660 | 15.556 |
| SVM3 | | | 9.658 | 15.518 |
| SVM4 | | | 9.883 | 13.886 |

**Table 3-7.** Several combined and weighted operating points friction-wear results (cycle test)

| | Hydro Power Loss [W] | Boundary Power Loss [W] | Total Power Loss [W] | Wear |
|---|---|---|---|---|
| RefSAE10W30 | 4.103 | 0.02784 | 4.131 | 1.668 |
| SVM1 | | | 3.324 | 2.073 |
| SVM2 | | | 3.328 | 2.043 |
| SVM3 | | | 3.329 | 2.033 |
| SVM4 | | | 3.435 | 1.695 |

# Chapter 4. Physical Testing Through Laser-Induced Fluorescence

Recall Item 2 from our list of project tasks: Light-Duty Diesel Engine and Oil Film Thickness Measurement System Installation based on Laser Induced Fluorescence Diagnostics. Another major aspect of our work included the design, development, and implementation of a laser-induced fluorescence (LIF) system whose purpose is to accurately detect oil film thickness along the power cylinder liner with high precision during engine operation at virtually any load and speed operating condition. Of particular interest is the development of film thickness between the piston rings and the cylinder wall across all crank angles and especially near top-dead center where oil thickness is at a minimum and ring-reversal occurs. At the time of this writing, MIT has had a rich history improving its LIF systems since the late 1980s following progressive development of the technique for the aforementioned application since the early 1970s [15, 16]. This method is important because it provides a means of testing power cylinder lubricant film thickness numerical models and modifying them for enhanced accuracy and reliability. The system developed for the purposes of this research represented another series of major improvements over previous iterations of the technology, and was successfully demonstrated on a fired Isuzu 4JJ1 engine at PTT Research and Technology Institute.

The application of an LIF diagnostic device for oil film analysis is particularly useful because of it can be designed to be non-destructive and non-interfering to the system under study. Furthermore, LIF has historically provided a highly linear correlation between its output single strength and absolute oil film thickness. Given the quantum-level nature of LIF, it is viewed as very precise in determining film thickness, with tolerances on the order of a fraction of a micron, which is the most relevant unit of measurement for oil film thickness along a firing engine cylinder. Smart and Ford, the originators of the LIF method, wrote that the range of thickness that can be measured for a light lubricating oil is typically 0.1 μm to 1 mm. Initial LIF techniques conducted at MIT yielded film thicknesses of around two microns near the top of the power cylinder [16]. Measurements conducted for the current research returned readings on the order of single-digit to triple-digit microns.

The LIF method involves doping of oil with a dye that fluoresces light at a longer wavelength than that which it absorbs from an impinging source. The amount of light fluoresced from the oil-dye mixture is designed to vary linearly with the thickness of the oil film at the particular location where light intensity is being sensed because the thicker the oil film, the more

"layers" of fluorescing molecules there are being excited by the incoming light and subsequently contributing to the measured intensity of fluoresced light. In other words, measurement of the fluoresced light "gives a quantitative estimate of the amount of fluorescent material [is] in the field of view common to the light source and detector" [16]. The oil-dye mixture used in these experiments was designed to emit light with an intensity peak at around 495nm wavelength (green), whereas the impinging laser used to induce that emitted radiation shone a 50mW beam of 442nm wavelength (blue) light.

Filters are installed to minimize contributions from ambient light and prevent impinging light from being reflected into the detector. This is a legitimate means of isolating light sources in part because of the substantial offset in the wavelength corresponding to peak intensity for both the incident and reradiated light. A new photomultiplier tube (PMT) with increased light sensitivity and lower anode dark current is used to measure the intensity of the fluoresced (and filtered) light. PMTs are vacuum tubes with extremely high sensitivity to light, as they amplify the current produced by light they detect by several million times. This enables, for example, individual photons to be detected when incident light flux is low, and more generally weak light signals to be detected above background noise levels. The Hamamatsu 4220p selected for this research has a gain of $1.2\times10^7$, cathode luminous sensitivity of 100 µA per lumen, and its specifications for average anode current and anode dark current are 0.1mA and 0.2nA, respectively. (cite Hamamatsu document) For obvious reasons, it was of critical importance to prevent the detection of any ambient or unintended light by the PMT.

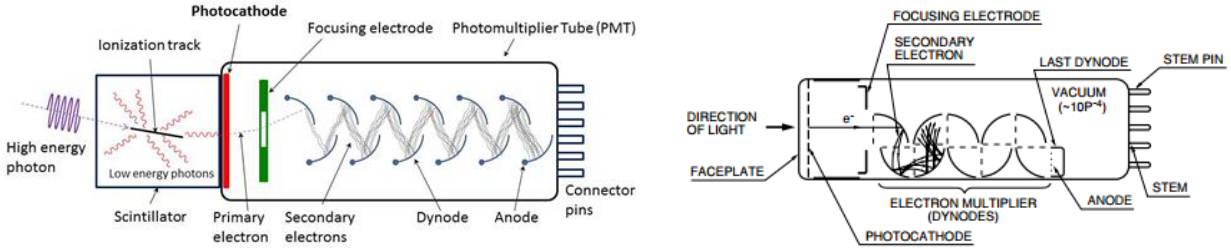


**Figure 4-1.** Two representatios of the design of a photomultiplier tube (PMT) [17]

## 4.1 Considerations for Dye Selection

Another ingredient in the development of the LIF system was the selection of an appropriate fluorescent dye for mixing with engine lubricating oil. As expressed by Peter Mulgrave, there are five primary requirements for the selection of a fluorescent dye [18]. The

first is a satisfactory ratio of fluoresced to impinging light intensity, which is a direct measure of fluorescent efficiency. This first requirement is quantitatively expressed as quantum efficiency. Another desired trait of a dye for the purposes of LIF is a significant offset in peak wavelengths between the incoming and fluoresced light signals.

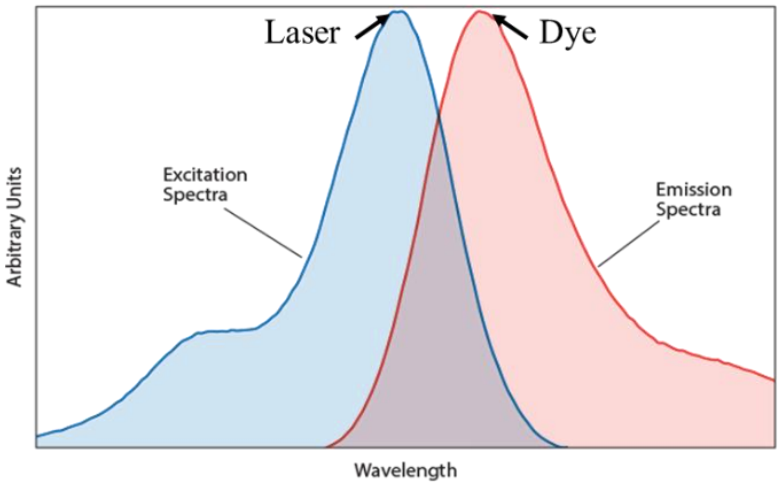


Such a characteristic reduces self-absorption of light, and more importantly provides a distinction between incoming and reradiated light. Third, the dye must have a high photochemical stability (i.e. it must not degrade quickly over time) such that it is able to provide consistent fluorescence over several operating cycles between replacements of the dye-oil mixture. A quickly degrading dye is of course not very useful for, for example, measuring oil film thickness of a firing engine over the course of an extensive driving cycle because detector readings for the same oil film thickness will exponential decrease over time. A fourth requirement mentioned by Mulgrave that the dye adequately absorb the impinging light and maintain a "population inversion required for stimulated emission" perhaps goes without saying [18]. Lastly, the dye has to be physically capable of mixing with oil into a stable, homogenous solution that is relatively unaffected by the particular operating conditions of the engine lubricated by the mixture, especially temperature and pressure. This final requirement can be quantitatively expressed through two parameters—for the purpose of the present application—as solubility and thermal stability. A dye with good solubility mixes and remains homogeneously mixed in oil, and high enough thermal stability would permit the dye to provide consistent fluorescence across the entire temperature range achievable by the engine during testing. High values for both parameters are therefore desirable. Additionally, it was important to select a dye with a high melting point in order to mitigate the possibility of fluorescence quenching due to what would effective be thermal bleaching. Historic LIF setups proved highly instructive in dye comparison across specific characteristics, and Coumarin 523 ($C_{16}H_{14}N_2O_2$) powder dye was ultimately

selected with solvent dichloromethane. The intensity of absorption spectrum of this mixture peaks at a wavelength 443nm, whereas the intensity of its emission spectrum peaks at a wavelength of around 495nm.

It has been noted that a two-dye setup in which one dye absorbs the spectrum of the other enhances signal resolution and may be considered if observing the desired signal outside of background noise proves challenging [19]. For more information regarding fluorescent dyes and dye selection, please see references [15] and [18] in the bibliography.

## 4.2 The LIF Optical Trains

### 4.2.1 Overview

Another critical aspect of the LIF system consists of several optical components that focus, collimate, transmit, and filter light appropriately and as required for the purposes of each section of the system. The LIF system has been described as being composed of two subsystem partitions: an "incoming" excitation train (or system) and an "outgoing" fluorescence system. The excitation train consists of the laser providing the impinging signal that induces excitation of the dye that is mixed with the oil, a series of focusing optics that transmits the laser signal through optical fibers and focuses that signal via probing optics onto a theoretical point along the oil film lining the engine cylinder under investigation. The dye-oil mixture at that point fluoresces light, which is transmitted through the fluorescence system to the PMT detector via an additional train of focusing optics consisting of collimators and filters. The output signal of the PMT corresponds to the intensity of the signal fluoresced from the oil along the engine liner, and consequently also the oil film thickness at that point where the detected light signal was emitted. Figure 4-1 is a relatively abstract, yet comprehensive, schematic of the entire LIF system.

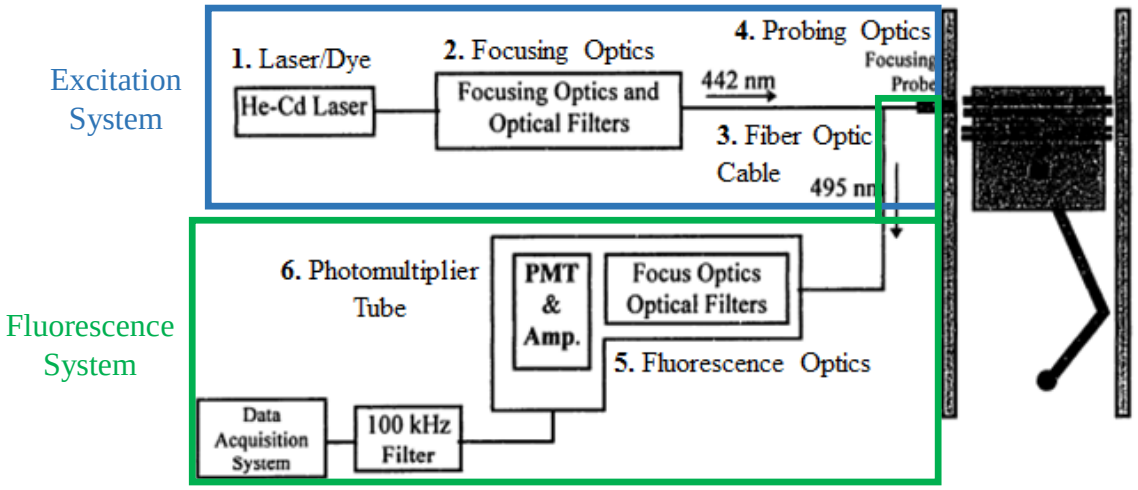


**Figure 4-2.** A schematic of the full LIF System

### 4.2.2 The Laser

A laser was foremost selected to provide a light signal corresponding to the wavelength at which the dye-oil mixture absorption spectrum peaks in its intensity. An additional requirement for the laser included adequate signal strength for sufficient molecular excitation such that oil film thicknesses between 1 and 100 microns could be distinguished from one another and correlated to PMT output signal in a linear manner. Furthermore, the laser had to produce a beam of size that was conducive to coupling into a wound bundle of optical fibers without damaging the fibers or significantly diminishing the transmitted signal. Additionally, the output signal of the laser had to be very precise and consistent such that no noticeable fluctuation in detected signal from the PMT could be traced to variation in laser output signal strength. Laser operational lifetime had to be sufficient for the purposes of testing. The size and price of the laser were also of consideration. Manufacturer reputation was therefore of great importance when deciding upon a laser for purchase. A Kimmon Koha IK4401R-D, 441.6 nm Helium-Cadmium (He-Cd) laser was selected, in part because Kimmon Koha is "the world's oldest and largest manufacturer of Helium Cadmium lasers. [20]" Its specifications include a power of 50mW, linear polarization, beam diameter of around 1mm, and beam divergence < 0.5mrad (~0.03 degrees). While this power is a few times greater than that used in similar previous LIF setups, attenuating light is not a difficult process and could be conducted if necessary.

### 4.2.3 Focusing Optics

The signal emitted by the He-Cd laser has to be transmitted through to the engine cylinder in an efficient manner such that it is not dramatically attenuated en route. This is accomplished first through a series of focusing optics that couple the laser beam into a wound bundle of optical fibers, which transmit the signal through to a separate set of optics referred to herein as "probing optics." The focusing optics train, as expressed in Figure 4-2, consists of a lens tube containing a manually adjustable aperture, a filter to eliminate the majority of ambient light that may skew detector readings and thus isolate the laser beam signal, retaining rings to fasten the filter in place, and a collimator/coupler mounted via a manually adjustable adapter that channels the laser beam into a much narrower space covered by the ends of the optical fibers through which the light signal must pass on its way to the power cylinder oil film. All elements of the focusing optics train were manufactured by Thorlabs. The component of this system that requires perhaps the most effort in the product selection process is the collimator/coupler. It must be compatible with the wavelength of laser light, and must focus that light into the fibers in such a way that the fibers are not damaged through exposure to excessive radiative power. It must furthermore adequately focus the laser light into the fibers so that it is not dramatically truncated and attenuated. The selected coupler/collimator was the Thorlabs F220SMA-A, a single unit enclosure with rated focal length 10.9mm, alignment wavelength 543nm, and numerical aperture 0.25. This was adequate for the coupling required in this project. Its Thorlabs KAD11F-SM1 Threaded Kinematic Pitch/Yaw Adapter had several degrees of freedom, permitting good alignment of the coupler to the incoming laser beam signal. One concern, however, was the taping required around the adapter to prevent the leakage of ambient light into the optical train. An already sealed adapter would be preferable to such required retrofitting of an optical device that should not require it. The mounting equipment displayed in the figure below was optional and applicable to setups involving optical tables.

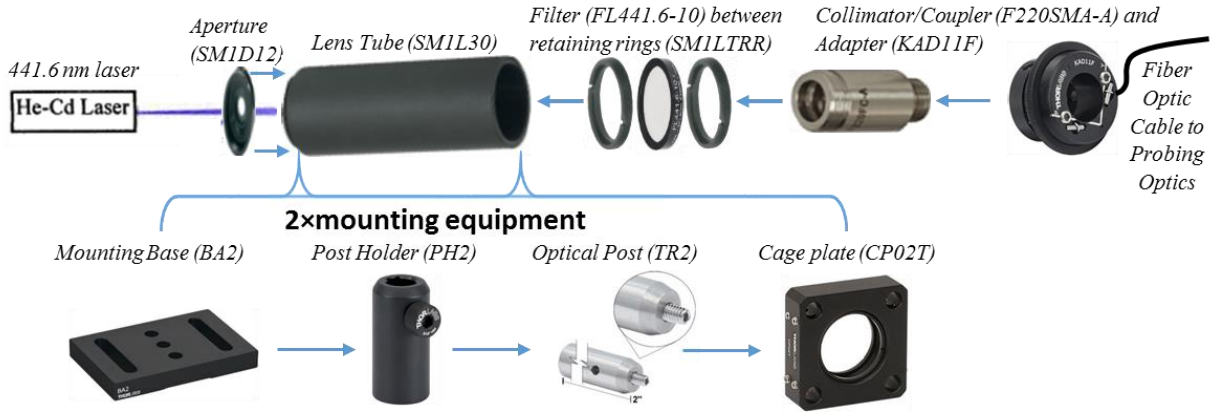


**Figure 4-3.** LIF Focusing Optics Train

### 4.2.4 Optical Fiber Cable

A single, fused silica optical fiber was connected to the coupler of the focusing optics for transmitting the laser signal to the oil film in the engine power cylinder. Six additional fibers were wound coaxially around the central incidence fiber at the site of the probing optics. This fluorescence bundle of six fiber independently carried the reradiated signal from the cylinder liner to the PMT detector in a different cable from the incident fiber. The entire fiber optics cable subsystem, therefore, was bifurcated at the focusing probe such that one end of the cable trailed back to the laser whereas the other progressed with the six-fiber bundle on to the fluorescence system and ultimately PMT detector assembly. This was depicted above in the overall LIF system schematic, Figure 4-3. The fibers were each 200 microns in diameter and rated to handle the signal power and frequencies that it would experience during experimentation. The performed this function over the course of the present research very well.

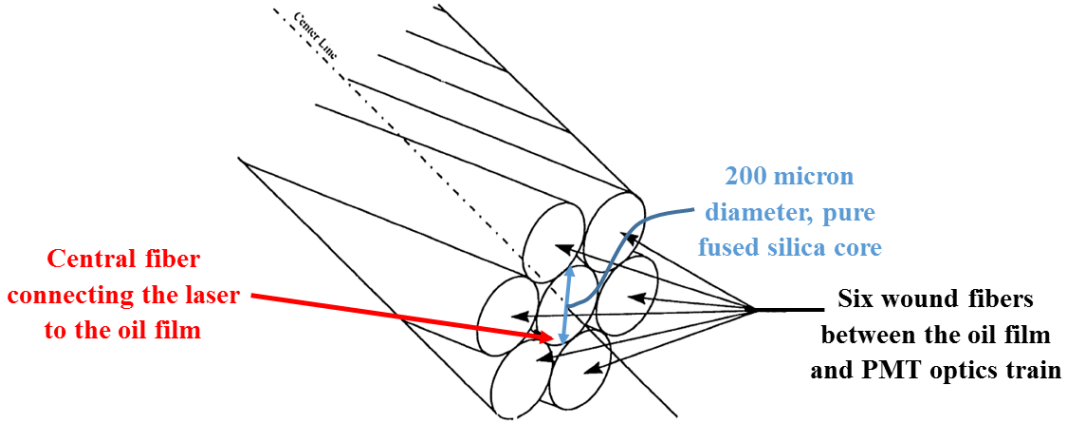


**Figure 4-4.** An illustration of the coaxial fiber bundle surrounding a single core fiber

### 4.2.5 Probing Optics

Probing optics were used in order to transmit the laser signal onto the oil-dye lubricating mixture located on the engine cylinder wall. They consisted of a series of tubes and lenses that sought to prevent engine fluids from interfering with the optical signal paths and promote as lossless a signal transmission as possible.

#### 4.2.5.1 Description

The probing optics were situated on and within the engine block. At the outside of the engine block, the laser signal was transferred from the fiber optics bundle to a coupler/collimator —the same one used above in the focusing optics—that collimated the signal through a removable optical passageway taking the form of a cylindrical probing device inserted into a channel bored through the engine block and into a power cylinder such that optical access from the exterior of the block to the cylinder oil film could be achieved. The probing optics then consisted of both a collimator/coupler unit attached to an adjustable inner tube that screwed into a fixed outer tube, which was fastened to the engine block via an NPT male swage fitting with tapered pipe threads. The exterior tube served to isolate the interior optics probe from the rest of the engine and enabled precise focusing and transmission of the light signal to and from the oil film region of interest. A collimator/coupler was screwed into the end of the interior tube such that the signal from the laser transmitted through an optical fiber would be collimated and passed through the interior tube to a transparent window placed along the edge of the engine cylinder. A plano-convex lens was screwed into the threaded interior tube such that the collimated light from the collimator/coupler unit is focused onto a small point along the oil film along the cylinder wall. In order to focus the light onto a very small region along the oil film, the lens was positioned approximately its back focal length distance away from entrance of the cylinder wall, since that is precisely where the oil film is first present. That same plano-convex lens collimates the fluoresced light back to the collimator/coupler, which then couples the reradiated signal back into the fluorescent optical fiber bundle surrounding the central fiber that transmits the light signal from the laser.

#### 4.2.5.2 Design and Manufacturing

The probing optics components were all either enclosed inside of, or attached to, a threaded tube that screws inside of a larger, stationary tube whose purpose is to shield the optical components from the engine combustion gases and coolant. It is this external cylinder that was fixed to the engine block via male NPT swage fitting. The internal cylinder can be adjusted within the outer shell in order to fine-tune the focusing of the concentric apparatus whose interior piece screws into and out of the stationary, exterior shell. O-rings and copper rings were used for sealing purposes on the outer shell and the inner tube, respectively.

The NPT male swage fitting mentioned previous served two functions: sealing of combustion gases and coolant inside the engine block and tightly fastening the removable optics tube to the engine block such that it would not vibrate, rotate, or translate during experimentation, especially while data is being acquired during fired engine operation. The one-inch fitting selected for this research given the diameter of the exterior, fixed tube is large compared to most fitting of its kind. It, however, performed as desired with sufficient clamping force, and through its dual-ferrule design successfully prevented the outer tube from moving during engine operation and sealed all combustion gases and coolant inside the engine block. Note that once the NPT fitting is tightened for the aforementioned dual purposes, it should be considered permanently locked. Such fittings are not designed to be repeatedly tightened and loosened and should thus be locked when experimentalists are confident in their existing implementation.

An additional component of the probing optics was a glass window inserted where the focusing probe passageway was bored through the cylinder liner. This was done, not surprisingly, to prevent the leakage of any combustion gases through the optical passage and to retain optical access to the oil film along the liner. The glass window had to be stable to the temperature and pressure fluctuations experienced in the engine cylinder during all anticipated operating conditions, and could not shrink or expand in a manner that would jeopardize either its structural integrity or the sealing function that it is supposed to provide. Clear fused quartz was selected for this LIF system. Of critical importance is proper dimensioning and tolerancing of the window so that it does not noticeably affect the rheological behavior of the fluid under study! Changes in film thicknesses or flow behavior due to the presence of the window and any

discontinuities that it introduces to the engine cylinder wall must be minimal and generally unobtrusive. Additional discussion regarding glass selection is provided by Mulgrave [18].

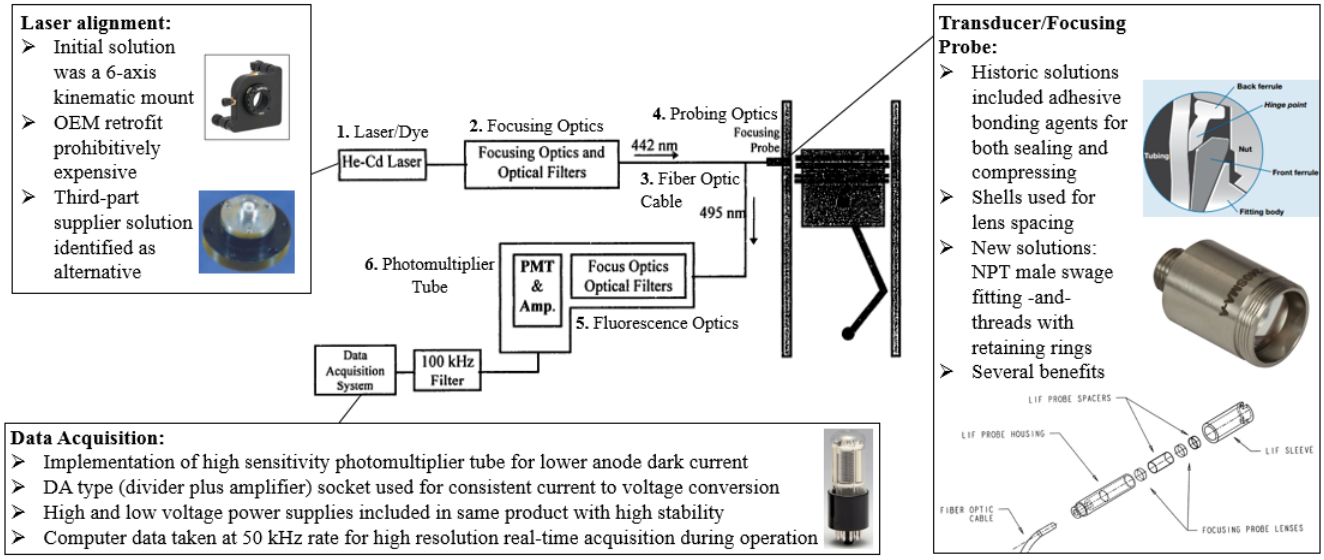


**Figure 4-5.** A holistic picture of the LIF setup applied in the present research effort

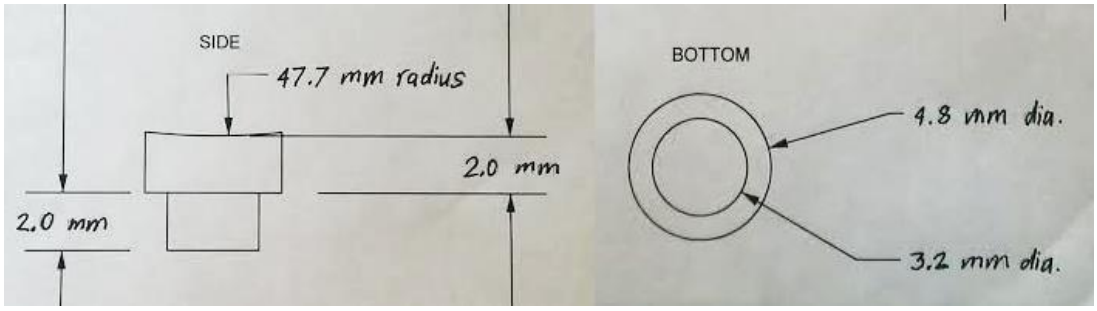


**Figure 4-6.** Quartz window dimensions

## 4.3 Calibration of the LIF System

The LIF system is designed to product a linear correlation between output signal and fluoresced light signal strength. The constant of proportionality, however, must be determined somehow. The means applied in this research is a combination of static and dynamic calibration. Static calibration was conducted in order to verify the presence of the linear correlation. Dynamic calibration was used to obtain an absolute value for proportionality constant that could be applied in a range of subsequent experiments wherein engine has reached a steady-state operating temperature, which is assumed to be relatively constant. After all, the LIF signal value

is known to be highly sensitive to lubricant temperature, expressed by Arthur Kariya, to whom much of the success of the author's LIF setup can be attributed [21].

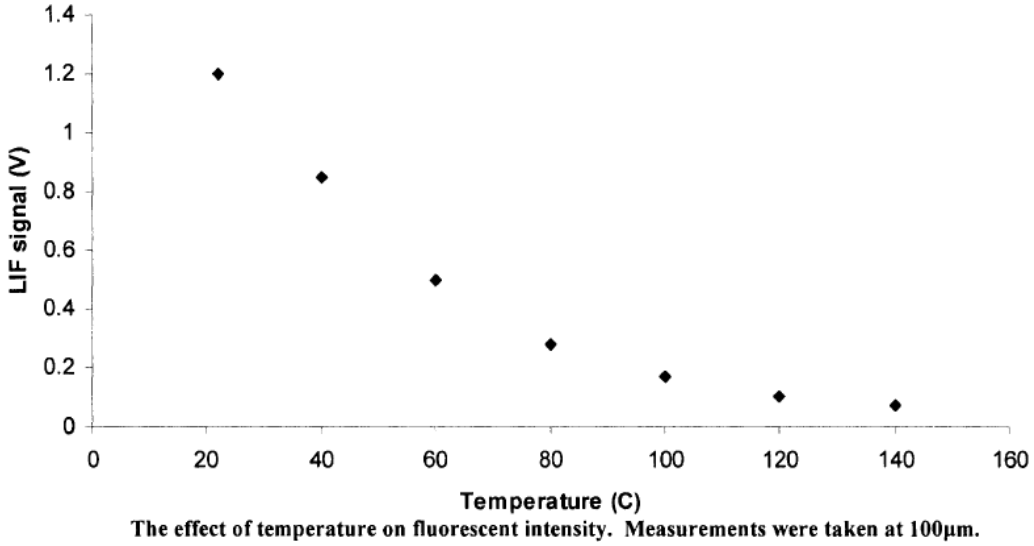


**Figure 4-7.** LIF signal strength drops sharply with increasing temperature

An important factor in determining the effectiveness of an LIF system is the concentration of fluorescent dye powder mixed with the dye selected as per previously described criteria. The nature of dye mixing involves preparing the dye in a mix of one liter of oil to 75 mL of dichloromethane to some mass of dye powder, where this mass can be simply determined by converting an optimal dye concentration to mass. A proper concentration minimizes the dye-lubricant mixture's absorbance while preserving a re-radiation signal that can be clearly observed in the LIF output trace above background noise. The selected PMT, which possessed noticeably weaker noise signals than previous versions used at MIT, was helpful. However, optimizing dye concentration was still an important step in LIF calibration. A concentration that is too great leads to full absorption of the incoming light by the top few layers in the lubricant film, preventing an experimenter from distinguishing between thin films of variable thicknesses. Since the oil films along engine cylinders vary from less than 1 micron to several tens of microns to upwards of 100 microns, a concentration that is able to retain a linear PMT signal-film thickness profile between 1 and 100 microns was desirable. Recalling studies by Kariya, a dye concentration of $\mathbf{5 \times 10^{-4}} \frac{\boldsymbol{mol}}{\boldsymbol{L}}$ was selected and verified. Figure 4-6 shows that as concentration increases, the signal-to-thickness ratio increases, but eventually plateaus past a threshold thickness because at some thickness, all of the incident light has been absorbed and no light

reaches the next layer of oil molecules, which prevents them from contributing any added fluorescent light.

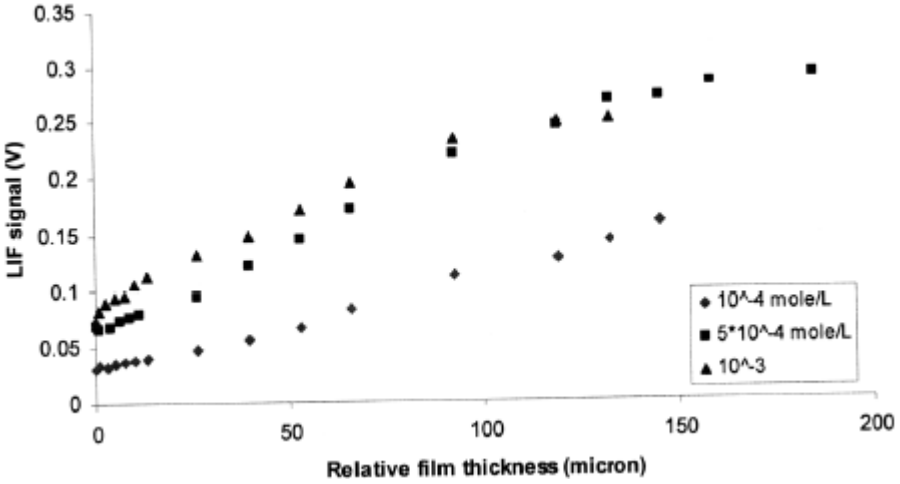


**Figure 4-8.** LIF signal ideally varies strongly and linearly with oil film thickness

A quantitative relationship describing the fluorescent signal transmitted to the PMT detector as a function of oil-dye mixture properties is given by the following equation, which is based on Lambert's Law and accounts for impinging light absorption at successive layers of dye lubricant molecules [21].

$$\boldsymbol{I_{fluor,detected} = S\frac{I_0 C_{dye}\epsilon_{dye}}{C_{dye}\epsilon_{dye}+2\sigma_{oil}}\left[1 - e^{-(C_{dye}\epsilon_{dye}+2\sigma_{oil})h}\right]\cdot\int_0^\infty f(\lambda)\varphi(\lambda)d\lambda,}$$

Where:

$I_{fluor,\ detected}$: intensity of the detected fluorescence

$I_0$: intensity of excitation laser light

S: shape factor, relating the position of the detector to the fraction of fluorescent photons detected

$C_{dye}$: concentration of the dye in the lubricant mixture

$\boldsymbol{\varepsilon_{dye}}$: dye absorptivity coefficient

$\boldsymbol{\sigma_{oil}}$: oil absorptivity

$\boldsymbol{h}$: oil film thickness

$\boldsymbol{\varphi(\lambda)}$: quantum yield efficiency at wavelength $\boldsymbol{\lambda}$

$\boldsymbol{f(\lambda)}$: filter transmittance at wavelength $\boldsymbol{\lambda}$

Note that the bounds of integration were general to encapsulate all possible wavelengths, and could have further specified both the minimum and maximum wavelengths permitted through the

long-pass filter through which the fluoresced signal passes before being transmitted through to the PMT detector.

Static calibration of the LIF system was conducted at a constant substrate surface temperature elevated above room temperature via hot plate, and consisted of recording LIF signals obtained from impinging a laser of constant power onto the surface of a series of metal substrates with grooves chemically etched into their surfaces. The focusing probe was screwed into the side of an aluminum block, whose interior's only other access to ambient light was through a slit on its top side into which the metal substrates slid for testing. In order to obtain a signal output versus oil film thickness relationship with acceptable fidelity, the oil film thickness along the substrates had to be controlled and known with reasonable accuracy on the order of 10% or less error. The process chemical etching itself was relatively straight-forward. A rectangular patch of space on each substrate measuring around 4mm × 2mm was marked, cleaned, and etched via a mixture of sodium hydroxide diluted in water. Note that NaOH reacts exothermically with water and should be mixed slowly and in a controlled environment. The corrosive blend was dropped onto the aluminum substrate surfaces from a pipette. The number of drops was noted for each substrate so that drop number could be correlated to groove depth. Groove depth was then measured via profilometer, whose principle is illustrated in Figure 4-7 below. No quick and inexpensive method was found for measuring the actual oil film thickness on an aluminum substrate. Ellipsometry was the final idea considered, and while promising, was not implemented. An optical method for accurately determining the oil thickness on the substrate would of course be highly useful for static calibration purposes.

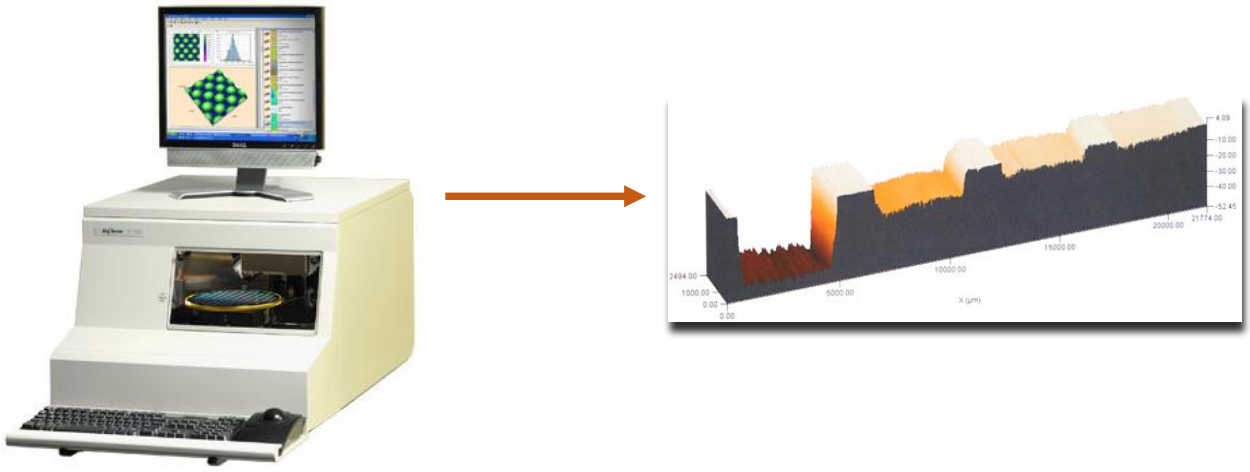

**Figure 4-9:** Tencor P-16 Surface Profilometer with resolution of 20 Angstroms to 1 millimeter

A lubricant mixed with fluorescent dye in the proper concentration was then introduced onto the substrate and excessive oil was wiped off so that the oil film surface was approximately even with that of the substrate surface surrounding the etched groove. Note that this method was not exact and greater precision would be a great idea for future improvement. The substrate was inserted into the rectangular aluminum enclosure and the laser signal impinging onto the substrate excited fluoresced light, which was filtered through to the PMT to yield an output signal strength. The signal strength for each substrate (and corresponding groove depth / film thickness) was recorded for what would ultimately constitute the static calibration.

| Profile Depths, Microns | PMT, Volts |
|---|---|
| 2 | 1.1 |
| 8 | 1.4 |
| 17 | 1.9 |
| 42 | 3 |

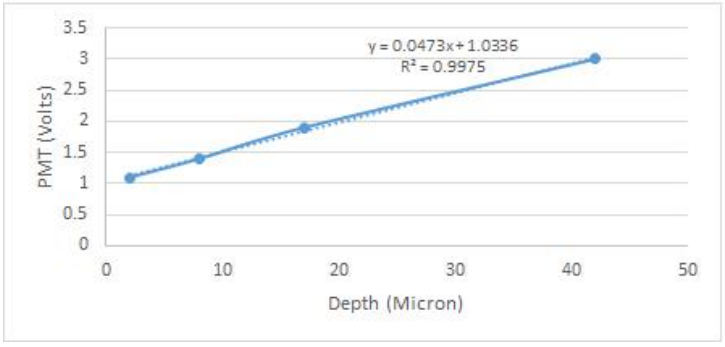


**Figure 4-10:** Static calibration results between film thickness and output signal, 75 Celsius

Dynamic calibration then followed, and involved determining the slope of the signal-thickness line by way of comparing signal strengths with that corresponding to a known film thickness. This can be accomplished by etching a groove of known depth directly into the piston cylinder, or detecting components of the piston of known geometric lengths, such as fine waves along its upper surface. An absolute proportionality constant can be determined from static calibration in which substrates are held at a velocity equal to that at which the optical access location along the cylinder wall is positioned. Figure 4-10 juxtaposes the numerical result for film thicknesses between the top ring and cylinder wall with output signal measured near TDC. What can be ascertained from these two plots is the notion that the ratio of peak to trough viscosities is constantly on the order of three-to-one for both methods. Furthermore, both models seem to present agreeing results for geometric features of the piston, which are all on the order of a millimeter. Since crank angle can be converted directly into physical distance, signal jump base

widths corresponding to a few millimeters were taken as reassuring signs of LIF precision and reliability. Furthermore, the relatively high resolution of the returned data set enabled investigation into the wetting (partial or full flooding) phenomena between the ring-pack and cylinder wall near TDC. It seemed the case that given a substantial convergence of the signal peak onto one point from both ends of the ring boundaries, there is considerable starvation, promoting the idea that a fully-flooded model does not accurately portray the physical reality of the system.

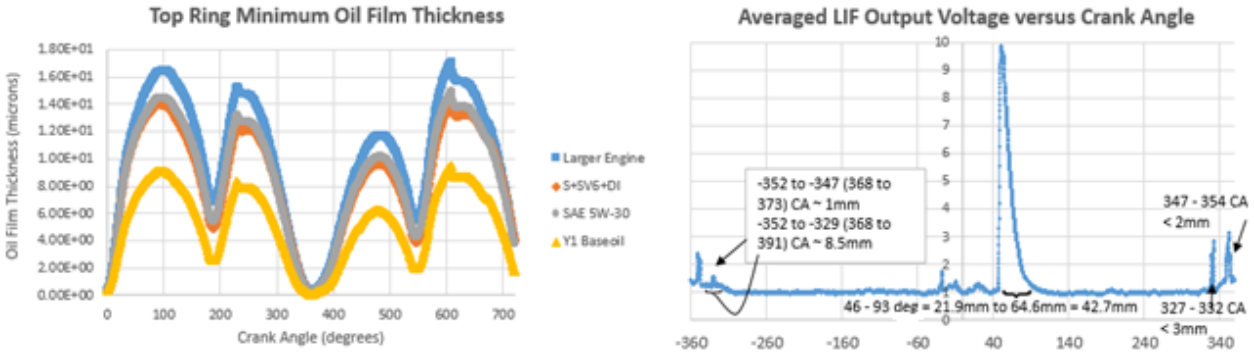


**Figure 4-11.** Film thickness results from numerical simulation (left) and LIF data (right)

The sharp spike in signal at around 2+ cm per the perspective of the optimal access point may be attributable ring reversal, during which the ring-pack contacts the cylinder wall perhaps traps a glob of lubricant that is dragged along the wall. This is possible because the spike occurs immediately following combustion, when perhaps the piston has been forced against the cylinder wall, and an amassing of lubricant results.

## 4.4 Engine Operation and Data Acquisition

The complete LIF system was setup and refined at PTT's RTI. Two optical channels were bored into an Isuzu 4JJ1 engine for fired-engine oil film diagnostic purposes. One was centered at approximately mid-stroke of a cylinder, and another was positioned near TDC so that minimum oil film thickness, engine wear, and phenomena associated with ring-reversal could be investigated. It is this latter probe near TDC that was of primary interest to the experimenters, since most of the peculiarities—and thus learning opportunities—associated with the behavior of the engine cylinder wall oil film occurred in the region near TDC. The mid-stroke probe was instructive for assessing the fidelity of the relatively high-speed, hydrodynamic predictions from numerical simulation. Both probes were further useful in detecting transient behavior of the oil

film, especially cycle-to-cycle variation and time required to achieve an effective equilibrium rheological behavior.

As far as data acquisition is concerned, of particular importance were the linearity of the mapping between output voltage and film thickness, and the resolution with which details of the

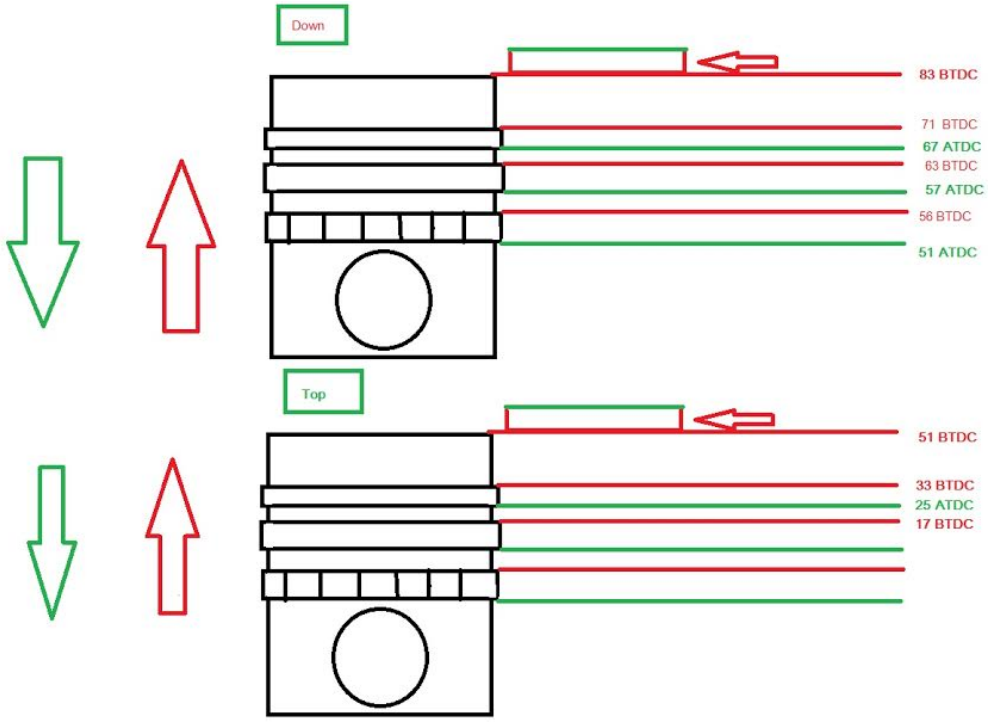


**Figure 4-12.** Piston feature crank angle measurements for both up stroke and down stroke

piston, including the skirt and ring-pack, could be detected via the LIF method. For example, with ring thicknesses on the order of 2mm and the degree of starvation—or proportion of a ring that is not attached to the oil film—playing an important role in understanding the fluid behavior in the power cylinder, it was important to obtain at least around ten data points per ring movement past the focusing point during each cycle of fired-engine operation so that a reasonable profile of lubricant behavior "under" each ring could be ascertained and modeled. Luckily, the LIF system latency was not noticeable and readings even on the very first system test proved more than adequately resolute for the purpose just described. The following Figure 4-11 denotes the crank angle position of each major piston component during the 4JJ1 engine operating cycle.

**Figure 4-13.** LIF Focusing Probe Installation into Engine Block via NPT Fitting

Once the LIF system was properly installed in the engine and tested for reliability and repeatability, data was collected at a rate of several thousand hertz, especially so that the film thickness profile along each ring could be determined with precision. Figure 4-12 below gives a simple output voltage reading from the PMT assembly for one engine revolution. The four peaks in the plot correspond to the two passages of the top two rings on the piston past the center of the optical passage in the engine block. Ring widths and other expressed piston dimensions had to be correlated to crank angles so that an effective starvation percentage—or fraction of the ring not wetted by the oil film—could be ascertained. Once this was accomplished, an approximate wetting diagram could be generated for each ring. The wetting of each ring places an important role in viscous dissipation stemming from the present of the lubricant between a ring and the cylinder wall. A sharp peak in LIF signal was noticed at around 60 degrees past TDC, or where the top piston land passed the focused light signal. It is believed that this peak stems from a scraping effect of the top of the piston in which a sizeable glob of lubricant is dragged along with the piston. This peak was not present during all cycles.

With such high resolution and precision in the output data, which was verified through manual mapping of piston features with the profile of the acquired data, great insight could be shed on the actual rheological behavior of the lubricant along the engine cylinder wall. This, in turn, enabled us to compare simulation results with data from the real-word engine operation.

## 4.5 LIF Data Acquisition and Results

Physical film thickness measurement through LIF is done in large part in order to validate the Reynolds equation-based friction model developed throughout this research effort. As explained in the theory section of this thesis, film thickness and hence viscosity play the governing roles in determining which form of friction dominates along the cylinder liner. It is important to note the general perspectives of both forms of modeling. The numerical solver returns the minimum oil film thickness between the ring and the cylinder wall, which refers to the distance between the trough of the ring's barrel-shaped profile and the wall surface underneath. Consequently, the film thickness results plotted for the ring are those for the ring at every point along the liner. In contrast, the LIF system's output over time (or crank angle) is the measured lubricant thickness at a given point along the cylinder wall over an engine's operating cycle. Consequently, there is a single point of comparisons between the two thickness diagnostic methods—namely, that in which the ring modeled in numerical simulation passes directly over the LIF optical access window. The ability of the physical LIF model to validate the values returned from numerical simulation will be substantially improved in subsequent research by implementing numerical solvers for all three rings (not just the top ring as it currently stands) and returning a discretized array of film thickness along the piston skirt as a function of time. Since the ring and skirt models are relatively independent in their present forms, such improvements would enable validation of the skirt friction model as well.

Let us recall Figure 4-11. The crank angle (θ) locations of LIF signal values can be mapped directly to location (x) along the cylinder wall via the geometric relationship, which is dependent on crank radius r and connecting rod length l:

$$\boldsymbol{x = r \cdot \cos(\theta) + \sqrt{l^2 - r^2 \sin^2 \theta}}$$

LIF data were shown to conflict with data reflecting manual measurements of physical piston ring-pack crank angle locations at the optical access point along the cylinder wall. Discrepancies between the two values can be attributed to movement of rings within their grooves, piston tilt, and accuracy of piston ring-pack feature crank angle measurements. Conservative estimates for these sources of LIF measurement error

An important part of LIF data analysis is the locating of ring positions within the data graphs. This is accomplished by combining a known mapping of physical ring crank angle location measurements with parabolic LIF data that reflect the shape of their corresponding

rings. The most important information provided by LIF data, however, is the minimum oil film thickness between the ring of interest and cylinder wall, since the minimum film thickness is the driving factor in determining both hydrodynamic and boundary frictional power loss values. A comparison of minimum film thickness across data sets enables the accurate prediction of relative wear rate and frictional power loss contributions. For example, film thickness in lubrication theory is known to scale with square-root of the viscosity—that is, $\boldsymbol{t} \sim \sqrt{\boldsymbol{\mu}}$. Viscosity determines load parameter, which can be mapped to a point on a system's Stribeck curve. Hence, it is critically important in the context of LIF analysis to ascertain the crank angle locations of oil between the ring and cylinder wall so that minimum film thickness values can be reliably obtained across several lubricant formulations. As temperature significantly affects LIF output signal strength, it is important that comparisons be made at the same operating conditions so that film temperatures are held approximately constant.

Considering a sample, characteristic LIF trace over time in the form of Figure 4-14, we notice different minimum oil film thicknesses between the upstroke and downstroke. This comes about largely due to the piston tilt change and ring reversal at TDC and should be considered when comparing across lubricant blends. The resolution of data in Figure 4-14 is not quite optimal, since troughs in the regions of oil underneath the rings are represented by just one or two data points. The peaks visible in this data represent individual rings to which oil attaches, and troughs are given by dips in the middle of the larger peaks.

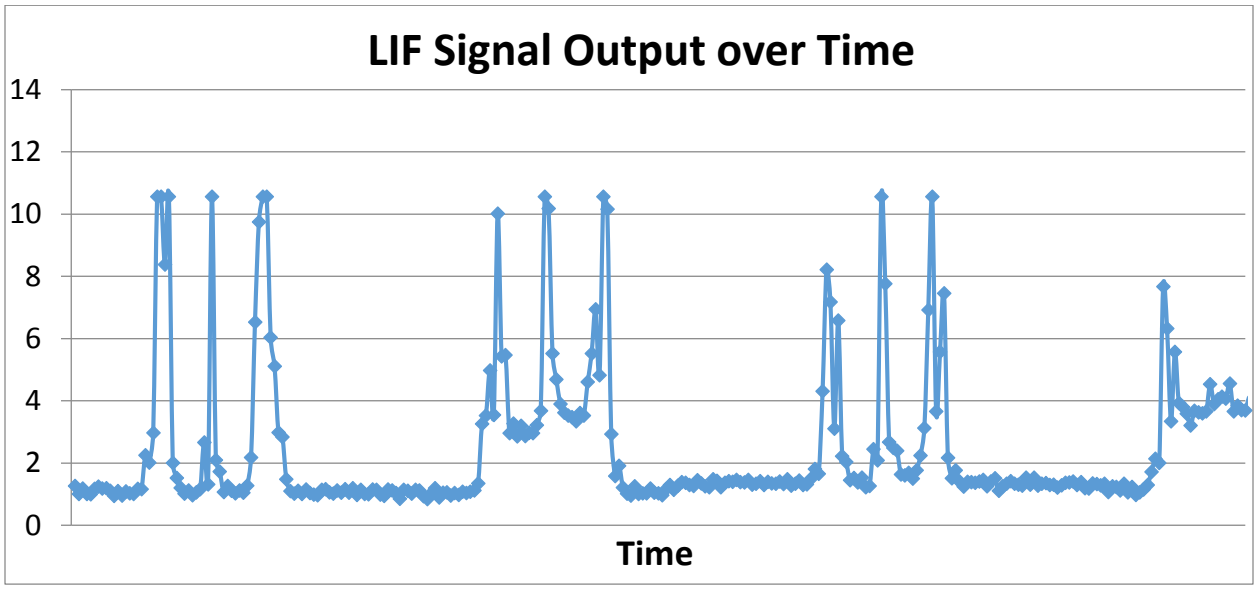


**Figure 4-14.** LIF Signal data representing ring-oil behavior

# Chapter 5 Advocating for SAE Oil Grade Classification Reform

It is self-evident that enhanced fuel economy in internal combustion engines has positive, far-reaching implications for the betterment of our society and planet in general. From reduced greenhouse gas emissions to the preservation of our world's precious non-renewable resources to nations' independence from one another with regard to those resources, reduction in fuel consumption from automobiles presents a panoply of benefits. It is therefore prudent that capable governments and their regulatory agencies enact policies that promote the reduction of unnecessary energy usage by vehicles. While standards and incentives programs for reducing engine emissions and fuel consumption do exist across several of the world's economic superpowers, stringent policies are not in place in several of the world's most populated developing countries where automobile use is ubiquitous. Such nations often apply U.S. SAE standards when classifying their lubricants, and go no further in tailoring lubricant formulations to the automobiles of their nations that may experience unique patterns of both prevailing driving and ambient weather conditions. We have expressed throughout this document the idea that the strategic application of viscosity modifiers to mitigate wear at high power cylinder wall lubricant temperatures is a very promising method for enhancing fuel economy while maintaining a constant power cylinder wear rate.

The previous statement may beg the question as to effects on valve train wear, since the mechanical elements surrounding an engine's camshaft operate at much lower temperatures than does the power cylinder. Reducing viscosity between, for example cam lobes and rocker arms, may promote increased scuffing on those components, which is clearly a deleterious consequence. However, current developments in split-system lubricating trains, which effectively involves channeling two different lubricants to the power cylinder and valve train mechanical components, seems quite promising. Were such a lubricating scheme be implemented in a global scale across automobiles, the present strategy of selective lubricant thickening at high power cylinder temperatures would leave effective wear rates of critical engine components relatively unaffected. Figure 5-1 below illustrates the distinction between the valve-train mechanical components whose friction components possess significant boundary components, and the power cylinder, which is dominated by viscous dissipation.

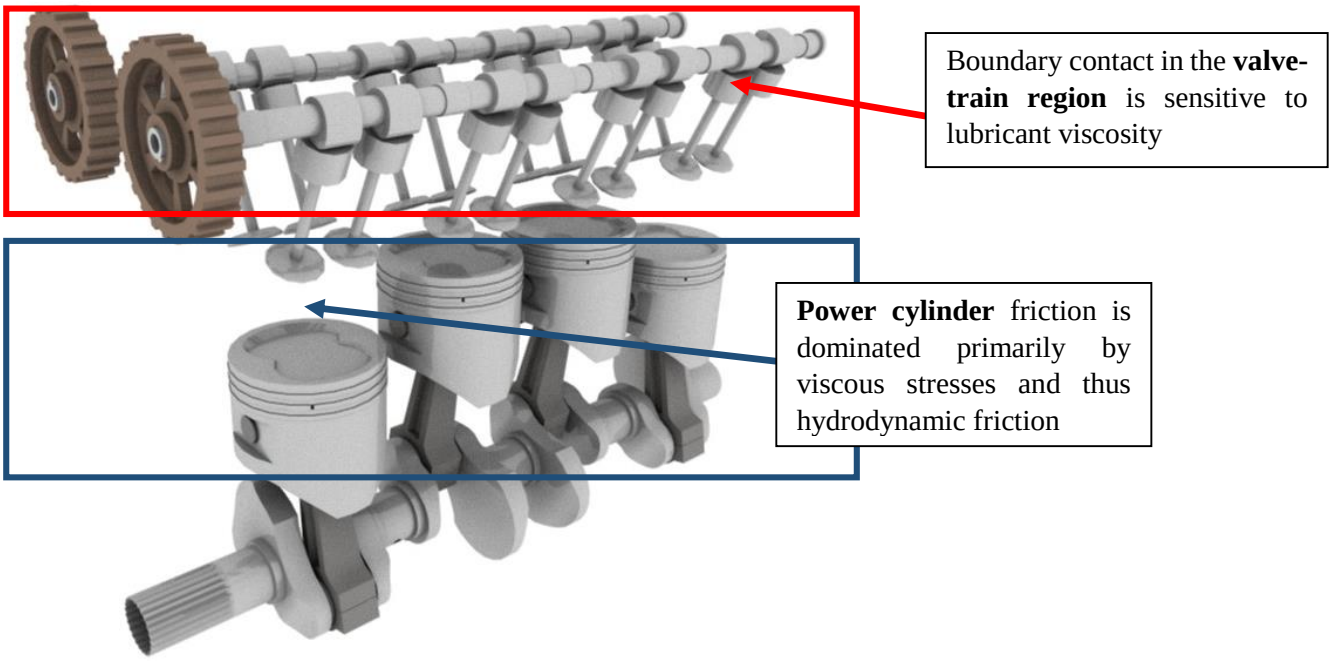


**Figure 5-1.** Boundary friction in the valve train and viscous dissipation in the power cylinder

While SAE's existing multi-grade motor oil classification system does consider the notion of viscosity index improvement and does include medium-temperature (150 Celsius) rheological behavior for high-temperature-high-shear (HTHS) operation, it does so only with respect to low temperatures and shear rates that do not reflect regions of high-temperature engine wear along an engine's cylinder wall. Such an operating point would be represented by a low-shear value at temperatures of around 170-200 Celsius. High temperatures (> 150 Celsius) within a power cylinder are attained at low shear rates with low engine speed. SAE partitions first based on whether oils are single- or multi-grade. Single-grade (or "straight weight") oils, as defined in SAE J300, are oils that possess the characteristics of one class of oil at both low (well below freezing) and high (100 Celsius) temperatures. Multi-grade oils are simply those with added viscosity modifiers, which are intended to result in oils with lower classes of viscosity at low temperatures than at operating temperatures, given the need for cold cranking that cannot always easily be accomplished through the use of single-grade oils. Thus, the method of oil classification that permeates the global lubricants industry considers only the low temperature and mid-range operating temperature viscometric behavior of motor oils. After all, the viscosity index, which is the most common form of characterizing the temperature sensitivity of a

lubricant's viscosity, is based on data points taken at and between 40 and 100 Celsius—low temperatures from the perspective of an engine's cylinder wall.

It is proposed that SAE incorporate the key idea of this thesis into its oil classification scheme such that consumers are informed of the "grades" of their lubricants in both the low and high oil film temperature regimes of their engine's power cylinder. Since the development of such an idea is premised on the notion that viscosity modifiers are no longer used to address cold start issues, but instead to reduce wear near TDC through selective oil thickening at high temperatures within the power cylinder, SAE can adopt a naming protocol "summer" as a corollary to its ubiquitous "winter" designator found in its current multi-grade classifications, such as 15W-40. Thus, the new classification would produce oil grades like (40S-0), where 40 represents typical single-grade oil rheological properties exhibited near TDC, and 0 is the reference to viscosity near mid-stroke. This classification should apply to warm climates such as those in Southeast Asia and even some locations domestically within the United States, including Hawaii and Los Angeles, whose immediate surroundings do not experience conditions that could lead to hazards during engine cold-start attempts.

This evolution of the current SAE lubricant rheological classification also implies the need for a downward shift in oil viscosities to address the optimal value of around 1 cSt near mid-stroke. Currently, the lowest viscosity classification is for the 16 single-grade oil, whose minimum viscosity at 150 Celsius is 2.3 cSt. Consequently, a 1 cSt lubricant formulation is simply not representable by current standards. Since 150 Celsius for HTHS conditions closely resembles piston behavior near the mid-stroke, oil viscosity is minimal in that region, and the standards could be rewritten accordingly.

Diffusion of adequate information to inform consumers of both the benefits and limitations of so-called "summer grade" oils would ensure that such lubricants are not used consistently in cold climates either intentionally or unwittingly. Such an implementation has unique constraints associated with it in comparison with "winter grade" oils because the latter can theoretically be used in any typical weather conditions around the world. That is, they do not have practical upper bounds on their allowable usage temperatures, whereas "summer grade" oils would of course be restricted to warm weather use. While such a restriction may seem cumbersome for many consumers, the author argues that it is perfectly appropriate for a

significant number of moderate to high power consuming vehicles, especially in Southeast Asia where diesel pickup trucks are common. In a place like Thailand, implementing a policy for mandating summer grade lubricants for at least commercial and government vehicles may well result in substantial savings in both fuel consumption and engine emissions.

In short, the existing single- and multi-grade standards may be kept in their existing forms, but an additional series of classifications to address the 150-200 Celsius operating regions for both low and high shear should be included so that consumers are enabled to select a lubricant that optimizes the operation of their engine for fuel economy. By considering their engine type, driving patterns, and ambient climate conditions, users could effectively use a grid to understand which lubricants satisfy their needs, and the tradeoff inherent in selecting one product over another. In essence, users are provided with greater information regarding the impact of their lubricant purchases on the efficiency and mechanical health of their automobile's engines. Users would thereby be able to switch between winter and summer grades depending on their individual circumstances, and no longer merely select a generic engine oil that satisfies cold cranking requirements that may be completely irrelevant for a particular consumer.

What the proposed protocol may also inspire is the creation of higher resolution grade intervals such as 12, 14, 16, etc. so that increasingly precise optimization can be achieved. For example, the current SAE lists a new oil grade at around 10% or more of the previous grade's listed medium-temperature (150 Celsius, HTHS) viscosity bound. A much finer segmentation of lubricant rheological properties may therefore be necessary to result in the multiple-percent fuel economy improvement demonstrated in the present research endeavor. For example, advanced-performance engine oils that command a high premium and significant profit margins for manufacturers and precisely "tune" for engine efficiency may prove to be greatly desired by auto enthusiasts and oil manufacturers alike. Further, the desire to operate with a given engine oil in both cold and warm temperatures may lead to the listing of both winter and summer grades on a given engine oil, the creation of viscosity modifier blends that effectively activate and deactivate at both low and high temperatures to address both cranking and fuel economy concerns, and consequently a newly defined market in the oil industry.

# Chapter 6 Summary and Conclusions

This thesis reviews some of the key milestones accomplished in a lubricants-focused collaboration between PTT and the MIT Sloan Automotive Lab. The goal of the project is to enhance engine mechanical efficiency by over 3% through strategic tailoring of lubricant formulations to specific engine geometries and operating conditions. Through selective iteration of lubricant candidates through a Reynolds based lubrication flow solver, the objective was accomplished with an approximate 3.5% mechanical efficiency improvement. An LIF diagnostic system was successfully developed and implemented in order to obtain real-world film thickness data that could be used as a reference against numerical results. Theoretical studies were undertaken to determine the limits of efficiency improvement, and an approximate 25% reduction in overall engine mechanical efficiency losses could be attained through power cylinder lubricant optimization. NEDC cycle analysis validates the notion that full cycle numerical tests should be run if a truly optimal lubricant is to be selected, since a single representative operating point for a cycle does not adequately capture the highly variable nature of the different cycle operating points. Further work that is focused on enhancing the features of the existing numerical model is forthcoming.

Several recommendations were made for improving the state of lubricants, their additives, and the policy that regulates how they are classified and used around the world. For example, it is clear that—according to the wear model applied in the present work—in order to maintain a given level of engine wear, the high temperature characteristics in the region of peak wear rate must be held approximately constant. In order to enforce this principle while minimizing power losses elsewhere, especially near mid-stroke, viscosity modifiers must be better understood and controlled. Specifically, it would be highly beneficial to be able to reliably control the uncoiling behavior of VMs in a manner that promotes thickening of the lubricant just prior to the region of peak wear and not near mid-stroke. This retains a thin oil film for as long as appropriate, and effectively transitions to a wear mitigation mode when boundary contact becomes an issue.

Furthermore, given the nature of the present work in applying VMs to address the high temperature regions of the engine rather than the more traditional cold-cranking, the means of classifying a multi-grade lubricant of this type should not be the same as that used to classify lubricants whose VMs' purposes are to mitigate cold weather pumping issues. Consequently,

adding a “summer” standard of oil grade to the SAE oil grade classification protocol should be considered as an alternative to the existing means of characterizing multi-grade lubricants.

As a side note, the author would point the reader to two publications, among many others, that are particularly related to his work, including “Development of an API SN, SAE 0W-20 Engine Lubricating Oil for Tropical Climate using a New Novel Viscosity Modifier and Verification of Its Performance via a Field Trial in Thailand” and “Optimizing Base Oil Viscosity Temperature Dependence For Power Cylinder Friction Reduction” [22, 23]. These documents directly reflect the product of the present research, and extend our findings to neighboring fields and possible applications. Considerable additional literature is available in the SAE journal library.

Additional work on this project will include enhancements to the existing friction-wear model and further insight into the implications of LIF output data results. Vaporization, oil composition, friction modifiers, and anti-wear agents will all hopefully be accurately represented in subsequent simulation editions. Accurate mapping of LIF traces to ring profiles is also an area of central interest to the author and his collaborators, as it is crucial to the validation of both simulation results and our understanding of the physical rheological phenomena that transpire within internal combustion engines. It is also hoped that the uncoiling behavior of viscosity modifiers will be better understood such that VM design is achieved in order to control the temperature range of uncoiling for maximal lubricant thickening near TDC and regions of peak wear, with a much lower viscosity present in lower temperature and high shear operating environments.

# Bibliography


[1] M. Molewyk, “In Situ Control of Lubricant Properties for Reduction of Power Cylinder Friction through Thermal Barrier Coating,” *MIT SM Thesis*, 2014.

[2] D. Richardson, "Review of Power Cylinder Friction for Diesel Engines," *Journal of Engineering for Gas Turbines and Power-Transactions of the ASME*, vol. 122, no. 4, pp. 506-519, 2000.

[3] Caines, Haycock, and Hillier. “Chapter 1: Introduction and Fundamentals.” In *Automotive Lubricants Reference Book*. Second ed. Warrendale, PA: SAE International, 2004.

[4] S. Hironaka, “Boundary Lubrication and Lubricants.” *Three Bond Technical News*, 1984.

[5] V. Wong, “Lubrication and Friction.” Cambridge, MA. 2013.

[6] T. Tian, “Modeling the Performance of the Piston Ring-Pack in Internal Combustion Engines,” *MIT PhD Dissertation*, 1997.

[7] Patir N, Cheng HS. An Average Flow Model for Determining Effects of Three-Dimensional Roughness on Partial Hydrodynamic Lubrication. ASME. *J. Tribol.*.1978;100(1):12-17.

[8] J. A. Greenwood and J. H. Tripp. The contact of two nominally flat rough surfaces. *Proceedings of the Institution of Mechanical Engineers*, 185(1):625-633, June 1970.

[9] B. Bhushan. “Chapter 7: Wear.” In *Introduction to Tribology*. New York: John Wiley & Sons, 2002.

[10] I.M. Hutchings, *Tribology: Friction and Wear of Engineering Materials* (CRC Press, Boca Raton, 1992).

[11] M. Molewyk, personal communication, October 2014.

[12] Materials provided in part by Dr. M. Plumley and G. Gu. 2014.

[13] Yamaguchi, Elaine S., et al. "Chapter 21: Additive Technology." In *Handbook of Lubrication and Tribology*. Second ed. Boca Raton, FL: CRC Press, 2012.

[14] Stachowiak and Batchelor, “Chapter 2: Physical Properties of Lubricants.” In *Engineering Tribology*. Third ed. Oxford: Elsevier Inc., 2005.

[15] “Calibration of Laser Fluorescence Measurements of Lubricant Film Thickness in Engines,” by D.P.Hoult, J.Lux, V.W.Wong, and S.A Billian, SAE Paper 881587, presented at the Int’l Fuels and Lubricants Meeting & Exposition, Portland, OR, October 1988; SAE Transactions Vol. 97, 1988.

[16] Smart A E and Ford R A J 1974 Measurement of thin liquid films by a fluorescence technique *Wear* 29 41–7.

[17] Hamamatsu. “Photomultiplier Tubes: Basics and Applications.” Third ed. Hamamtsu Photonics K. K., 2006.

[18] P. Mulgrave, “Development of a Laser Induced Fluorescence System for Measuring Oil Film Thickness in Two Dimensions in a Reciprocating Engine,” *MIT SM Thesis*, 1997.

[19] Presentation in Lubrication Fundamentals at STLE’s 2015 Annual Meeting & Exhibition.

[20] Kimmon Koha. “He-Cd Laser.” Kimmon Koha Co., Ltd.

[21] A. Kariya, “Development of a Multi-Regime Tribometer and Investigation of Zinc Dialkyldithiophosphate Tribofilm Development in the Presence of Overbased Calcium Sulfonate,” *MIT SM Thesis*, 2009.

[22] Predapitakkun, S. and Sukajit, P., "Development of an API SN, SAE 0W-20 Engine Lubricating Oil for Tropical Climate using a New Novel Viscosity Modifier and Verification of Its Performance via a Field Trial in Thailand," SAE Technical Paper 2014-01-2779, 2014.

[23] Plumley, M., Wong, V., Molewyk, M., and Park, S., "Optimizing Base Oil Viscosity Temperature Dependence For Power Cylinder Friction Reduction," SAE Technical Paper 2014-01-1658, 2014.

# Appendices

## Appendix A1. Engine Input Parameter Code

```
2,1200.,240.,150.,125.0,
0.5,32,150.,0.285,
0.1,130.,0.285,0.1
0.115,879.0,993.4,103.8,2.5,0.0225,0.88,1.0,
195.,100.,1,1,
70.,95.,1,1.E-4,
124.5,64.0,94.85,250.0,
200.0E-6,220.0E-6,0.0,0.00138,0.02644,41.55E-4,
-0.001855,2.733,1.122,3.185,0.33,
0.4,0.01,0.1,0.1,
11,19,50.0e-6,50.0e-6

TYPICAL values for MM11....actual values used are read from list
above:
N_Cyc:  Number of Cycles to run [dimensionless]: 1
RPM:    Crankshaft Rotational Speed [rpm]: 1200.0
LCR:    Connecting Rod Length [mm]: 245.5
()
STROKE: Stroke [mm]: 150.0
()
BORE:   Bore [mm]: 125.0
()

RA_TOP: Compression (TOP) Ring: Roughness [microns]: 0.5
()
TR_TOP: Compression Ring: Tension Force [N]:32.0
()  (measure or see SAE Piston Ring Standards J1997)
E_TOP:  Compression Ring: Modulus of Elasticity (i.e. Young's Modulus)
[GPa]: 150.     (can range from 85-150)
PS_TOP: Compression Ring: Poisson's Ratio [dimensionless]:0.285

RA_LINER: Liner Roughness Rq [microns]: 0.1                    ()
E_LINER:  Liner Modulus of Elasticity (Young's Modulus) [GPa]: 130.
PS_LINER: Liner Poisson's Ratio [dimensionless]: 0.285
rgfcoe: ring coefficient of friction

OIL_K:  Oil Viscosity Parameter: Vogel equation: k [centiStokes]:
0.115
OIL_DEN: Oil Parameter: Density [kg/m^3]:879   (Infineum 15W40)
OIL_TH1: Oil Viscosity Parameter: Vogel equation: Theta 1 [degrees
C]:921.2
OIL_TH2: Oil Viscosity Parameter: Vogel equation: Theta 2 [degrees
C]:103.2
OIL_A:  Oil Viscosity Parameter: Critical Shear Rate Equation: a (or
c1) [dimensionless]:2.5
```

```
OIL_B:  Oil Viscosity Parameter: Critical Shear Rate Equation: b (or
c2) [degrees C]^(-1):0.0225
OIL_R_VIS: Oil Viscosity Parameter: Cross Equn: ratio of high shear
visc to low shear visc (mu_infinity/mu_0): 0.88
OIL_M:  Oil Viscosity Parameter: Cross Equation: m [dimensionless]:1.0

T_TDC:  Oil Viscosity Parameter: Woschni Correlation: T_TDC [degrees
C]:170
T_BDC:  Oil Viscosity Parameter: Woschni Correlation: T_BDC [degrees
C]:100
I_TEMP_READ: IF 0, USES T_TDC,T_BDC; IF 1 USES INPUT_TEMP_LINER FILE
I_NOTE: 1 if you want to add note, 0 if you don't

FOLLOWING ADDED FOR SKIRT CODE (also in order of values above):
      PLANDS=  70              distance from top ring to middle of
skirt (for temp calcs)
      T_BDC_sk= 95       temp expected where skirt reaches bdc
      i_temp_read_sk=1       !0 for Woschni hybrid, 1 for lookup .dat
      TOL=1.0E-4         convergence tolerance

      PSTDIA = 124.5    nominal skirt diameter (mm)
      SKIRTL = 64.     length of skirt (mm)
      SKIRTW = 94.85   calculated length of skirt in angular direction
(mm)
      cylinl = 250.      cylinder length (mm)

      rofs = 200.e-6    offset of ring section relative to skirt in
radial direction (m)
      PLCLR =220.E-6     clearance of top of skirt to wristpin (m)
      CP = 0.0           wrist pin offset (m)
      CG = 0.00138      horiz distance piston cg to wrist pin (m)
      A = 0.02644       Vert distance top of skirt to Mansouri had
0.0428 (m)
      RIPP = 41.55E-4   piston mom of iner,mansouri=137.45E-4,scaled
by m,L^2 (kgm2)

      BCG = -0.001855   vert distance skirt top to piston CG (m)
      RMPST = 2.733         !piston mass (kg)
      RMWRST = 1.122        !wristpin mass (kg)
      RMCONR = 3.815        !conrod mass...Mansouri had 11.3 (kg)
      CRMEFR = 0.33         !% of conrod mass at wristpin

      WAVHGT = 0.4       !mansouri used 10E-6  (micr)
      WAVLEN = 0.01         !surface waviness wavelength  (m)
      ROUGHS = 0.1       !surface roughness skirt&liner (micr)
      skfcoe = 0.1        !contact friction coefficient, skirt

      NXIN = 11           !number grid points, mansouri=11
      NYIN = 19           !mansouri=19
      haref= 50E-6        !initial film thickness on liner antithr
side (m)
      htref= 50E-6        !
```

## Appendix A2. Lubricant Input Parameter Code

```
VM1_Vis100_9_Den800,1.6577,800.,210.68,24.531
VM2_Vis100_8.5_Den800,1.2361,800.,255.22,32.369
RefSAE10W30,0.12338,789.7,915.45,102.78
```

## Appendix B. Focusing Probe Images

*End onto which the collimator/coupler is screwed*

*Threaded tunnel bored through the engine block*

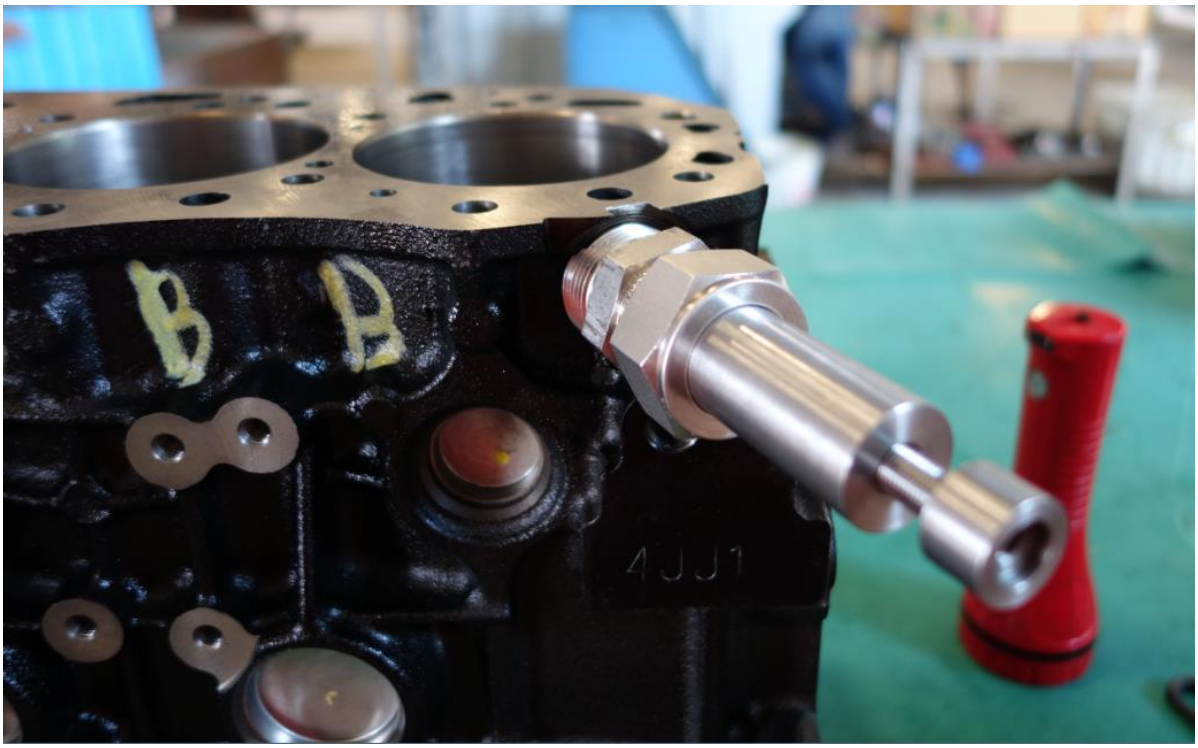


*Focusing probe installed near Top-Dead-Center (TDC)*

## Appendix C. Focusing Probe Drawing

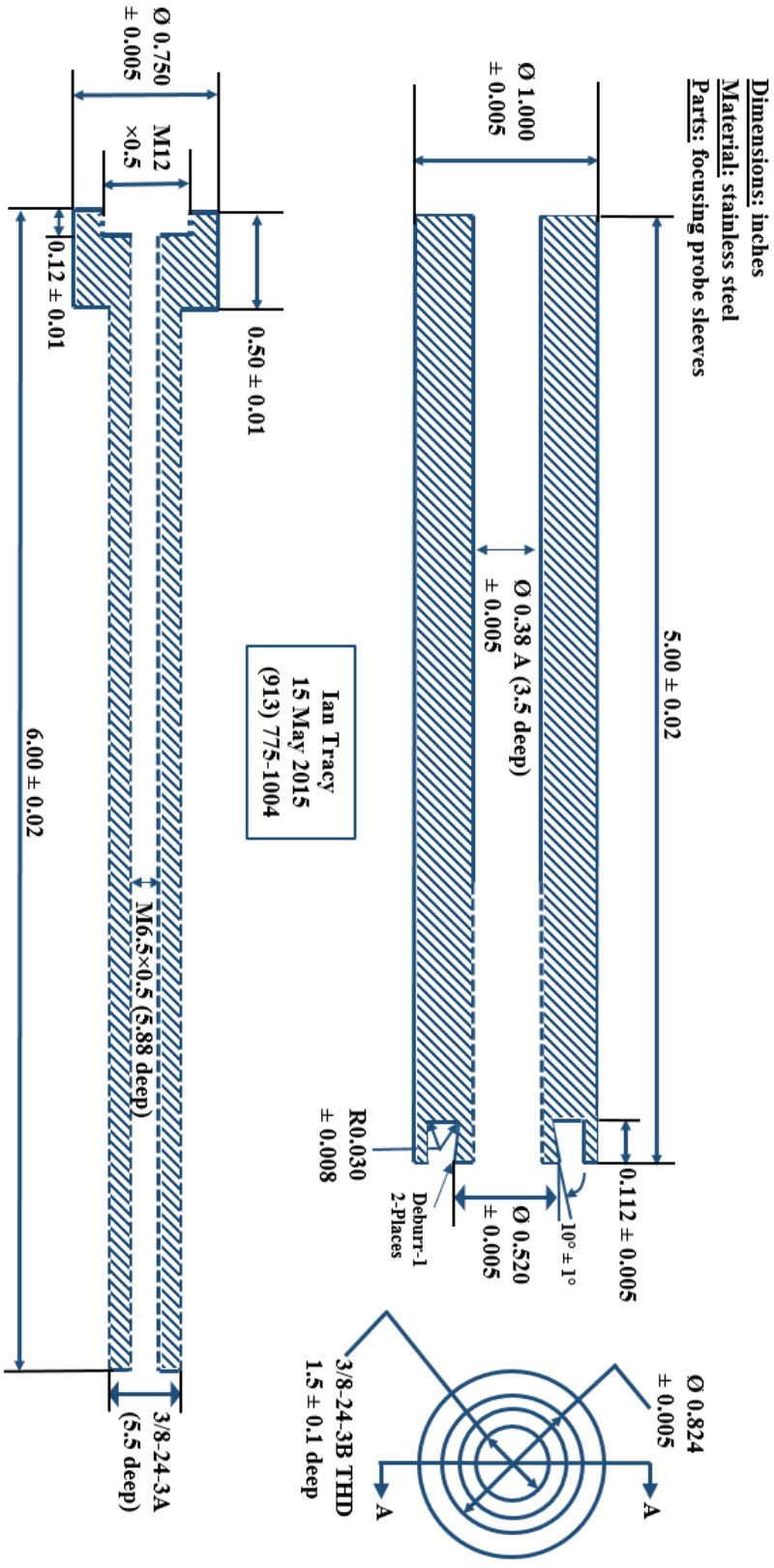

# Appendix D. Laser Specifications

## Kimmon Koha Co., Ltd.

**Model IK4401R-D**
**50mW @ 442nm $TEM_{00}$**
**HeCd Laser System**

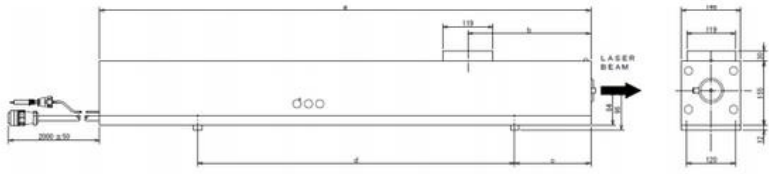


| a | b | c | d |
|---|---|---|---|
| 850 | 380 | 128 | 605 |

All dimensions in millimeters

## SPECIFICATIONS

| | |
|---|---|
| Model | IK4401R-D |
| Wavelength | 441.6nm |
| Output Power | 50mW |
| Transverse Mode | $TEM_{00}$ |
| Mode Spacing (C/2L) | 194 MHz |
| Spectral Bandwidth | 3 GHz |
| Coherence Length | 10 cm |
| Polarization | Linear, Vertical |
| Polarization Ratio | > 500:1 |
| Peak-To-Peak Noise (30kHz-2MHz) | > 10% |
| R.M.S. Noise (30kHz-10MHz) | > 2% |
| Beam Diameter ($1/e^2$) | 1.1 mm① |
| Beam Divergence | 0.5 mrad |
| Beam Pointing Stability (25°C constant temp) | ±25 μrad<br>±12.5 μrad② |
| Warm Up Time (90% power) | 20 minutes |
| Power Stability (25° C constant temperature) | ±2%/4 hours |
| Power Stability (10°-40°C) | 20% |
| Environmental Condition (operation) | Temp. 10°-40°C, Hum. 90%RH③ |
| Environmental Condition (storage) | Temp. -10°-50°C, Hum. 90%RH③ |
| Vibration (operation) | 0.25 G |
| Vibration (storage) | 2 G |
| Shock (with Kimmon packaging) | 20 G④ |
| Dimensions | 850 x 146 x 197 mm |
| Weight | 16 kg |
| CDRH Laser Classification | Class IIIb |
| Power Supply Model | KR1801C |

① - Measured 100mm from output coupler
② - With remote cooling fan
③ - Non-condensing
④ - Vertical direction


## Appendix E. Coumarin 523 Dye Specifications

| Lasing Wavelength Max. (nm) | Range (nm) | Pump Source (nm) | Solvent | Concentration (molar) | Abs λ-max | Fl λ-max |
|---|---|---|---|---|---|---|
| 514 | 500-560 | FL[69] | $MeOH/H_2O$ | $8 \times 10^{-5}$ | 443[e] | 485[e] |
| 520 | 501-545 | FL[69] | $MeOH/H_2O$,1/1 | $1 \times 10^{-4}$ | | |
| 522 | | FL[19] | Ethanol | | | |

$MeOH/H_2O$=methanol/water, e=ethanol